MONASH University

Intelligent Vehicle Control Strategies for Cooperative Eco-driving on Road Networks

A. S. M. Bakibillah

A thesis submitted for the degree of Doctor of Philosophy at
Monash University in 2020
Mechatronics Engineering, School of Engineering

Copyright notice

Abstract

Fuel consumption and emissions of a vehicle are greatly infulenced by driving behavior. In particular, signalized intersections, roundabouts, and road-geometry characteristics, such as, rolling terrains and horizontal curves are the major sources of bottlenecks. This brings the necessity of the development of intelligent vehicle control strategy for cooperative ecological (eco) driving at road networks. Infrastructure-to-vehicle (I2V) and vehicle-to-vehicle (V2V) communications along with automated vehicle (AV) technologies can play an important role to improve traffic flow performance through control algorithms. However, full autonomy of vehicles and proper infrastructure development for V2V and I2V communications are currently not widespread. The work in this thesis proposes novel intelligent vehicle control strategies for cooperative eco-driving at road networks that generate the optimal velocity trajectory for the vehicle. The strategies are based on learning efficient driving from driving data, efficient driving based on model predictive control (MPC) and fuzzy-tuned MPC, and intelligent vehicle coordination using a cloud-based system or a centrlized controller. We develop machine learning approach to predict traffic flow behavior better at signalized intersections, non-linear MPC to improve traffic flow at rolling terrains and horizontal curved roads, fuzzy interence techniques to tune MPC for smooth variation of speeds on sloples, and receding horizon control approach for vehicle coordination at roundabouts. To evaluate the performance of the proposed scheme, microscopic traffic simulations are conducted and benchedmarked with the existing traditional systems. The results show significant performance improvement in fuel economy, CO_2 emission, and travel time, while ensuring driving safety.

Declaration

This thesis is an original work of my research and contains no material which has been accepted for the award of any other degree or diploma at any university or equivalent institution and that, to the best of my knowledge and belief, this thesis contains no material previously published or written by another person, except where due reference is made in the text of the thesis.

Signature:

Print Name: A. S. M. Bakibillah

Date: 20/11/2020

Publications during enrolment

Journals:

1. **A. S. M. Bakibillah**, M. A. S. Kamal, Chee Pin Tan, Tomohisa Hayakawa, and Jun-Ichi Imura, “Event-driven Stochastic Eco-driving Strategy at Signalized Intersections from Self-driving Data,” *IEEE Transactions on Vehicular Technology*, vol. 68, no. 9, pp. 8557-8569, 2019. **[Q1, IF 5.37]**

2. **A. S. M. Bakibillah**, M. A. S. Kamal, Chee Pin Tan, Tomohisa Hayakawa, and Jun-Ichi Imura, “Fuzzy-tuned Model Predictive Control for Dynamic Eco-driving on Hilly Roads,” *Applied Soft Computing*, pp. 106875, 2020. **[Q1, IF 5.47]**

3. **A. S. M. Bakibillah**, M. A. S. Kamal, Chee Pin Tan, Susilawati, Tomohisa Hayakawa, and Jun-Ichi Imura, “Coordinated Merging of Connected-Automated Vehicles at Roundabouts for Smooth Traffic Flow,” *IEEE Transactions on Intelligent Transportation Systems,* Under Review. **[Q1, IF 6.31]**

4. **A. S. M. Bakibillah**, M. A. S. Kamal, Chee Pin Tan, Tomohisa Hayakawa, and Jun-Ichi Imura, “Dynamic Eco-driving on Horizontal Curves using MPC Under Various Road-surface Conditions,” *IEEE Transactions on Control Systems Technology,* Submission Stage. **[Q1, IF 5.31]**

Conference Proceedings:

1. **A. S. M. Bakibillah**, M. A. S. Kamal, and Chee Pin Tan, “Sustainable Eco-driving Strategy at Signalized Intersections from Driving Data,” in *Proc. Annual Conference of the Society of Instrument and Control Engineers of Japan (SICE)*, Accepted, 2020.

2. **A. S. M. Bakibillah**, M. A. S. Kamal, Susilawati, and Chee Pin Tan, “The Optimal Coordination of Connected and Automated Vehicles at Roundabouts,” in *Proc. 58th Annual Conference of the Society of Instrument and Control Engineers of Japan (SICE)*, pp. 1392-1397, 2019. **[Top 3 out of 400 papers]**

3. **A. S. M. Bakibillah**, M. A. S. Kamal, Chee Pin Tan, Tomohisa Hayakawa, and Jun-Ichi Imura, “Eco-driving on Hilly Roads Using Model Predictive Control,” in *Proc. IEEE Joint 7th International Conference on Informatics, Electronics & Vision and 2nd International Conference on Imaging, Vision & Pattern Recognition*, pp. 476-480, 2018.

Acknowledgements

First of all, I would like to express my deepest gratitude to my supervisor A/Prof. M. A. S. Kamal for his supervision and continuous support of my Ph.D. work. His profound knowledge and guidance helped me to better understand my field of research. It was really enlightening to discuss with him my thoughts for finding answers to the problems. I couldn't have imagined a better advisor for my Ph.D. work.

Next, my deepest appreciation to my supervisor A/Prof. Tan Chee Pin for his advice and motivation throughout my Ph.D. candidature. His constructive criticism and feedback helped to boost my research and writing of my Ph.D. thesis. His patience and generosity have encouraged an incredibly friendly research environment and therefore, obtain the best possible outcome.

Besides my supervisors, my sincere gratitude goes to A/Prof. Tomohisa Hayakawa and Prof. Jun-ichi Imura for their insightful comments and hard questions, which inspired me to extend my work from different perspectives.

I would like to acknowledge Japan Society of the Promotion of Science (JSPS) Grant-in-Aid for Scientific Research (A) 18H03774 and (C) 20K04531 for supporting my Ph.D. research and publications.

Last but not least, I would like to thank my family members for supporting me spiritually throughout my Ph.D. study.

Contents

List of Figures

List of Tables

List of Abbreviations

ACC	Adaptive Cruise Control
ADAS	Advanced Driver Assistance Systems
AHS	Automated Highway System
AIM	Autonomous Intersection Management
API	Advanced Programming Interface
AHS	Automated Highway Systems
BN	Bayesian Network
BBI	Ball Bank Indicator
CACC	Cooperative Adaptive Cruise Control
CAV	Connected and Automated Vehicle
CMEM	Comprehensive Modal Emissions Model
COG	Center of Gravity
CV	Connected Vehicle
CVIC	Cooperative Vehicle Intersection Control
DP	Dynamic Programming
ECO	Ecological
EDS	Eco-driving System/Strategy
EV	Electric Vehicle
GHG	Greenhouse Gas
GIS	Geographic Information Systems
GDP	Gross Domestic Product
GPS	Global Positioning System
GPR	Gaussian Process Regression
IDM	Intelligent Driver Model
I2V	Infrastructure to Vehicle
ITS	Intelligent Transportation Systems
MPC	Model Predictive Control
MTC	Multi-level Traffic control
MOBIL	Minimizing Overall Braking Induced by Lane Change
OBU	On-board Unit
ORNL	Oak Ridge National Laboratory
PHEV	Plug-in Hybrid Electric Vehicle
RCU	Roundabout Coordination Unit
RCS	Roundabout Coordination System

RLS	Recursive Least Square
RHC	Receding Horizon Control
SAE	Society of Automotive Engineers
SPAT	Signal Phase and Timing
SQP	Sequential Quadratic Programming
SAS	Speed Advisory System
SLFD	Single-line Flow Diagram
TDS	Traditional Driving System
TRS	Traditional Roundabout System
V2V	Vehicle to Vehicle
VICS	Vehicle Intersection Coordination Scheme

Chapter 1

1 Introduction

1.1 Research Background

In recent decades, despite growing development of vehicular technologies and mobility systems, traffic congestion, fuel consumption, and greenhouse gas (GHG) emissions remain an issue due to increase in the demand for transportation on the road network. A report on urban road mobility shows that traffic congestion resulted in a total cost of 160 billion USD per year to American drivers to travel extra 6.9 billion hours and purchase extra 3.1 billion gallons of fuel (Schrank et al., 2015) and this cost is increasing every year as shown in Figure 1.

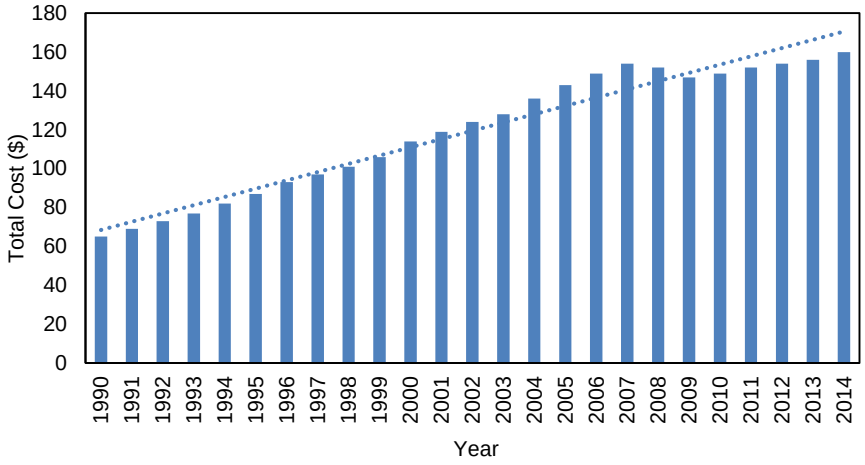

Figure 1: Total cost due to traffic congestion in the U.S. (1990-2014).

According to European Commission, the external costs of road traffic congestion alone amount to 0.5% of Community GDP and by 2050, the congestion cost will increase by about 50% (European Commission, 2011). In the U.S., road transportation accounts for about 28% of energy use (U.S. EIA, 2019), and is the second largest source of GHG emissions, which accounts for about 29% of the total U.S. GHG emissions (Desai & Harvey, 2017). Similarly, road transportation causes about 23% of the total GHG emissions in the European Union (EU), and is the largest source of NOx emissions (Guerreiro

et al., 2014). Specifically, emissions from gasoline-fuelled vehicles contribute 55%, 36%, and 28% of carbon monoxide (CO), nitrogen oxides (NOx), and hydrocarbons (HC), respectively (Zhang & Frey, 2006). Such large amount of emissions from transportation is the primary source of air pollution and global warming. Thus, automotive researchers and policymakers have been focusing on various sustainable road transportation technologies that can reduce both fuel consumption and GHG emissions.

A vehicle's fuel consumption and emissions are affected by several physical factors, such as its engine characteristics, power train system, structure against aerodynamic drag, and fuel type (Barth et al., 2006; Bishop et al., 2007). The development of advanced engine technology, hybrid power train, lightweight automobiles, eco-fuel, and electric vehicle (EV) helped to realize energy-efficient transportation systems (Mendez & Thirouard, 2009; Ngo et al., 2012). However, recent studies have revealed that driving behaviour has a potential influence on vehicle fuel consumption and emissions, because it is very hard for a human driver to apply intimate knowledge of the engine dynamics (for fuel-efficient driving) by perfectly anticipating surrounding road traffic situations (Berry, 2010; Knowles et al., 2012). For example, frequent acceleration and braking due to aggressive driving behaviour can increase fuel consumption up to 33% on highways and 5% on urban ways (Saboohi & Farzaneh, 2009). Specifically, signalized intersections and roundabouts are the main sources of bottleneck, where human drivers frequently perform idling, acceleration, and braking (Margiotta & Snyder, 2011; Tang et al., 2017).

A report on “Smart drive” by the energy conservation centre, Japan studied the impact of driving action on fuel consumption and found that consumption during start/acceleration and slowing down makes up about 50% of the whole fuel consumption as illustrated in Figure 2 (Toyota, 2006). Field studies revealed that stop-and-go vehicles cause 14% more fuel consumption and emissions than vehicles drive at constant speed (Xia et al., 2012). Thus,

speed regulation considerably affects fuel consumption and emissions of a vehicle as shown in Figure 3 (Liu et al., 2015).

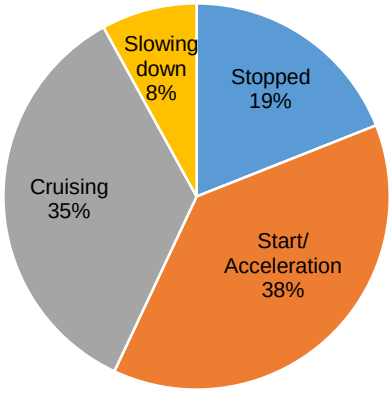

Figure 2: Effect of driving action on fuel consumption.

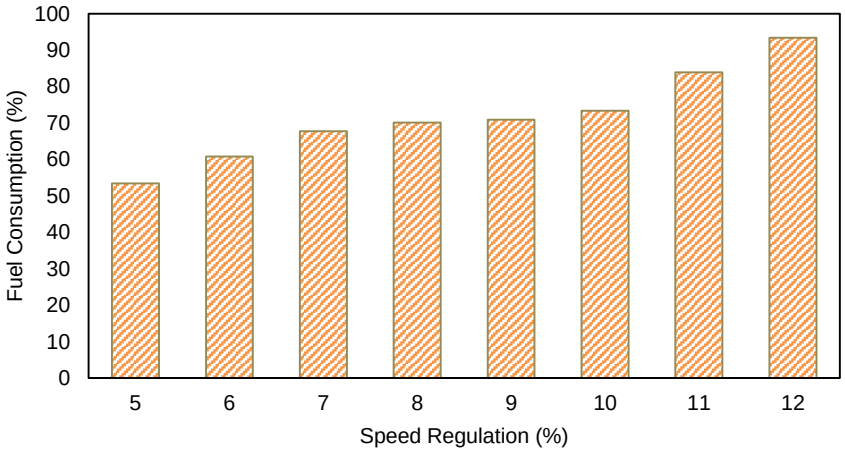

Figure 3: Fuel consumption variation with speed regulation in the complex driving cycle.

Moreover, road-geometry characteristics, such as roadway grades in a hilly road profile and horizontal curved roads seriously impact human driving behaviour as well as real-world fuel consumption and emissions of a vehicle. For example, fuel consumption of vehicles is approximately 5% to 20% more on uphill sections of a hilly road compared to a flat road because high power is required to overcome the gravitational force (Boriboonsomsin & Barth, 2009; Carrese et al., 2013). Some researchers found an average increase of 2–64% in fuel consumption and CO_2 emission, 3–47% in HC, 4–73% in CO, and 24–380% in NOx by varying the road grade from 0% to 8% in steps of +1% for a

5 km road with an average vehicle speed of 70 km/h (Silva et al., 2006). Likewise, Ko et al. (2015) found that a vehicle driving on horizontal curved roads at a speed of 70 km/h consumes 34% extra fuel and produces up to 91% more emissions when the radius is 50% lower than the minimum standard.

In contrast, a series of driving tests show that it is possible to reduce fuel consumption by approximately 5-25% through driving in an economical style (Mierlo et al., 2004; Cheng et al., 2013). Among various efficient driving strategies, ecological driving (eco-driving) is one such strategy that gives various solutions and techniques for improving fuel efficiency, reducing traffic congestion, and emissions (Barth et al., 2011; Hu et al., 2016). The main concept of eco-driving is to control acceleration, deceleration, and idling by optimizing velocity profile, and facilitate anticipatory and cooperative driving.

In the literature eco-driving has been evaluated in two major scenarios; on the freeways (Kamal et al., 2011; Wang et al., 2014; Hu et al., 2016) and on the signalized intersections and merging roadways (Barth et al., 2011, Xia et al., 2013a; Rakha & Kamalanathsharma, 2011). Xia et al. (2012) carried out both simulation and field testing using a cloud based server to demonstrate the potential of an eco-approach application and obtained 13.6% fuel saving at a signalized intersection. An experimental study using the vehicle's on-board logging device and GPS tracking system showed long-term impact of an eco-driving training course with 5.8% fuel improvement (Beusen et al., 2009). A dynamic eco-driving strategy based on real-time traffic sensing and telematics along with a traffic management system achieved approximately 10-20% fuel savings without a significant increase in travel time (Barth & Boriboonsomsin, 2009). Another research implemented eco-driving using the hardware-in-the-loop method to test optimal velocity trajectories on an engine test bench, and reduced fuel consumption by 17-25% on urban roads (Mensing et al., 2013). In Europe, eco-driving programs showed substantial improvement in fuel economy in the range of 5-15%. The eco-driving flow-chart is shown in Figure 4.

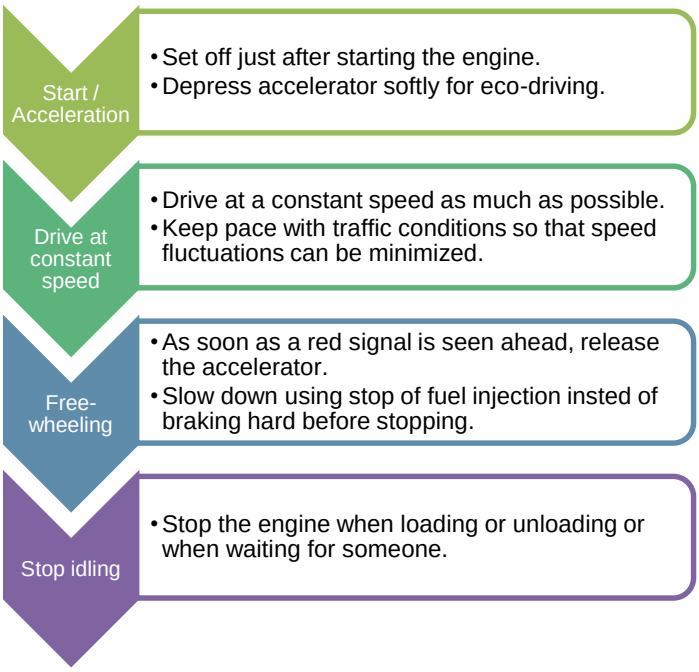

Figure 4: Eco-driving steps showing fuel efficient way of driving.

Several fuel consumption models have been developed to estimate fuel consumption of vehicles for eco-driving. Post et al. (1985) proposed a power-based fuel consumption model, which estimates total fuel consumption for vehicles within 2% of real-world fuel usage. The model was developed from 177 in-use vehicles chassis dynamo-meter experiments. Later, the accuracy of the model was enhanced by Akcelik (1989) considering various vehicle speed and road geometry data. Barth et al. (2000) developed another energy/emissions model called Comprehensive Modal Emissions Model (CMEM) that predicts the instantaneous fuel consumption rate of a vehicle based on its engine size, engine speed, engine friction, and engine power. The CMEM is capable of estimating fuel consumption of 30 different vehicle categories from small light-duty vehicles to class-8 heavy duty trucks and the estimation accuracy of the model is within 5% of actual fuel consumption. The researchers of Linkőpings University developed a fuel consumption model using vehicle gear shifting and topographic information (Hellinga et al., 2000; Fröberg et al., 2006).

Simpson (2005) developed a fuel consumption model called PAMVEC based on parametric analysis of road-load equations that uses simple on-vehicle feature inputs for estimating fuel consumption with an error below 20%. Rakha et al. (2004) another fuel consumption model called VT-Micro model was developed experimentally with nine normal emitting light-duty vehicles in a laboratory at Oak Ridge National Laboratory (ORNL). Under this model, various polynomial combinations of velocity and acceleration were tested using chassis dynamo-meter data collected at the ORNL. Kamal et al. (2012) developed a fuel consumption model based on the torque–speed characteristic map of the engine of a typical vehicle. The model estimates fuel consumption rates of a vehicle using its instantaneous velocity and acceleration.

With recent advancements of intelligent transportation systems (ITS), connected and automated vehicle (CAV) technologies, geographic information systems (GIS), global positioning systems (GPS), and databases such as Google Maps Elevation advanced programming interface (API), it is possible to obtain relevant information of upcoming road segments in advance and control the trajectory and movement of individual vehicle for eco-driving (Li et al., 2014, Gáspár & Németh, 2014). The connected vehicle (CV) environment facilitates two-way wireless communications; namely, vehicle-to-vehicle (V2V) and/or vehicle-to-infrastructure or infrastructure-to-vehicle (V2I or I2V) communications as shown in Figure 5 (Azizi, 2015; Hamida et al., 2015). Moreover, it is possible to coordinate between vehicles and infrastructure with either a centralized or decentralized controller to improve traffic flow performance and safety by cooperative driving in specific traffic scenarios, such as signalized intersections and roundabouts (Yang et al., 2016; Rios-Torres & Malikopoulos, 2017). The idea of coordinated and cooperative traffic system has attracted great attention in traffic flow control as it solves multiple issues posed by traditional human driving, such as stop-and-go driving and traffic accidents. The vehicles are expected to follow the command given by the controller to ensure maximum efficiency of traffic flow. Moreover,

coordination can be repeated frequently to include state feedback for smooth operation, even if a vehicle does not follow the command or if unexpected disturbances occur. Thus, it is possible to arrange the whole system in the exact required way, which is very difficult for a human driver. Though with the advances in V2V and I2V communication technologies, cooperative control incorporating under a fully Connected Vehicle (CV) environment enables cooperation between vehicles and infrastructure to improve the traffic management but unfortunately, CAV technologies are not widespread. Hence, more practical and adoptable driving methods need to be developed to deal with current road-traffic situations.

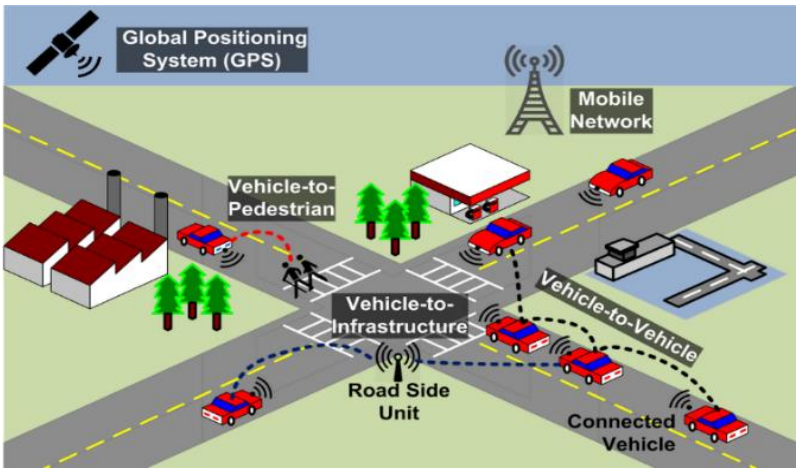

Figure 5: Various vehicular communication technologies (Hamida et al., 2015).

1.2 Research Scope

The scope of eco-driving at different scenarios of road networks is illustrated in Figure 6. The work in this thesis is mainly focused on developing intelligent and advanced vehicle control systems for cooperative eco-driving at signalized intersections, free roads with explicit road-geometry characteristics, such as rolling terrains (with various up and down slopes) and horizontal curves (with various curvature and road-surface conditions), and four-leg roundabouts. The work in this thesis target to achieve vehicle autonomy levels 2 and 3 as shown in Figure 7 (SAE, 2014). In recent years most new vehicles have some built-in safety features or driver assisting technologies, which meet

SAE Level 1, such as adaptive cruise control, lane alignment, and crash avoidance, making Level 0 almost obsolete.

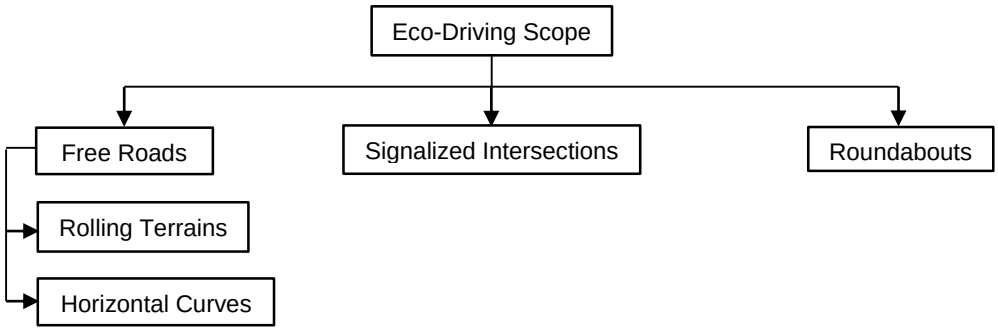

Figure 6: Eco-driving research scope.

Level	Name	Execution of steering and acceleration / deceleration	Monitoring of driving environment	Fallback performance of dynamic driving task	System capability (driving modes)
Human driver monitors the driving environment					
0	No Automation				n/a
1	Driver Assistance				Some driving modes
2	Partial Automation				Some driving modes
Automated driving system monitors the driving environment					
3	Conditional Automation				Some driving modes
4	High Automation				Some driving modes
5	Full Automation				All driving modes

Figure 7: Levels of driving automation for on-road vehicles (SAE, 2014).

1.3 Research Objectives

The main objective of this thesis is to develop intelligent vehicle control strategies for cooperative eco-driving in different road-traffic scenarios based on the research gap. The overall objectives of this thesis are as follows:

1. To study energy and environmental impacts from traditional traffic flow behaviour on road networks in various context and traffic scenarios.
2. To develop vehicle control strategy using advanced and intelligent control methods for fuel-efficient driving.

3. To develop machine learning techniques to predict traffic flow behaviour better.
4. To develop cooperative eco-driving system for better coordination of vehicles.
5. To evaluate the performance of the proposed system and its impact on overall traffic flow behaviour and environment.

1.4 Research Methodology

The work plan of this thesis consists of several interrelated tasks as given below:

- **Task 1: Develop traffic simulator**

  After studying the traditional traffic flow behaviour on road networks in various context and traffic scenarios, a traffic simulator is developed using MATLAB. The MATLAB platform facilities modeling of microscopic and macroscopic traffic flow behaviour, implementation of advanced vehicle control systems, and machine learning algorithms.

- **Task 2: Develop intelligent vehicle control strategies**

  Advanced and intelligent vehicle control methods, such as non-linear model predictive control (MPC), fuzzy-tuned MPC and receding horizon control systems are developed by computing real-time trajectory for fuel-efficient driving on road networks for different driving contexts.

- **Task 3: Develop machine learning techniques for better prediction**

  As traffic flow is susceptible to various disturbances /uncertainties and road-traffic conditions, hence, machine learning techniques, such as Bayesian Gaussian process and fuzzy inference algorithms are developed to predict stochastic nature of traffic flow behaviour for better control of vehicles.

- **Task 4: Develop cooperative eco-driving systems**

  In various scenarios of traffic flow on road networks, such as signalized intersections, hilly roads, curved roads, and roundabouts the

cooperative eco-driving systems are developed for better coordination of vehicles, which outperformed the existing eco-driving systems.

- **Task 5: Evaluate the performance of the proposed systems**

  The effectiveness of the proposed eco-driving systems are evaluated in various context and traffic scenarios on road networks using microscopic traffic simulation and compared with the existing driving systems. Also, the impact of overall traffic flow behaviour, fuel consumption, and environment are analysed.

1.5 Main Contributions

The main contributions of this thesis are as follows:

1. We have developed a traffic simulator that replicates real traffic scenarios and measures driving information, such as change of traffic signal, vehicle's position, velocity, and acceleration. This simulator can be used by others to evaluate various microscopic and macroscopic traffic flow behaviour in various context and traffic scenarios.
2. We have developed an event-driven eco-driving strategy (EDS) at signalized intersections by learning driving patterns, i.e., velocity profiles from vehicles self-driving data. Specifically, the main contribution of the EDS is the incorporation of machine learning technique with stochastic optimization. The developed method is very suitable for real-world traffic scenarios as the developed model is not deterministic; but rather it considers disturbances and uncertainties during the learning process.
3. We have developed a dynamic EDS based on fuzzy-tuned MPC that fully utilizes gravitational energy on a slopping road and significantly reduces fuel consumption and CO_2 emission, while ensuring a collision free traffic flow. Also, we have investigated the traffic flow performance in a dense traffic.

4. We have developed a dynamic EDS using MPC that substantially reduces fuel consumption and CO_2 emission of the vehicle on horizontal curves, while ensuring driving safety. We derived a method to accurately calculate road-curvature from the digital road map data.
5. We have developed an intelligent roundabout coordination system for eco-driving using receding horizon control approach. The system ensures safe and smooth traffic flow for various traffic demands.

Chapter 2

2 Literature Review

Technological advancements in sensors, electronics, control systems, artificial intelligence, and vehicular technologies have rapidly increased the capabilities of modern vehicles. In 1970, the automatic guidance and control of vehicles emphasized its importance for both traffic-related problems and accidents (Fenton, 1970). After few years later, the communication requirements in the longitudinal control of vehicles were investigated for allocation of control computation and associated trade-offs for maintaining an acceptable level of vehicle performance in automated transit systems (Pue, 1979). In the same year, the hierarchical controller functions in vehicle management for automated vehicle system and automated highway system (AHS) were proposed (Caudill et al., 1979). The goal of the AHS was to reduce traffic congestion, reduce energy consumption and emissions, and improve safety. In the 1980s, the concept of platooning of vehicles became a popular system-level approach to address traffic congestion, where vehicles in a platoon could accelerate, decelerate, and maintain high speed simultaneously. Later in 1991, the research on lateral and longitudinal control of vehicles was summarized (Shladover et al., 1991). The longitudinal control for a platoon of vehicles was proposed in 1993 without requiring the lead vehicle to communication with the following vehicles (Sheikholeslam & Desoer, 1993). The main features of automated intelligent vehicle-highway systems were extensively discussed by Varaiya (1993). The implementation of a platoon based integrated control system consisting of eight fully automated vehicles was reported in (Rajamani et al., 2000). Over the last decade several advanced driver assistance systems (ADAS) have been developed by researchers and manufacturers for eco-driving that provided significant improvement in vehicle control systems and adopted efficient driving

behaviour. The following subsections give literature review on vehicle control strategies for eco-driving at signalized intersections, hilly roads, horizontal curved roads, and roundabouts.

2.1 Vehicle Control Strategies at Signalized Intersections

When approaching a signalized intersection, the knowledge of traffic signal timing remains unavailable to the driver. Therefore, a sudden change in traffic signal forces the driver to perform aggressive braking to stop and remain idle for the entire red signal period; this causes a significant amount of fuel consumption and emissions (Li et al., 2009).

A number of studies on vehicle control systems at signalized intersections have been proposed in the literature. Early research focused on the development of dynamic and adaptive traffic signal controllers and control algorithms based on the information of vehicle queue lengths (Li et al., 2004; Nishuichi & Yoshii 2005; Cools et al., 2013) or the position and velocity information of connected vehicles (Priemer & Friedrich, 2009; Kamal et al., 2012). Nair and Cai (2007) developed a fuzzy logic controller for an isolated signalized intersection to control signal timings and phase sequence under both normal and exceptional traffic conditions. Some similar works developed fuzzy logic controller for signalized intersections (Shen et al., 2002; Murat & Gedizlioglu, 2005). But, it is very expensive to upgrade the design of traffic signal infrastructure (Maccubbin et al., 2008).

Some researchers developed *adaptive cruise control* (ACC) system with autonomous driving features, which could adapt to various traffic environments by accelerating or braking to control the velocity whilst maintaining proper gap between ACC vehicle and preceding vehicle (VanderWerf et al., 2002; Ioannou & Stefanovic, 2005; Kesting et al., 2008; Pananurak et al., 2009). The ACC system is an improved version of conventional cruise control systems, which were designed to maintain a certain desired speed, which were not flexible nor adaptive. The ACC vehicle

is equipped with a radar or infrared sensors to detect the velocity of the immediate preceding vehicle and adjust its velocity accordingly. If there is no preceding vehicle the ACC vehicle travels at its desired velocity. The concept of ACC system is shown in Figure 8, where prediction of the velocity trajectory of the preceding vehicle (blue) is in demand to obtain optimal velocity profile. An investigation showed that implementation of fuel optimal ACC system leads to fuel saving of about 15% in case of a FTP-like cycle. The main disadvantage of the ACC vehicle is that it can only predict the velocity trajectory of the preceding vehicle. The technological advancement in wireless communication further improved ACC systems with the integration of vehicle-to-vehicle (V2V) communication where the position, velocity, and acceleration information of any vehicle can be transmitted to other vehicles within the transmission range and called cooperative adaptive cruise control (CACC) systems (van Arem et al., 2006; Shaldover et al., 2009; Naus et al., 2010; Öncü et al., 2014). The schematic of CACC is shown in Figure 9, where it is necessary to determine the optimal velocity trajectory of the predecessor (orange vehicle). The precise traffic information is available via I2V communication.

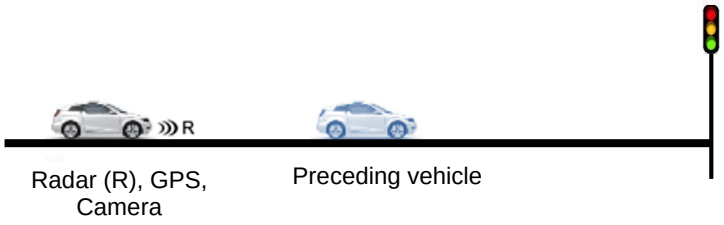

Figure 8: The first vehicle (grey) is equipped with ACC system.

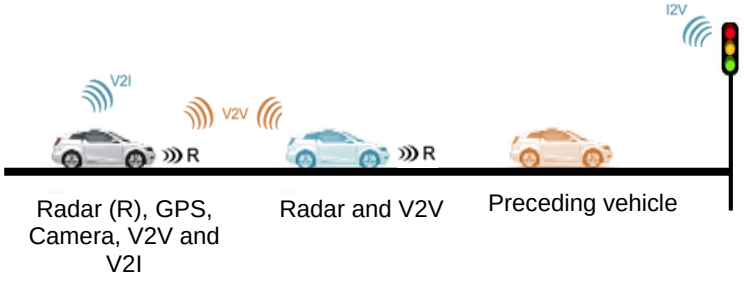

Figure 9: The first vehicle (grey) is equipped with CACC system.

Some researchers have proposed speed advisory systems (SAS) to reduce waiting time at the red signal, fuel consumption, and CO_2 emissions by utilizing traffic signal phase and timing (SPAT) information in advance (Mandava et al., 2009; Asadi & Vahidi, 2011; Kamal et al., 2015; Jiang et al., 2017). While these works have assumed that the signal phase and timing information is known accurately, it is difficult to obtain accurate SPAT information in practice because of timing drift in fixed time traffic lights. A probabilistic SPAT prediction approach has been proposed by combining historically averaged timing data with real-time traffic signal phase data (Mahler & Vahidi, 2014), where a deterministic dynamic programming (DDP) method was used to solve an optimal control problem; however, this is costly in terms of memory and CPU usage, and often is not feasible for real-time implementation. Some similar works on optimal velocity advisory algorithms for signalized intersections have been reported in (Morsink et al., 2008; Spyropoulou & Karlaftis, 2008), where the main focus was to develop in-car speed assistance systems to improve speed management for driving safety by helping drivers select a suitable speed.

Some approaches developed a cooperative vehicle intersection control (CVIC) system (Lee & Park, 2012), and a vehicle-intersection coordination scheme (VICS) (Kamal et al., 2015) for futuristic autonomous vehicles without using traffic lights under connected vehicles environment. As an alternative to traditional traffic control systems, some work proposed an approach of autonomous intersection management (AIM) based on reservation algorithms (Dresner & Stone 2008; Fortelle, 2010; Huang et al., 2012; Li et al., 2013). Zohdy and Rakha (2016) developed an intersection management system through vehicle connectivity that optimizes the movement of CACC vehicles. Some other studies proposed cooperative vehicle intersection schemes for the coordination of automated vehicles in an intersection based on optimization of the travel time (Li & Wang, 2006; Yan et al., 2009; Jin et al., 2012). Mirheli et al. (2018) proposed a signal-head-free intersection control system for connected and autonomous vehicles using dynamic programming to optimize

the intersection throughput. Other studies have utilized Model Predictive Control (MPC) for efficient vehicle control systems and manoeuvres to obtain sub-optimal trajectories with preceding vehicle information and changing traffic signals at intersections (Kamal et al., 2013; Makarem et al., 2013; Cao et al., 2015). A similar MPC approach is developed for the application in a hybrid vehicle (Yu et al., 2015). Nunzio et al. (2013) proposed a graph discretising method along with optimal velocity pruning algorithm for an electric vehicle, where the complete knowledge of SPAT in the network is considered in advance. Another research proposed an eco-driving strategy for connected electric vehicles at signalized intersection with queue movement prediction (Dong et al., 2000).

2.2 Vehicle Control Strategies on Hilly Roads

Various up and down slopes in a hilly road profile have significant impact on vehicle fuel consumption and GHG emissions. A study showed that emissions from three light-duty gasoline vehicles increased by 40–90% for CO_2, 60–110% for HC, 60–140% for CO, and 180–450% for NOx when road grades are higher than 5% compared to 0% grades (Zhang & Frey, 2006). Another study demonstrated that the vehicle fuel consumption and emission rates increase in excess of 9% for a 1% increase in road grade (Park & Rakha, 2006). Cicero-Fernández et al. (1997) reported an average increase of 3 g CO/mi and 0.04 g HC/mi with 1% increase in road grade.

Several studies have explored vehicle control strategies for eco-driving on hilly roads. Early research mainly suggested that fuel consumption is substantially minimized by running at constant velocity on constant road slopes. Specifically, the first attempt to minimize fuel consumption on hilly roads was to adjust the velocity on different road slopes using a feedback control system (Schwarzkopf & Leipnik, 1977). The optimal velocity was derived by combining the Pontryagin's maximum principle with a nonlinear vehicle model and a constant velocity turns out to be optimal for certain constant slopes. A similar study found the optimal velocity for conserving fuel,

when vehicles are traveling at a constant velocity within certain bounds on a constant road slope (Chang & Morlok, 2005). Saerens and Bulck (2013) developed an eco-driving control method for a point-mass vehicle using Pontryagin's maximum principle for a constant road slope. These methods are developed on the premise of constant road slopes and not applicable to real-world scenarios for hilly roads with varying slopes.

Another promising approach for hilly roads is dynamic programming (DP), provided that the information of entire driving cycle is available in advance. Hellstörm et al. (2009) proposed a look-ahead controller on-board to optimize the velocity trajectory of a diesel truck using future road topography information. They used dynamic programming (DP) method to solve an optimal control problem and showed a reduction of fuel consumption by approximately 3.5% without an increase in travel time. Kirschbaum et al. (2002) derived the fuel optimal control strategy using DP for the entire driving cycle when the vehicle speed is fixed. Luu et al. (2010) solved a DP-based optimal control problem considering variations in speed and road gradient to reduce fuel consumption of a light-duty vehicle. Likewise, another study proposed a fuel-optimized control problem for up and down slopes using local and global optimization, and showed fuel savings of about 5.5% (Wang et al., 2014). These DP-based approaches are useful to find the global optimum, but are not convenient for real-time implementation because requiring the information on the entire driving cycle before the trip is not feasible. Hu et al. (2016) proposed an optimal controller for a plug-in hybrid electric vehicle (PHEV) to minimize fuel consumption when traveling on rolling terrain or up-down slopes, whereas Li et al. (2016) experimentally developed a braking downshift controller to increase the energy efficiency of an EV during regenerative braking.

On the other hand, several implementable MPC-based frameworks are proposed for sloping roads. Kamal et al. (2011) developed an MPC framework for eco-driving considering road slope information, vehicle dynamics, and engine fuel consumption characteristics, whereas Kaku et al. (2013)

developed MPC for ecological vehicle synchronized driving with different aerodynamic drags and road shape information. Another work (Yu et al., 2015) developed MPC for hybrid vehicle eco-driving using traffic signal and road slope information. Although MPC is found effective to derive the optimal vehicle control input for eco-driving, it always tries to keep the speed of a vehicle close to the desired speed because the weights in the cost function are fixed. This fact typically implies that the controller tends to brake on the downslope to suppress increasing velocity due to gravity, and this braking action permits energy dissipation. Hence, these MPC-based methods may not be suitable for maximizing fuel economy on hilly roads.

2.3 Vehicle Control Strategies on Horizontal Curved Roads

When entering a horizontal curve, a driver usually slows down due to safety reasons, puts more effort to control the vehicle, and accelerates back to the initial velocity after crossing the middle of the curve. Such motions of the vehicle, deceleration, and then acceleration affect fuel consumption and emissions on a curved road. In particular, small radius of curvature seriously affects speed and acceleration of a vehicle, which results additional fuel consumption.

Existing research on horizontal curves mainly evaluated the impact of different curve features, such as curve length, degree of curvature, shoulder width, sight distance, superelevation rate, side-friction coefficient, and traffic volume on design speed and operating speed of vehicles using regression techniques to determine highway design standards for improving traffic safety (Fitzpatrick et al., 2000; Schurr et al., 2002; Misaghi & Hassan, 2005; Gong & Stamatiadis, 2008; Shallama & Ahmed, 2016; Wang et al., 2018; Cvitanić & Maljković, 2019). Other studies investigated driving behaviour in horizontal curves using naturalistic driving data to analyse traffic safety and the risk of crashes (Hamzeie, 2016; Machiani et al., 2016; Dhahir & Hassan, 2018). This is due to the fact that fatal crashes occur more frequently on horizontal curves than other types of road segments (Schneider et al., 2009; Chen et al., 2010;

Khan et al., 2013). Some other studies explored the effect of horizontal alignments on vehicle's fuel consumption and emissions (Kang et al., 2013; You, 2017; Llopis-Castelló et al., 2018).

On the other hand, very little research developed optimal control systems for eco-driving in horizontal curves. Zhang et al. (2013) developed a driver speed model for an adaptive cruise control (ACC) system for curved roads using recursive least-square (RLS) method. The speed control algorithm was based on individual driver's curve speed behaviour rather than ecological driving. Also, the model was only applicable when there was no preceding vehicle. Nissan launched an adaptive speed control system that warned a driver to reduce vehicle speed when approaching a curve using information of path radius ahead (Matsumoto et al., 2008). The target speed was determined based on the deviation of estimated total driver load and a reference total driver load, without considering ecological driving. Chang and Morlok (2005) used Lagrangian method to calculate the optimal velocity profile of a vehicle traveling on tangent or curved road. They concluded that fuel consumption will be minimum for a constant speed despite variations in road curvature and other conditions, which is not applicable in real-world scenarios. Similarly, Fröberg et al. (2006) showed that the fuel optimal approach is to drive at constant speed.

Gruppelaar et al. (2018) proposed a perceptually inspired driver model for speed control in curves. They used a binary classification method to capture speed adaptation of individual drivers for analysis of road geometry and for the development of driver support assistance devices. In (Ding & Jin, 2018), a dynamic programming (DP) algorithm is used to obtain the optimal speed profile for eco-driving in circular curves, and showed fuel savings of about 5.34% to 17.64%. While the DP-based solver yielded a global minimum, it is not suitable for real-time implementation because the information of entire driving cycle is required before the trip. Moreover, the studies above did not consider road-surface conditions for eco-driving on horizontal curves.

2.4 Vehicle Control Strategies at Roundabouts

A roundabout is a specific case of merging intersections or unsignalized roadways, where vehicles merge at low speed for safe interaction with other circulating vehicles, traverse the roundabout, and eventually exit to their desired directions. In general, the speed of approaching vehicles is dependent on the entry lane width, roundabout curvature, as well as the volume of both incoming and circulating traffic. Since an approaching vehicle requires an extra gap to enter the roundabout, increased traffic volume at the merging point can have a severe impact on the roundabout capacity. Consequently, the fuel consumption and the delay entering the roundabout can increase substantially.

In the literature, a number studies on vehicle control strategies at roundabouts have been reported. Early research mainly focused on the improvement of roundabout mobility and safety during rush hours using ramp metering with traffic signal control. In line with this expectation, a traffic signal control method was proposed to solve safety problems by eliminating conflict points and weaving sections at a multi-lane roundabout with different traffic flow rates (Yang et al., 2004). The authors introduced a second stop line for the left turn traffic on the circulating lanes. Zohdy and Rakha (2013) proposed a cooperative adaptive cruise control system to optimize velocity trajectories of vehicles when approaching a single lane roundabout using vehicle to infrastructure communication. The idea suggested was somewhat close to the design of single-lane entry ramps.

Hummer et al. (2014) developed a single-lane and a two-lane microscopic roundabout models to observe the effectiveness of metering signal with different traffic demand. The objective was to guide U.S. traffic signal designers on the use of metering signal. Gasulla et al. (2016) discussed the benefits of metering signals to mitigate operational problem at roundabouts with unbalanced flow, where the authors studied gap acceptance behaviour when the traffic demand reaches near the capacity. Another approach developed a multi-level traffic control (MTC) system that combines hybrid yield

control and fully actuated control at the large four-leg roundabouts to facilitate time varying vehicular demands automatically (Xu et al., 2016). Some other works reported environmental impacts at the roundabouts (Ahn et al., 2009; Gastaldi et al., 2014). A recent work proposed optimal coordination of Connected and Automated Vehicles at a two-lane roundabout (Zhao et al., 2017). The authors investigated the benefits on fuel consumption and travel time at different market penetration levels of CAVs, however they did not investigate different traffic demands on the roundabout capacity.

The work in the next few chapters will improve on these works and address the afore-mentioned gaps. Particularly, in the following chapters, we develop novel eco-driving strategies for signalized intersections, hilly roads, horizontal curved roads, and roundabouts, respectively.

Chapter 3

3 Eco-driving Strategy for Signalized Intersections

In a signalized intersection, injudicious driving reacting to sudden changes in traffic signal can lead to additional fuel consumption and increase of travel time. Existing eco-driving strategies for signalized intersections (Section 2.1) depend on connected and automated vehicle (CAV) technologies (at least partially), which provide cooperation between vehicles and infrastructure to improve intersection traffic flow. However, full autonomy of vehicles and proper infrastructure development for vehicle-to-vehicle (V2V) and infrastructure-to-vehicle (I2V) communications are not widespread currently. It is anticipated that full market penetration of CAV technologies are not feasible until 2060s (Alessandrini, 2015). Therefore, to improve driving scenarios in the existing signalized traffic environment, here we have developed a novel event-driven eco-driving strategy at the vicinity of a signalized intersection, by learning driving patterns, such as velocity profiles from vehicles self-driving data. Specifically, the main feature of our proposed eco-driving strategy is the incorporation of a machine learning technique with stochastic optimization of vehicle speed.

We use a traffic simulator that replicates real traffic scenarios, and measures driving information, such as signal events, vehicle's velocity, acceleration, and distance from the intersection. The driving data collected from the simulator are used to train a learning model known as a Bayesian Gaussian process, which is then used to predict the intersection crossing time and probability of crossing. From the crossing probability, and using a stochastic optimization algorithm, the optimal driving strategy for semi-autonomous mobility is developed without CAV technologies. The probabilistic Gaussian process modeling with Bayesian network allows flexibility as the parameters of the prediction nodes are not linked. The performance of the

proposed system is verified through microscopic traffic simulation to evaluate the improvement in fuel economy and travel time of vehicles compared to traditional driving. This work in this chapter has been published in the IEEE Transactions of Vehicular Technology, in (Bakibillah et al., 2019).

The rest of the chapter is organized as follows. In Section 3.1, at first we describe our real study area, the traffic flow modeling of conventional vehicles, and the effect of signal events on different trajectories of a vehicle. Then in Section 3.2, we discuss the driving data modeling by investigating the traffic flow behaviour at the signalized intersection. Secondly based on our findings, we develop a probabilistic Bayesian Gaussian process model in Section 3.3 and an eco-driving decision system in Section 3.4, and formulate an optimization framework in Section 3.5, which gives the minimum fuel. In Section 3.6 we illustrate the simulation results, and finally, Section 3.7 provides the summary of the chapter.

3.1 Background and Motivation

In this work, we use a typical model of moderate and non-congested traffic flow to mimic the driving behaviour of vehicles on an urban road when the vehicles are approaching the signalized intersection. We consider single lane traffic for simplicity, and therefore, lane changing and overtaking manoeuvres are not considered. However, we consider disturbances caused by merging, turning and crossing of vehicles from/to the link roads connected along the road. The durations of green (and yellow) and red signals are harmonized according to a real traffic scenario such that vehicles are able to cross the intersection from a certain distance within one traffic cycle. The vehicle environment is conventional, i.e., no V2V or I2V communication is considered in the vicinity of the signalized intersection.

To assess the performance of the proposed eco-driving system (EDS), a real road section (Jalan Subang 3 in Subang Jaya, Malaysia, which fits well into our chosen traffic flow model) connected to a T-intersection is chosen for

study as shown in Figure 10. The road section is a single-lane road located in an industrial area with moderate non-congested traffic flow at most times of a day. The traffic lights are visible to vehicles from a distance of 500 m. From multiple observations, it is found that the traffic flow is susceptible to sudden interventions by trucks/cars on both sides of the road and from the opposite directions (as shown in Figure 11); these random events sometimes force the vehicle to slow down, i.e., the velocity of the vehicle is affected. As a result, there is always some uncertainty in the projected arrival time at the intersection. Several other intersections in this area (e.g., Jalan Subang 5) also show similar traffic flow patterns. In these intersections, the duration of green signals and a short yellow signal for different approaches is between 20 sec to 30 sec.

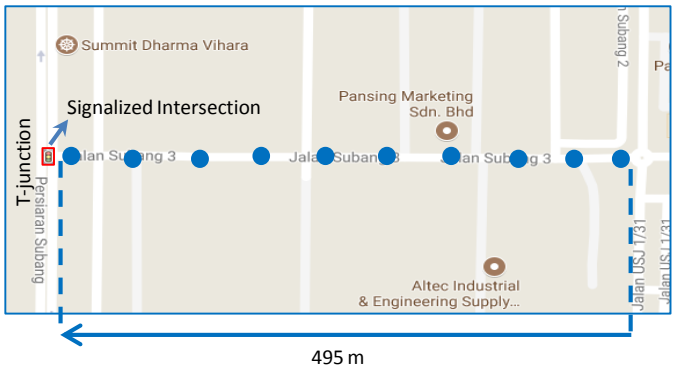

Figure 10: The study area which is a single lane road section consisting of one signalized intersection in Subang Jaya, Malaysia.

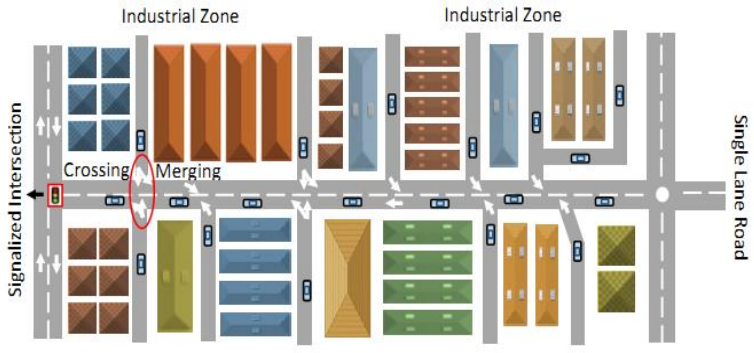

Figure 11: Traffic flow scenario in the test road located in an industrial area in Subang Jaya, Malaysia.

Our past self-driving experience in this route is utilized to realize similar traffic simulations (using a microscopic traffic simulator) and to develop a Bayesian learning model from simulated self-driving data. The model can dynamically suggest optimum speed profiles to drivers considering the current driving status, e.g., position, velocity, and the changing condition of the signal from visible distances.

3.1.1 Traffic Flow Modeling

This section presents the mathematical formulation of traffic flow modeling for traditional vehicles. A microscopic traffic model (Treiber et al., 2000) with discrete-time framework is considered for our traffic simulator, which includes the vehicles, the traffic lights, and the road section at which the vehicles travel. Generally, microscopic traffic models express acceleration and deceleration of each vehicle as a function of velocity of the preceding vehicle, speed difference, and safe headway (or distance) between vehicles (Nagel et al., 2003). Car-following models are used to infer driving behaviour at signalized intersections (Liebner et al., 2012). In the car-following process, only the longitudinal motion dynamics of vehicles are considered on an urban road segment with one signalized intersection and are expressed in a discrete-time framework indexed by *t* as

$$x_i(t+1) = x_i(t) + v_i(t)\Delta t + 0.5u_i(t)\Delta t^2, \qquad v_i(t+1) = v_i(t) + u_i(t)\Delta t, \tag{3.1}$$

where x_i, v_i, and u_i are the position, velocity, and acceleration of vehicle i, respectively, and Δt is the step size. The dynamic behaviour of vehicles depends on input acceleration u_i in (3.1), which is calculated according to a microscopic car-following model called the Intelligent Driver Model (IDM) that mimics human driving behaviour (Treiber et al., 2000) and it is a well-accepted model for single-lane traffic flow. The instantaneous acceleration $u_i(t)$ of vehicle i with its preceding vehicle i-1 is calculated as

$$u_i(t) = a\left[1 - \left(\frac{v_i(t)}{v_d}\right)^4 - \left(\frac{s^*\left(v_i(t), \Delta v_i(t)\right)}{\Delta x_i(t)}\right)^2\right],$$
$$s^*(v_i(t), \Delta v_i(t)) = s_0 + v_i(t)t_{hd}^* + \frac{v_i\,\Delta v_i}{2\sqrt{ab}}, \tag{3.2}$$

where the model parameters v_d, s_0, t_{hd}^*, α and b denote the desired velocity, minimum spacing from the preceding vehicle, safe headway time, maximum acceleration, and comfortable deceleration, respectively, and $\Delta x_i = x_i - x_{i-1}$ and $\Delta v_i = v_i - v_{i-1}$ are the space gap and velocity difference, respectively. In the case when the signal is red, it is assumed that a virtual vehicle is idling at the intersection, i.e., $v_{i-1} = 0$ and $x_{i-1} = x_{\mathrm{J}}$, where x_{J} is the position of the intersection stop bar in absolute coordinate system. The driving behaviour described above is termed as the Traditional Driving System (TDS).

3.1.2 Investigation of the Signal Events

Next, we investigate two possible scenarios of a vehicle, termed as the *host vehicle*, during the green and red signal events. In the first scenario, **Event A**, the host vehicle under the TDS enters the “visible signal zone” at a velocity v_1 and observes a change in traffic signal from red to green at a distance $d_1 = x_{\mathrm{J}} - x_1$, from the intersection, where x_{J} and x_1 are the positions of the intersection and the host vehicle, respectively. In this case, two trajectories of the vehicle are possible (Figure 12); firstly the signal stays green and the host vehicle crosses the intersection smoothly at cruising speed, and secondly the signal turns from green to yellow and if the host vehicle is very close to the intersection, it accelerates harshly to attempt crossing the intersection before the end of yellow but the signal turns red instead. Therefore, the vehicle performs aggressive braking to stop and remains idle for the entire duration of the red signal.

In the second scenario, **Event B**, the host vehicle under the TDS enters the “visible signal zone” and observes the signal changing from green to yellow and then red. It then decelerates to stop at the intersection, since it cannot

pass the intersection within the green-yellow signal (Figure 13). It is not possible to cross the intersection smoothly due to the long red signal period. In both events, when driving under the TDS, fuel consumption and travel time may increase as the information of signal timing and surrounding traffic are unknown (Li et al., 2009; Sivak, 2013). However, it is possible to improve driving performance under this situation if signal patterns and its influence can be learned or estimated, and share the information to the cloud/centralized controller for cooperation with other vehicles. Specifically, if a model is developed and trained using past driving data of the vehicle, it is possible to predict future driving patterns well in advance to improve fuel economy and travel time of the host vehicle as well as other traditional connected vehicles ensuring cooperative eco-driving within the analysis boundary.

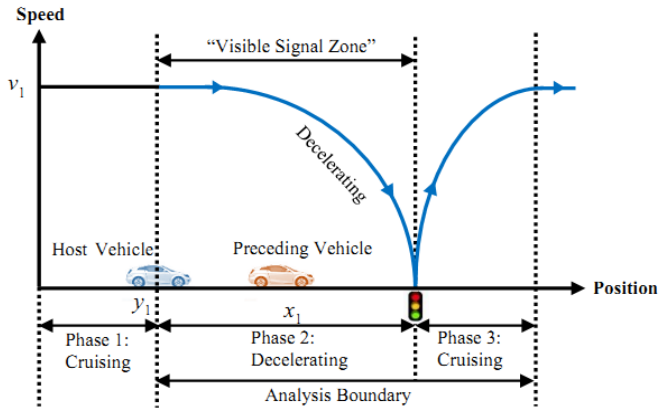

Figure 12: Vehicle under the TDS when approaching the green signal.

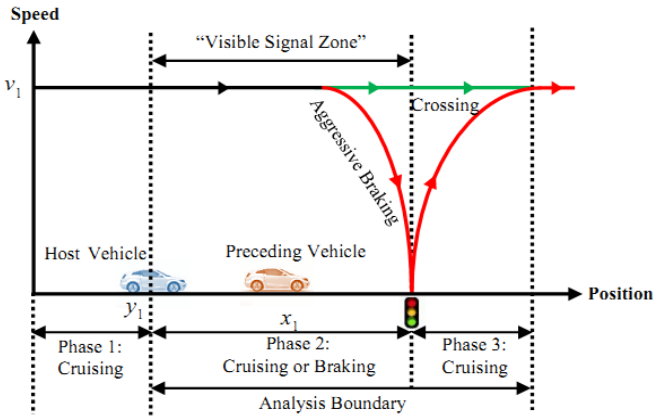

Figure 13: Vehicle under the TDS when approaching the red signal.

3.2 Driving Data Modeling

Firstly we investigate the traffic flow behaviour and identify the important factors influencing the crossing time (time takes to cross the intersection) of a vehicle from multiple observations of each event. In particular, at observation n the following information is recorded:

- Time at occurrence of an event, t_{en} and time at crossing of the intersection, t_{cn}
- Types of Event, $\delta_n(t_{en}) = \{0, 1\}$, where $\delta_n(t_{en}) = 1$ denotes signal switching from red to green and $\delta_n(t_{en}) = 0$ denotes signal switching from green (to yellow and then) to red
- Velocity, $v_n(t_{en}) \in \mathbb{R}^+$(real number space)
- Distance to the intersection, $d_n(t_{en}) \in \mathbb{R}^+$

It is noticed that when $\delta_n(t_{en}) = 1$, a fast-moving vehicle near the intersection is more likely to cross without stopping. However, if the vehicle is far from the intersection, then in the most cases it fails to cross and brakes aggressively to stop for the red signal. On the contrary, when $\delta_n(t_{en}) = 0$, a vehicle may or may not cross the intersection depending on the velocity and distance from the intersection; however, the possibility of crossing is very low and the vehicle will most likely have to decelerate to stop and wait until the red signal period ends. Therefore, $\delta_n(t_{en})$, $v_n(t_{en})$, and $d_n(t_{en})$ are the predictor variables that influence the crossing time of each vehicle, i.e., $\tau_n = t_{cn} - t_{en}$. Furthermore, as explained in Section 3.2, it is found that due to disturbances and different traffic flow patterns, the crossing time is subject to some uncertainty. Due to such stochastic nature of the crossing time, we consider a probabilistic model (instead of a deterministic model) to capture the uncertainty. Although we utilize past driving data of a vehicle on a single intersection only, in the near future, this method can be used for multiple intersections easily by retrieving traffic data of multiple intersections from cloud-based systems.

3.3 Bayesian Gaussian Process Model

The Bayesian Network (BN) is a method to solve inference problems with probability theory and has been widely used in modelling uncertain knowledge and building the probabilistic model from a set of data (Koller & Friedman, 2009). BN gives a graphical model representation of probabilistic relation between a set of variables and their conditional dependencies. We seek to predict the crossing time t_{cross} of an intersection based on signal event, vehicle velocity, and distance from the intersection. Hence, the Bayesian treatment of linear Conditional Gaussian models (CG) is used to determine conditional distribution of the response variable given the inputs. To do that, the host vehicle is selected and a simulation is performed to obtain the training dataset $D = \{(f_n, \tau_n) \mid n = 1,2, \dots \dots \dots N\}$, where $f_n = \{d_n, v_n, \delta_n(t_{en})\} \in \mathbb{R}^3$ denotes an input vector and $\tau_n \in \mathbb{R}$ denotes an output vector, which is the response variable, i.e., the crossing time of the intersection considering the effects of disturbances and uncertainties in traffic flow. It is important to note that τ_n is the intersection crossing time of the host vehicle obtained during data collection and is used to train the Bayesian learning model, whereas t_{cross} is the predicted crossing time of the intersection when the trained model receives new inputs. Next, a kernel-based probabilistic model called Gaussian Process Regression (GPR) model f_{GPR} is defined to fit the training dataset into the model. The GPR model is chosen because it predicts better than the parametric models and overcomes the problems of overfitting and underfitting. The output of f_{GPR} is a multivariate Gaussian with mean μ_n and covariance matrix Σ_n such as $\begin{bmatrix} f_n \\ \tau_n \end{bmatrix} \sim N\left(\begin{bmatrix} \mu_{fn} \\ \mu_{\tau n} \end{bmatrix}, \begin{bmatrix} \Sigma_{fnfn} & \Sigma_{fn\tau_n} \\ \Sigma_{\tau_n f_n} & \Sigma_{\tau_n \tau_n} \end{bmatrix}\right)$, where $\mu_n = [\mu_{fn}, \mu_{\tau n}]^{\mathrm{T}} \in \mathbb{R}^4$ denote the mean of input variables and response variable, and the covariance matrix $\Sigma_n = \Sigma(f_n, \tau_n)$ indicates a measure of the similarity of f_n and τ_n. The elements of the covariance matrix is determined using squared-exponential kernel function. Then, the conditional probability distribution is given as

$$P(\tau_n|\, f_n, \delta_n(t_{en}) = j) = \left|2\pi\Sigma_{nj}\right|^{-\frac{1}{2}} e^{\left\{\left(-\frac{1}{2}\right)\left(\tau_n-\mu_{\tau_{nj}}\right)^T \Sigma_{nj}{}^{-1}\left(\tau_n-\mu_{\tau_{nj}}\right)\right\}}, \quad (3.3)$$

where $P(\tau_n)$ is continuous-valued distribution conditioned on continuous-valued input variables d_n, v_n, and discrete-valued variable $\delta_n(t_{en})$. $|\Sigma_{nj}|$ denotes the determinant of Σ_{nj}. Then, the trained model f_{GPR} uses the new input vector $f_{new} = (d_{new}, v_{new}, \delta_{new})$ to predict the value of response variable t_{cross}, as shown in Figure 14, where the circles and the rectangle are used to differentiate inputs in continuous and binary values. The conditional probability of t_{cross} is given by

$$P(t_{cross}|\tau_n, f_n, f_{new}) = \frac{P(t_{cross}, \tau_n|f_n, f_{new})}{P(\tau_n|f_n, f_{new})}. \quad (3.4)$$

where the term in the numerator is called *joint probability distribution* and the term in the denominator is called *normalizing constant* or *marginal likelihood*. Once the crossing time distribution t_{cross} is predicted from the model $f_{GPR}(d_{new}, v_{new}, \delta_{new})$, we obtain the mean μ_{cross} and covariance matrix Σ_{cross}, i.e., $t_{cross} \sim N(\mu_{cross,} \Sigma_{cross})$. Then, the standard deviation σ_{cross} is obtained from the covariance matrix and the probability P_{cross} of a vehicle crossing the intersection for any arbitrary time is calculated using the Gaussian cumulative distribution function given as

$$\begin{aligned} P_{cross} &= P(t_{cross} \le t_r), \\ \Rightarrow\ P_{cross} &= P\left(Z_r \le \frac{t_r - \mu_{cross}}{\sigma_{cross}}\right), \end{aligned} \quad (3.5)$$

where t_r is the red signal timing and Z_r follows the standard normal distribution. The failure probability of crossing P_{fail} is the complement of P_{cross}.

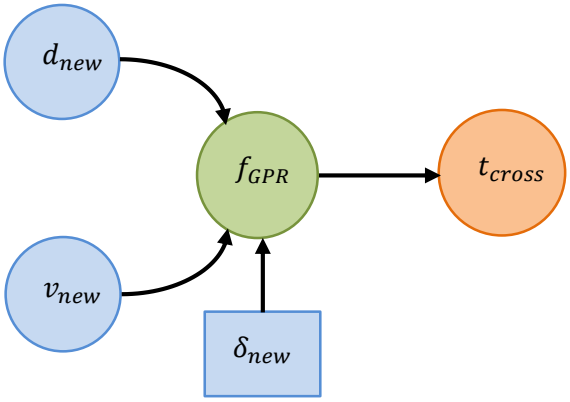

Figure 14: Bayesian network representation of Conditional Gaussian model.

3.4 Eco-Driving Decision System

Based on P_{cross}, which is the probability of the host vehicle crossing the intersection, we develop an EDS that provides a dynamic decision for optimal velocity to the vehicle when it is in the "decision zone" from where it can observe a change in the signal event and adjust its speed accordingly. We investigate both events A and B using the proposed EDS.

In **Event A**, there are three possible optimal trajectories as shown in Figure 15. Depending on P_{cross}, the EDS can suggest either to maintain constant cruising speed through the intersection or to increase acceleration appropriately in order to have higher probability of crossing the intersection without stopping. However, in both cases, there is still the probability of failing (to cross) and aggressive braking may occur if sudden disturbance occurs. Moreover, a vehicle fails to cross the intersection when the movement of the preceding vehicle prevents the host vehicle from reaching its recommended speed at some time instant. We estimate the crossing time distribution and the mean crossing time t_p of the preceding vehicle from the model. It is assumed that if the preceding vehicle is able to cross the intersection then it will continue at the current speed until $x_J + d$. Otherwise, the vehicle will stop at the intersection at a constant braking, idle, and manoeuvre again at a constant acceleration until $x_J + d$. Thus, the crossing time of the host vehicle will then

increase and is given by $t_h = (x_\mathrm{I} - x_p)/(v_p + t_\mathrm{s})$, where x_p and v_p are the position and velocity of the preceding vehicle, respectively, and the factor t_s is the saturation flow time gap at the intersection. The saturation flow time gap implies the safe car-following headway in seconds between vehicles in a dense flow of traffic for a specific intersection lane group and it is a direct function of vehicle speed and separation distance. The vehicle can increase its velocity up to $v_\mathrm{max} = (x_\mathrm{I} - x_h)/t_h$, where x_h is the position of the host vehicle. In exceptional cases, a vehicle can cruise at a lower velocity if the probability of crossing the intersection (at lower velocity) is still relatively high. In contrast, if the probability of crossing the intersection is very low, a vehicle can slow down smoothly to reduce idling time at the intersection.

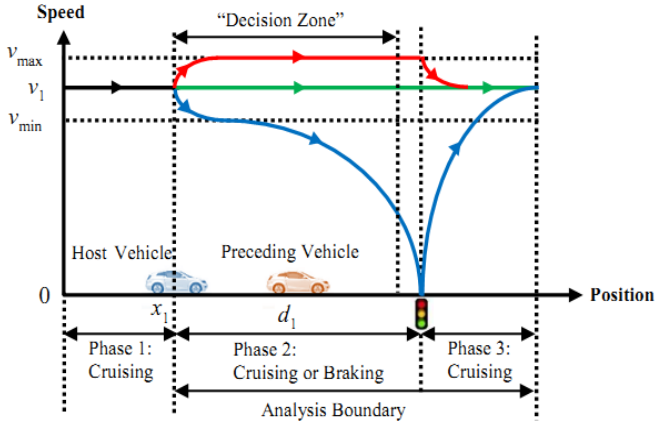

Figure 15: Vehicle under the EDS when approaching the green signal.

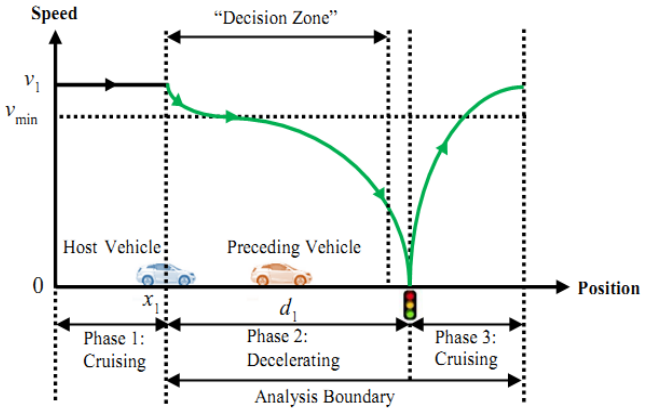

Figure 16: Vehicle under the EDS when approaching the red signal.

In **Event B**, when the vehicle is approaching the intersection, the EDS suggests the vehicle to slow down early to the minimum desired velocity and approach the intersection. The optimal trajectory profile is shown in Figure 16.

3.5 Formulation of Optimization Problem

Recall that the car-following model described in (3.2) where the parameter v_d denotes the desired speed of vehicle i. The EDS of the host vehicle can be implemented using the same car-following model (3.2) by tuning the desired speed v_d termed as the *set speed*. In the EDS, v_d needs to be optimized subject to the occurrence of the event by minimizing a performance index. This simplifies the optimization, as only one control variable needs to be determined. However, instead of changing v_d directly, we choose it to be a function of another variable v_δ and time, and the actual v_d is tuned gradually with time.

For a better explanation, let the actual set speed be represented by $v_d\ (t, v_\delta)$. At first we define a deterministic performance index J to optimize the set speed v_δ of the host vehicle at any event as

$$J(v_\delta) = \sum_{t-t_{en}}^{T_f} \left[f_v\big(v_i(v_\delta), u_i(v_\delta)\big) w_1 + (v_d\ (t, v_\delta) - v_{\mathrm{R}})^2 w_2 \right], \tag{3.6}$$

where t is the discrete time with step size Δt, t_{en} is the time when a change in signal is observed, T_f is the time to travel up to a distance d after the intersection located at x_{J}, f_v denotes the fuel consumption rate, whilst v_δ and v_{R} represent the desired velocity and reference velocity, respectively, and w_1 and w_2 denote weighting factors. The first term of the performance index J represents cost due to fuel consumption per second (ml/sec) and the second term is the cost due to deviation from a reference speed. The weighting factors w_1 and w_2 are tuned manually, such that the host vehicle can drive at reasonably high speed without affecting other traffic when it is far from the intersection. At the same time fuel consumption is also optimized.

Instantaneous speed and acceleration are two major dynamic factors that contribute to the fuel consumption rate of a vehicle. Using the instantaneous acceleration and velocity, fuel consumption rate f_v (in ml/s) is estimated as (Kamal et al., 2011)

$$f_v(v_i, u_i) = b_0 + b_1 v_i + b_2 {v_i}^2 + b_3 {v_i}^3 + \bar{u}_i(c_0 + c_1 v_i + c_2 {v_i}^2), \qquad (3.7)$$

where $b_0, b_1, b_2, b_3, c_0, c_1,$ and c_2 are the consumption parameters, which are known for a particular vehicle, whilst $\bar{u}_i$ is the positive acceleration and given by

$$\bar{u}_i = \begin{cases} u_i + g \sin\theta, & if\ u_i + g \sin\theta \geq 0, \\ 0, & otherwise. \end{cases} \qquad (3.8)$$

where g denotes the gravitational force and θ is the road slope angle, which can be obtained from the digital road-map. In our case, the experimental test-bed is a flat road ($\theta = 0$) and therefore, $g \sin\theta = 0$.

The goal is to optimize the performance index J (at the occurrence of an event) by choosing the optimal value of v_δ, which is constrained by $v_{\min} \leq v_\delta \leq v_{max}$, where $v_{\min} = 30$ km/h and $v_{max} = 60$ km/h. To simplify the optimization process we choose the optimal set v_δ^* from a pre-specified set of possible solutions such that $v_\delta^*(t) \in \{v_k\} = \{v_{\min} + k\Delta v\}$ where $k = 0,1,2, \ldots, K$ with $K = (v_{max} - v_{\min})/\Delta v$ and $\Delta v = 0.1$ km/h increment step. For each set velocity v_k the trajectory of the host vehicle is calculated using (3.1) and (3.2) in the horizon t_{en} to T_f considering small time step and assuming a preceding vehicle, if any, running at a steady speed. The corresponding v_i and u_i of each time step in the entire horizon is obtained, which are used to determine the performance index (3.6). Therefore, $K + 1$ possible values of the performance index J_k are obtained from the given set of possible solution. The value of v_k that yields the minimum J_k is taken as the optimal solution.

In the event of change in signal, the optimal speed is decided through optimization. Based on that speed, the host vehicle decides its acceleration

using IDM, which includes acceptable limits of acceleration. If a speed-up recommendation is given, the vehicle will not produce acceleration higher than the parameter a in (3.2). On the other hand, sudden drops in the desired velocity v_d in (3.2) can cause very large deceleration. Therefore, the slowdown recommendation is gradually implemented in the simulation by tuning v_d for any given v_δ in the horizon as

$$v_d\,(t, v_\delta) = \begin{cases} v_\delta, & if\ v_\delta \geq v_d(t-1), \\ \lambda v_d(t-1) + (1-\lambda)v_\delta, & otherwise. \end{cases} \tag{3.9}$$

where $\lambda < 1$ is the multiplication factor. Once the vehicle crosses the intersection, its desired velocity is reset to v_{R}. In the prediction horizon, once the vehicle is near the intersection, the possible signal status, e.g., red or green-yellow signal, is considered based on the learned behaviour. In the case of the red signal, the vehicle stops at the line (or behind the preceding vehicle), and once the signal becomes green it speeds up again.

Recall that there is always some uncertainty in the intersection crossing time due to disturbances and different traffic flow patterns. For each possible value of v_k, a vehicle may cross the intersection before the red signal, or fail to cross with some probability as obtained by the Gaussian regression model. Two possible trajectories of the vehicle obviously provide different values of the performance index J_k, namely, J_k^{cross} and J_k^{fail}, considering crossing and failing probabilities, respectively. An illustration of some velocity trajectories with crossing and failing probabilities is shown in Figure 17, where the "critical zone" is the distance that the vehicle may travel to cross the intersection during the yellow signal period. Therefore, we propose that the optimal solution should be decided based on the expected value of the performance index $E(J_k)$ considering the probability of crossing the intersection. Hence, the expected value $\bar{J}_k$ of performance index J_k in a stochastic manner is given as

$$\bar{J}_k = E(J_k) = \left(P_{cross}(v_k).J_k^{cross} + P_{fail}(v_k).J_k^{fail}\right). \tag{3.10}$$

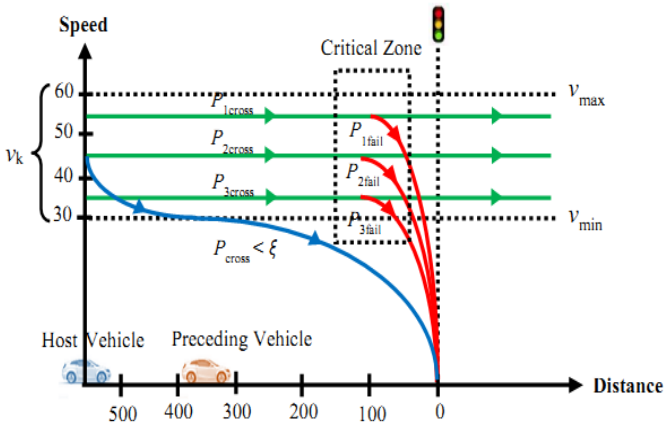

Figure 17: Recommended velocity trajectories of a vehicle when approaching the signalized intersection.

Note that the consideration of the crossing time of the preceding vehicle still remains an important factor, which is determined from the Bayesian learning model described earlier. In some cases or events, the probability of crossing, or failing before the red signal remains zero and the performance index (3.10) becomes the same as (3.6). In this way, we solve the optimization problem in a bi-level framework, i.e., the optimal decision is calculated in two-steps. In the first step, we consider all possible recommended velocities and obtain the corresponding performance index values and crossing probability. In the next step, we calculate the expected value of the performance index considering the probability of crossing the intersection using (3.10). Thus, at the occurrence of an event the optimal set speed of the host vehicle is obtained stochastically and used in the EDS to execute it as a speed advisory system (SAS). We summarize the overall procedure of the proposed EDS in Algorithm 1. Note that F_k^{cross} and F_k^{fail} gives the performance index related to the fuel consumption.

Algorithm 1: Proposed Eco-driving System (EDS)

---

1) Initialize $v_{\delta 0}^{*} = v_{\min}, v_{\max}, \Delta v$, and $K \coloneqq 0$
2) Set event δ_n at $t_{en} = t$
3) Measure $x_i(t_{en}), v_i(t_{en})$, and $\delta_n(t_{en})$

4) Estimate t_p from f_{GPR} having x_p and v_p

5) Predict $t_{cross} \sim N(\mu_{cross,}\, \Sigma_{cross})$ from f_{GPR}

6) Calculate $K = (v_{\max} - v_{\min})/\Delta v$

7) Loop 1:

   $k = 1 : K$

   Set $F_k^{cross} := 0, F_k^{fail} := 0$, and $t := 0$

8) Loop 2:

   Calculate $u_i(t)$ using (3.2) and

   Update states $x_i(t+1)$ and $v_i(t+1)$ using (3.1)

   If $x_i(t-1) > x_J$ and $x_i(t) > x_J$ then $t_{cross,\kappa} = t$

   Compute $F_k^{cross} = F_k^{cross} + f_v\big(v_i(t, v_\delta), u_i(t, v_\delta)\big)\,\Delta t$

   Set $t := t + 1$

   If $x_i(t) \leq (x_J + d)$ continue loop 2

   End loop 2

9) $t := 0$

10) Loop 3:

    Calculate estimated green-yellow and red signal time

    $(t_g \;\&\; t_r)$

    Calculate $u_i(t)$ and update states $x_i(t+1)$ and $v_i(t+1)$

    using (3.1)

    Compute $F_k^{fail} = F_k^{fail} + f_v\big(v_i(t, v_\delta), u_i(t, v_\delta)\big)\,\Delta t$

    Set $t := t + 1$

    End loop 3 if $x_i(t) > (x_J + d)$

11) Compute $\bar{J}_k(v_\delta^*)$

    Calculate $v_{k+1} = v_{\min} + k\Delta v$

    End loop 1

12) Find k for minimum $\bar{J}_k$ and set desired speed v_δ^*

    End

3.6 Simulation Results and Discussion

To implement the proposed EDS on a real-world traffic scenario with a signalized intersection, we have used a traffic simulator built in MATLAB. In order to obtain realistic traffic flows, the arrival of cars in the simulator is determined randomly using a probability distribution. The parameters of the car-following models are also randomly chosen from a pre-specified distribution. The traffic light is implemented with a fixed cycle and splits, where the last 3 sec of the green period is replaced by the yellow signal, i.e., actual durations of green and yellow signal are 27 sec and 3 sec, respectively, and a 2 sec all-red period is introduced before starting a green signal on the other approach. In the simulator, each vehicle follows the signal, and if necessary, brakes at yellow signal or passes through the intersection when the vehicle is already close to it. However, in taking the decision in advance, the yellow signal is simply treated as part of the green signal (since vehicles are allowed to cross during yellow signal). Then, the driving performance of the EDS is evaluated using microscopic traffic simulations.

The selected road (Jalan Subang 3) has a single lane with total length of 1.5 km and the intersection is located at 1.0 km. In order to evaluate fuel consumption and travel time, the analysis boundary of the road section is set to 500 m before and 100 m after the intersection. The EDS of the host vehicle gives the optimal driving decision when the host vehicle observes the event at a distance between 100 m and 500 m and velocity of 20 km/h to 65 km/h. The lower bound of distance from the intersection is set to 100 m so that the vehicle can adjust its driving strategy. In the simulation, all vehicles are assumed to be of the same size and length. The green-yellow and red traffic signal durations are set as $\beta_1 = 30$ sec (i.e., 27 sec green and 3 sec yellow), $\beta_2 = 60$ sec, respectively, and the traffic flow rate is considered to be moderate and non-congested. The parameters of the IDM are set as $v_d = 40 - 60$ km/h, $s_0 = 2$ m, $T = 1.0 - 2.2$ sec, $a = 1.5$ m/sec^2, and $b = 2.5$ m/sec^2. The acceleration and braking of the preceding vehicle are considered as 2 m/sec^2 and -2 m/sec^2,

respectively. The saturation flow gap time is considered 2 sec. The simulation is run in a discrete time framework with step size of $\Delta t = 0.5$. To predict all possible cases of traffic flow, the range of input variables x_{new} and v_{new} are taken as 0 m to 550 m and 25 km/h to 65 km/h, respectively. The fuel consumption parameters are $b_0 = 0.1569$, $b_1 = 2.450 \times 10^{-2}$, $b_2 = -7.415 \times 10^{-4}$, $b_3 = 5.975 \times 10^{-5}$, $c_0 = 0.07224$, $c_1 = 9.681 \times 10^{-2}$ and $c_3 = 1.075 \times 10^{-3}$ as calibrated for a typical car.

3.6.1 Learning Outcome

Firstly, we collect the data from driving on the test road. Then the Bayesian network is formed off-line using data samples for estimating the probability of a vehicle crossing the intersection when an event occurs. The intersection crossing time τ_n of the host vehicle is normalized with respect to green-yellow and red signal durations for simplicity, i.e., if $\delta_n(t_{en}) = 1$, then $\bar{\tau}_n = (\tau_n - \beta_1)/\beta_1$ and if $\delta_n(t_{en}) = 0$, then $\bar{\tau}_n = (\tau_n - \beta_2)/\beta_2$. The model is tuned each time with new data. During data collection we find that in the most cases the host vehicle has a moderate speed, e.g., around 40 km/h when an event is observed. In such cases, we train the model in 1-D using 30 data samples to estimate the crossing time of the intersection. However, such 1-D approximation is not sufficient when the speed variation of the host vehicle is large because the crossing time significantly varies with respect to both speed and distance. In this case, we train the model in 2-D using 170 data samples to attain better approximation of the crossing time. Note that the performance of the model remains consistent when we train it with increased data samples. After training the network, we tested the results (the mean crossing time in a normalized value) in both 1-D (with 95% confidence interval) and 2-D input spaces as shown in Figure 18(a) and (b), respectively. Here we show the learning outcomes of Bayesian optimization for **Event A** only due to some

uncertainty of crossing the intersection. In **Event B** the vehicle always has to stop at the intersection.

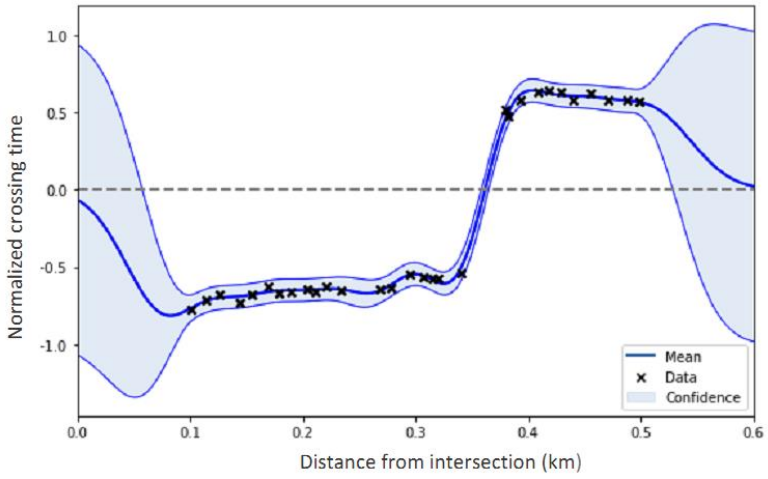

(a)

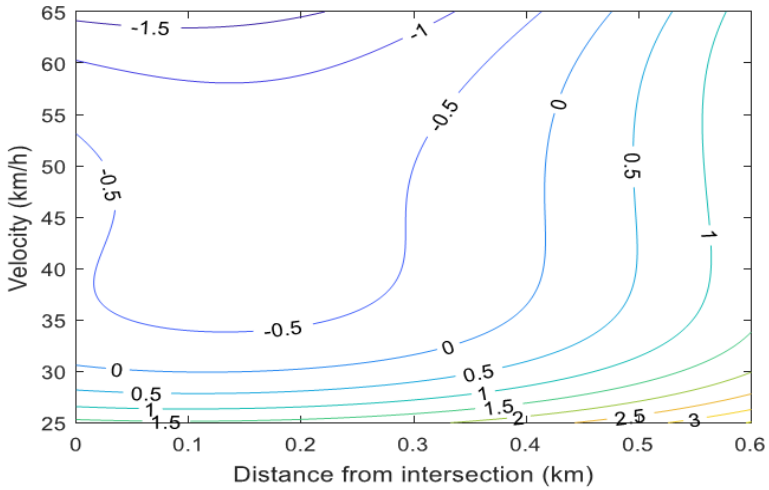

(b)

Figure 18: The normalized crossing time of the host vehicle when **Event A** occurs (a) 1-D plot and (b) 2-D contour plot.

When $\bar{\tau}_n = 0$, it means the crossing time is 30 sec (i.e., critical to cross the intersection), which is equal to the duration of green-yellow signal. When $\bar{\tau}_n = 1$, the crossing time is 60 sec. The normalized output (crossing time) of Bayesian network is transformed into the original scale after the learning process. The model is then used on-line to obtain the recommended velocity for the host vehicle.

3.6.2 Performance Evaluation

Secondly, the performance of the proposed EDS based on the Bayesian model is evaluated and compared with the TDS in a free flow traffic scenario. The distance-velocity, distance-fuel, and distance-time plots for green and red traffic events are shown in Figure 19. In Figure 19(a), the vehicle observes a change from red to green signal at about 450 m away from the intersection. In TDS, the vehicle maintains constant cruising speed at its initial velocity of 50 km/h and has to perform aggressive braking near the intersection due to a change to the red signal and idles for the entire red period before crossing the intersection. In the proposed EDS, the vehicle is recommended to increase its velocity to about 60 km/h; this maximizes the expected value of performance index (to have higher probability of crossing the intersection); it then speeds up and manages to cross the intersection before the red signal starts. This manoeuvre significantly reduces the cumulative fuel consumption and travel time. On the other hand, if the vehicle currently has a maximum speed meeting the speed limit and the probability of crossing the intersection is low, then it will be recommended to slow down early to the optimum velocity. In Figure 19(b), the vehicle comprehends a switch to red signal at about 450 m away from the intersection. In the TDS, the vehicle decelerates following the IDM and stops at the intersection; it reaches the intersection early and waits for the rest of the period before crossing the intersection again. However, for the proposed EDS, the vehicle is recommended to decelerate early to minimum velocity of 30 km/h to avoid lengthy idling period at the intersection. Thus, the cumulative fuel savings of the EDS vehicle outperforms the TDS vehicle though travel time of both vehicles is similar due to long red signal period.

Finally, the performance of the EDS and the TDS are compared in dense but under saturated traffic flow. A total of 200 trials are conducted to observe traffic flow behaviour with the aforementioned parameters and traffic

characteristics with and without the EDS. In each trial, a fixed sample of 35 vehicles is selected for analysis and the simulation is run for 10 minutes.

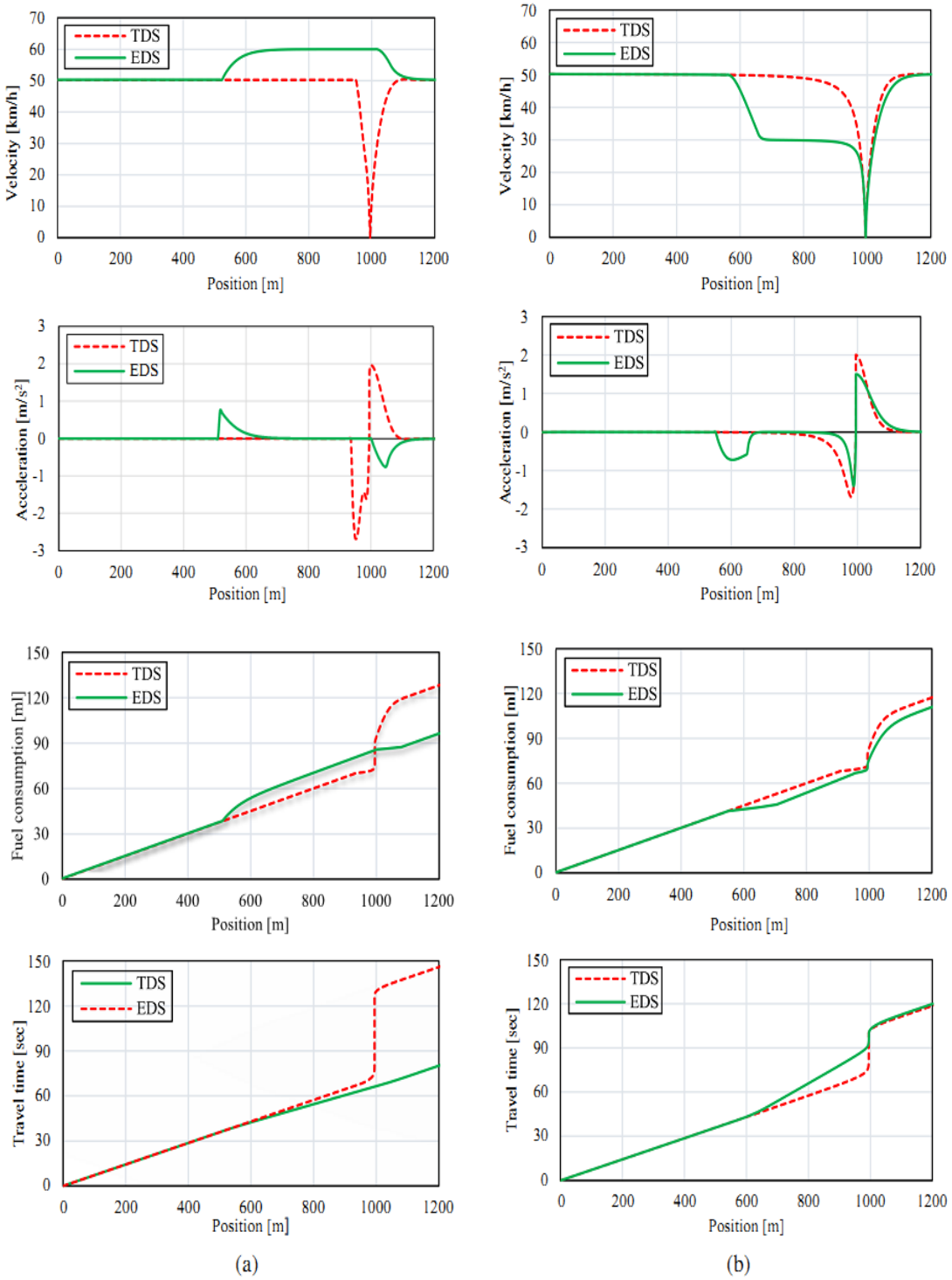

Figure 19: Comparison of driving performance between the eco-driving system (EDS) and the traditional driving system (TDS) for (a) **Event A** and (b) **Event B**.

The histograms of fuel economy and travel time for 200 trails are shown in Figure 20(a) and (b), respectively. The percentage improvement in fuel economy and total travel time are given in Table 1. It is observed that the proposed EDS has improved the fuel consumption and travel time by +3.9% and +7.8%, respectively, in the context of traffic conditions considered in this study. The histograms show that after optimization the distributions for both fuel economy and travel time have shifted to the left. In the most cases, the vehicle has sufficient distance or headway from its preceding vehicle to adjust its driving manoeuvres to the recommended velocity due to moderate and non-congested traffic flow.

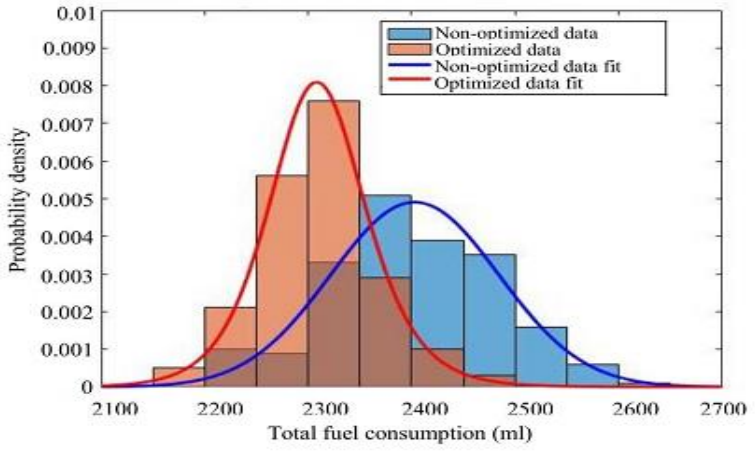

Figure 20: Histogram of driving performance of the EDS and the TDS. (a) Total fuel consumption and (b) total travel time.

Table 1: Performance Comparison in Fuel Consumption and Travel Time

	Fuel Consumption	**Travel Time**
Mean Value	TDS: 2402.9 ml EDS: 2309.5 ml	TDS: 2754.0 sec EDS: 2539.2 sec
Percentage Improvement	+3.9%	+7.8%

When the traffic signal switches to green, vehicles under the EDS accelerates to have higher probability of crossing the intersection. On the other hand, vehicles with high failing probability (of crossing) slows down earlier and cruises at minimum speed towards the intersection. When the EDS vehicle perceives a red signal, it slows down earlier and the vehicles behind are also restricted to follow. The host vehicle under the EDS will only start to adjust its driving behaviour when an event is detected. Although the improvement in travel time is significantly high, the improvement of the fuel consumption remains at a moderate level. This is because the acceleration behaviour depends on the parameter of the car-following model. Since the red period of 60 sec and the green-yellow period of 30 sec are used, if a vehicle can escape the red signal by speeding up in a non-congested traffic, its travel time improves significantly. On the other hand, even if the vehicle slows down to avoid idling at the red signal, it does not increase its crossing time or average speed. However, such escaping of red signal is associated with aggressive acceleration, which compromises fuel efficiency. Such behaviour is reflected in the collective performance of fuel and travel time improvement.

3.7 Summary

In this chapter, we have developed an event-driven eco-driving strategy from self-driving data for a signalized intersection with moderate and non-congested traffic flow. The proposed driving system takes into consideration the presence of disturbances and preceding vehicles, and the EDS suggests

the recommended optimal velocity through stochastic optimization. The vehicle either maintains constant cruising speed or an appropriate acceleration level to avoid the red signal when it observes a switch to green signal. When there is a shift to the red signal, the vehicle slows down to its minimum velocity and slowly travel across the intersection. The simulation results show that the proposed EDS has better efficiency in fuel and travel time than the TDS. Though the proposed system performs eco-driving without using V2V or I2V technologies, it can be a very promising technology for semi-autonomous vehicles in the near future. Also, our method will be able to handle unknown characteristics of multiple intersections in the near future because traffic data of multiple intersections could be retrieved easily using cloud-based systems.

The extension of the existing eco-driving using stochastic model predictive control, by incorporating such probabilistic models, logical decisions at the signal change, safety constraints and a long prediction horizon, is not feasible due to huge computational complexity and requirement of repeated optimization. However, our proposed framework opens an opportunity to incorporate model predictive control to optimize the acceleration of the vehicle further based on the optimal set speed in a bi-level framework. Such implementation will obviously improve the fuel efficiency of the vehicle beyond what is achieved by the proposed method. Such extension of the proposed EDS along with experimental observation and analysis of real driving at intersections will be our next research.

Also, in the future, this system can be extended to multiple intersections and double lane roads with the implementation of lane change model called MOBIL. The system can be extended to analyse traffic flow with mixed vehicles.

Chapter 4

4 Eco-driving Strategy for Hilly Roads

When a vehicle drives on hilly terrain, road grades impact fuel consumption and emissions considerably. In this chapter, we develop a dynamic eco-driving system (EDS) based on fuzzy-tuned model predictive control (MPC) for a host vehicle that fully utilizes the gravitational energy on various sloping roads. Previous vehicle control strategies for hilly roads (Section 2.2) using MPC used fixed-weight cost functions regardless of the driving context, such as road slopes. This fact typically implies that the controller tends to brake on the downslope to suppress increasing velocity due to gravity, and this braking action permits energy dissipation. Our proposed EDS adjusts a weight of the cost function (depending on the states of the road, and both host and preceding vehicles) to better utilize the host vehicle's gravitational potential energy, and consequently, further improve the fuel consumption behaviour with the same travel time. Compared to the previous DP-based methods, our proposed method does not require information of entire driving cycle before the trip. Thus, our method is suitable for real-time implementation.

In the proposed EDS, we formulate a nonlinear optimization problem with an appropriate prediction horizon, and an objective function based on the factors affecting vehicle fuel consumption. The velocity related weight of the objective function is tuned through fuzzy inference techniques. By considering the longitudinal motion dynamics of the host vehicle, state of the preceding vehicle, and road slope information (obtained from the digital road map), the optimization generates velocity trajectories for the host vehicle that minimizes fuel consumption and CO_2 emission, whilst ensuring a collision free traffic. We also investigate the driving performance of following vehicles (behind the host vehicle) that are driven by the traditional driving (human-based) system (TDS)

in synchronous and dense traffic on real hilly roads located in Fukuoka City, Japan. This was not considered in existing works on hilly roads.

It is found that the fuzzy-tuned MPC EDS significantly reduces fuel consumption and CO_2 emission of the host vehicle compared to the TDS, for the same travel time. In dense traffic, the fuel consumption and CO_2 emission of following vehicles are noticeably reduced. Hence, this work also contributes towards the development of eco-driving methods that can improve the driving strategy of a group of vehicles on various road grades in the dense traffic environment. This work in this chapter has been published in the Applied Soft Computing, in (Bakibillah et al., 2020).

The rest of the chapter is organized as follows. In Section 4.1, we describe the fundamental concept of our proposed EDS and in Section 4.2, we formulate the model of vehicle motion dynamics on hilly roads. Then we develop the model predictive control algorithm in Section 4.3 and tuning of the objective function using fuzzy inference in Section 4.4. Section 4.5 presents key simulation results on typical and real hilly road scenarios, and finally, Section 4.6 gives the summary of the chapter.

4.1 Fundamental Concept

It is well known that driving behaviour and road conditions significantly affect fuel consumption and emissions of a vehicle. For example, aggressive acceleration, braking, and speeding waste considerable amount of fuel, whereas uphill slopes consume more fuel and downhill slopes have the potential to save fuel. Forecasting future road traffic situations and driving states (including road grade information) is very useful for driving in an ecological manner, but such anticipations are hardly possible for human driving. Therefore, an eco-driving system can be a promising solution to assist a driver improve fuel-efficiency.

The fundamental concept of our proposed fuzzy-tuned MPC EDS on a hilly road is illustrated in Figure 21. The EDS uses the host vehicle's

longitudinal motion dynamics (while following a preceding vehicle) and information of road grades ahead to calculate the optimal velocity over the traveling interval. The preceding vehicle and following vehicles are assumed be TDS vehicles. The dynamic behaviour of those vehicles is modelled based on a microscopic car-following model known as the Intelligent Driver Model (IDM), which imitates human driving behaviour (Treiber et al., 2000). The IDM is defined by the acceleration function in terms of the dynamics of position and velocity of each vehicle, and it captures the impact of road grades on the acceleration of a vehicle and generates the control input to ensure steady speed on the slope. We also assume that the vehicles are traveling in a group, in synchronous traffic flow. The EDS knows the road grade information of the trajectory, which is obtained from the three-dimensional (3D) digital road map data, whereas the vehicle's location is acquired from the GPS. To evaluate the effectiveness of the proposed EDS, a suitable objective (cost) function is formulated and one of its weights is tuned using fuzzy inference techniques to obtain smooth variation of speed on road slopes. The fuzzy inference is based on the instantaneous speed and the road slope angle. The following sections

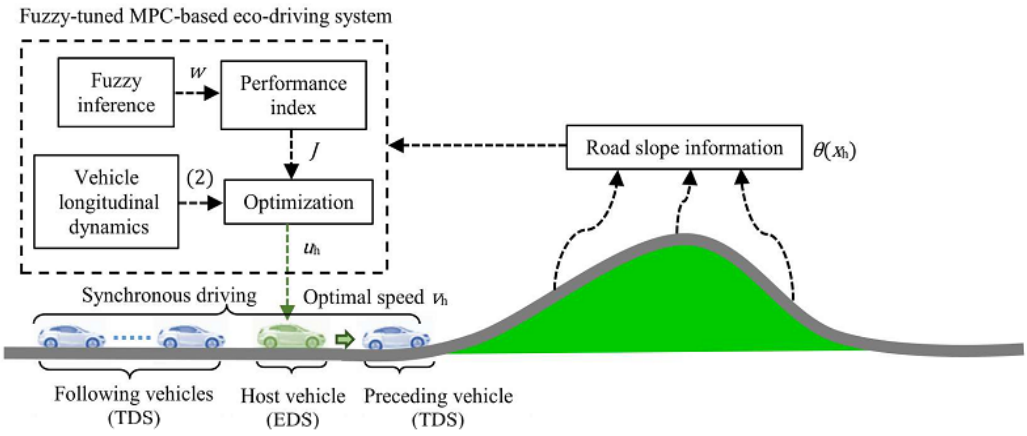

describe the problem formulation and the fuzzy based control method in detail.

Figure 21: Fundamental concept of the proposed EDS on a hilly profile with up-down slopes using fuzzy-tuned MPC.

4.2 Vehicle Dynamics on Hilly Roads

Fuel consumption and CO_2 emission of a vehicle are directly related to the longitudinal motion dynamics (Mihaly & Gáspár, 2013). Hence, we consider only the longitudinal motion dynamics of the host vehicle in the optimization, and controlling the lateral dynamics (for lane keeping and lane changing) is the responsibility of the driver. Since the host vehicle must maintain a safe gap with its preceding vehicle, the states of the preceding vehicle are considered as a dynamic reference. The nonlinear state equation of the vehicle in the longitudinal direction at time t can be expressed as

$$\dot{y}(t) = f(y(t), u_h(t), z(t)), \tag{4.1}$$

where $y(t) = \left[x_h(t), v_h(t), x_p(t), v_p(t)\right]^{\mathrm{T}} \in \mathbb{R}^4$ denotes the state vector representing position x_h and velocity v_h of the host vehicle, position x_p and velocity v_p of the preceding vehicle, respectively, u_h is the control input relating to the traction force, and $z(t)$ is a time varying external parameter representing acceleration u_p of the preceding vehicle, whose value can be approximated by the measured speeds.

The motion of the host vehicle is determined by the total forces acting on it as shown in Figure 22 and is given as

$$M_h \frac{dv_h(t)}{dt} = F_T(t) - F_R(t), \tag{4.2}$$

where M_h, $F_T(t)$, and $F_R(t)$ represent the equivalent mass of the host vehicle, the traction force, and the sum of all motion resistance forces, respectively.

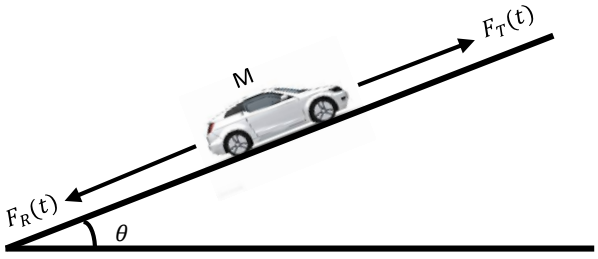

Figure 22: Forces acting on the vehicle while running on a hilly road.

Note that $F_R(t)$ consists of aerodynamic drag, rolling resistance, and gravitational force due to the slope and is given by

$$F_R = \frac{1}{2} C_D \rho_a A_v v_h^2(t) + \mu M_h g \cos\theta\,(x_h) + M_h g \sin\theta\,(x_h), \tag{4.3}$$

where C_D, ρ_a, A_v, μ, and $\theta(x_h)$ respectively are the drag coefficient, the air density, the vehicle frontal area, the rolling friction coefficient, the gravitational acceleration, and the road slope angle associated with the host vehicle position x_h. The traction force is given by the product of the mass of the vehicle and the equivalent acceleration as $F_T(t) = M_h u_h(t)$. Thus, the function in (4.1) is written as

$$f\big(y, u_h(t), z(t)\big) = \begin{bmatrix} v_h \\ -\frac{1}{2M_h} C_D \rho_a A_v v_h^2 - \mu g \cos\theta\,(x_h) - g \sin\theta\,(x_h) + u_h(t) \\ v_p \\ u_p(t) \end{bmatrix}, \tag{4.4}$$

where the term $-\frac{1}{2M_h} C_D \rho_a A_v v_h^2 - \mu g \cos\theta\,(x_h) - g \sin\theta\,(x_h) + u_h(t)$ is the apparent acceleration. The control input u_h of the host vehicle is applied through its throttle or brake. The road altitude information is available from the digital road map, which is used to calculate θ (road slope angle at position x_h) as

$$\theta(x_h) = tan^{-1}\left(\frac{R_{alt}(x_h + \Delta x_h) - R_{alt}(x_h)}{\Delta x_h}\right), \tag{4.5}$$

where $R_{alt}(x_h)$ is the road elevation at position x_h and Δx_h is the horizontal span. For simplicity, $\theta(x_h)$ can be written as θ.

4.3 Model Predictive Control

It is known that a vehicle's acceleration and braking rates are directly associated with the input force and variation of engine torque. A high level of acceleration or braking is not beneficial for energy efficiency as well as driving

comfort. We propose a fuzzy-tuned MPC based dynamic EDS that measures the states of the host vehicle at any time t and derives the optimal velocity trajectory required for an efficient and safe manoeuvring in the prediction horizon. Specifically, we formulate an optimization algorithm to calculate the optimal velocity. The constraints of the optimization problem include the constraints for velocity, acceleration, and safe headway. A suitable value of the prediction horizon (analogous with anticipation of human drivers) is considered; since traffic flow experiences significant variation, a long horizon would not be beneficial. The safe headway (distance) s_d of the host vehicle from the preceding vehicle is given as

$$s_d(t) = s_0 + t_{hd}^* v_h(t), \tag{4.6}$$

where s_0 is the minimum spacing between vehicles and t_{hd}^* is the safe (reference) headway time while following the preceding vehicle.

To implement the MPC with state dynamics (4.1) and (4.4), an optimal control problem is solved, where an objective function is minimized at each time t and expressed as

$$J\big(y(t), u_h(t)\big) = \int_t^{t+T} [w_1(v_h(t), \theta(t))(v_h(\tau|t) - v_d)^2 + w_2 u_h^2(\tau|t) + w_3(1 + e^{-\sigma(t_{hd}^* - t_{hd}(\tau|t))})^{-1}]\, d\tau, \tag{4.7}$$

Subject to

$$v_{\min} \le v_h(\tau|t) \le v_{\max}$$
$$u_{\min} \le v_h(\tau|t) \le u_{\max}$$
$$x_p(\tau|t) - x_h(\tau|t) \ge S_d(\tau|t)$$

where T denotes the prediction horizon from current time t on which the optimum trajectories are computed, v_d is the constant desired velocity, σ is a positive constant, $t_{hd}(\tau|t) = (x_p(t) - x_h(t) - s_0)/(v_h(t) + \xi)$ is the instant time headway that includes a positive threshold ξ to evade singularity at $v_h(t) = 0$, $w_1(v_h, \theta), w_2$, and w_3 are the weighting factors related to the

velocity, acceleration, and safe distance terms, respectively. The first term of the objective function is the cost due to deviation of the current velocity from v_{d}. The second term is the cost of the vehicle's acceleration force considering the effect of gravitational force on the slope. The third term implies a penalty due to deviation from the reference headway, which is calculated dynamically to provide a large value when the host vehicle is approaching to the preceding vehicle and a negligible small value when the preceding vehicle is sufficiently faraway. Note that here we choose a sigmoid function instead of a quadratic function so that this cost only appears when the instant time headway t_{hd} reduces significantly from the safe time headway t_{hd}^{*}. The value of weight $w_1(v_h, \theta)$ is tuned depending on the driving context, whereas high values are chosen for weights w_2 and w_3. Specifically, weight $w_1(v_h, \theta)$ is tuned by means of fuzzy inference described in the next section so that the variation of speed on the slopes can provide better utilization of the kinetic energy, and consequently, the fuel efficiency and CO_2 emission of the host vehicle are improved.

4.4 Tuning of Objective Function using Fuzzy Inference

The fuzzy inference technique is a powerful tool, which presents objects in an abstruse way similar to the concepts and thought process of a human. Fuzzy logic control allows range-to-range or range-to-point control unlike point-to-point control in classical control strategy. The concept of fuzzy logic was invented by L. A. Zadeh in 1965 as a mathematical tool to deal with uncertainty (Zadeh, 1965). However, this invention received attention almost after ten years when E. H. Mamdani applied in a real application for controlling a steam engine by incorporating a set of linguistic control rules (Mamdani & Assilian, 1975). Since the 1980s, works on fuzzy implementations have been developed rapidly including its applications in automatic control, automobile production, industrial manufacturing, academic education, hospitals, and so on. Moreover, different fuzzy technologies have been proposed using classical control methods, e.g., PID-fuzzy control (Er & Sun, 2001), phase-plan mapping fuzzy

control (Li & Gatland, 1995), adaptive fuzzy control (Hsu & Fu, 2000), neuro-fuzzy control (Jang & Sun, 1995), and switched fuzzy sampled-data control (Shi et al., 2019). The most popular fuzzy inference methods are Mamdani, Sugeno, and Tsukamoto methods that work with crisp data as inputs (Iancu, 2012). Among these methods, the fuzzy inference technique of Mamdani is the most widely used. In this work, we develop a new concept called fuzzy-tuned MPC or fuzzy-MPC and utilize the fuzzy inference method of Mamdani. We apply three consecutive steps to implement fuzzy logic, which are fuzzification, fuzzy inference, and defuzzification.

4.4.1 Fuzzification

In the fuzzification process we consider the instantaneous velocity $v_h(t)$ of the host vehicle and the road slope angle $\theta(t)$ as crisp inputs to tune $w_1(v_h, \theta)$, and represent them with linguistic variables. i.e., 'Low' (L) and 'High' (H) for velocities and 'Negative' (N) and 'Positive' (P) for slopes. Then, we derive the membership functions to obtain the proportion of these inputs corresponding to the appropriate fuzzy sets. The members of a fuzzy set have smooth boundaries compared to the classical set. Generally, there are different types of membership functions, such as the Gaussian waveform, bell-shaped waveform, triangular waveform, trapezoidal waveform, S-curve waveform, and sigmoidal waveform. Because of the dynamic nature and variation of traffic flow in a short period of time, we choose and define trapezoidal shaped membership functions for velocity $v_h(t)$ and road slope angle $\theta(t)$ as shown in Figure 23(a). The centre of velocity and road slope angle membership functions are located at v_d and 0, respectively. Then, we determine the corresponding membership values for velocity $\{\mu_L(v_h), \mu_H(v_h)\}$ and road slope angle $\{\mu_N(\theta), \mu_P(\theta)\}$.

4.4.2 Fuzzy Inference

In the next step, we define the fuzzy control rule as shown in Figure 23(b), which is the kernel of the fuzzy inference process. In fuzzy inference,

expert knowledge is required to design the control rules; in this case, a vehicle's fuel consumption characteristics on slopes can be improved in the following ways

- At the down slope and low speed, $w_1(v_h, \theta)$ should be low because the speed will increase automatically due to the down slope.
- At the down slope and high speed, $w_1(v_h, \theta)$ should be moderate to avoid braking, which will wasting kinetic/potential energy and cause ride discomfort.
- At the up slope and at normal or low speed, $w_1(v_h, \theta)$ should be high to let the vehicle speed be close to its desired speed.
- At the up slope and high speed, $w_1(v_h, \theta)$ should be moderate to avoid braking as the vehicle will slow down naturally (due to gravity and drag).

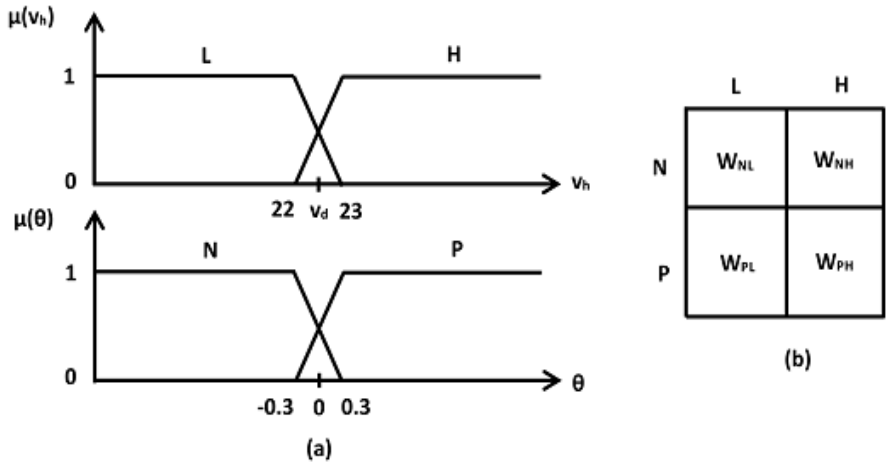

Figure 23: Fuzzy inference technique (a) trapezoidal shaped membership functions, (b) fuzzy control rules.

In our case, we use the above expert knowledge to design the fuzzy rules. Then, we apply the fuzzified inputs to the predecessors of the fuzzy rules. In this implementation, there are two predecessors of fuzzy rules, and hence, the fuzzy operator AND is used to get a single value, which gives the result of predecessor evaluation. The conjunction of rule predecessors is evaluated as

$$\mu_{ij}(t) = \mu_{i\in\{L,H\}}(t) \cap \mu_{j\in\{N,P\}}(t) = \min\{\mu_i(v_h), \mu_j(\theta)\}. \quad (4.8)$$

Then, we associate the membership functions with the fuzzy rules to determine the control output as

$$F_z(v_h, \theta) = \sum \mu_{ij}(v_h, \theta) W_{ij}, \quad (4.9)$$

where $W_{ij}, ij \in \{NL, NH, PL, PH\}$, are the constant fuzzy weights. Since the speed $v_h(t)$ and the road slope angle $\theta(t)$ vary with time, $\mu_{ij}(v_h(t), \theta(t))$ is also time varying.

4.4.3 Defuzzification

Finally, we transform the fuzzy output back to the crisp output using defuzzification (*D*) method called Center of Gravity (COG), which is widely used in real applications. The COG output is calculated as

$$w_1(v_h, \theta) = DF_z(v_h, \theta) = \frac{F_z(v_h, \theta)}{\sum_{ij\in\{NL,NH,PL,PH\}} \mu_{ij}(v_h, \theta)}. \quad (4.10)$$

Figure 24 shows smooth variation in $w_1(v_h, \theta)$ when both the speed $v_h(t)$ of the host vehicle and the road slope angle $\theta(t)$ vary. A smooth variation in $w_1(v_h, \theta)$ yields significant improvement in fuel consumption as well as CO_2 emission for the same travel time.

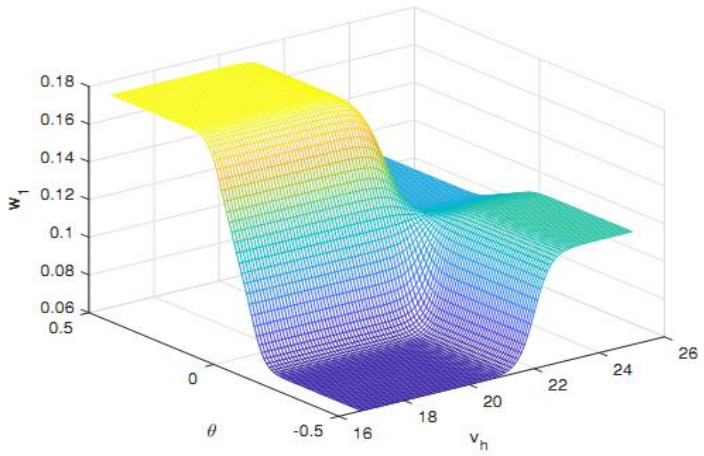

Figure 24: Fuzzy inference of the weight $w_1(v_h, \theta)$ when both the speed v_h of the host vehicle and the road slope angle θ vary.

4.5 Simulation Results and Discussion

To implement and validate the proposed EDS for real hilly road traffic scenarios, we developed a simulation framework in MATLAB (which has been proven to be mathematically reliable and used to simulate many real world scenarios) and solved a nonlinear optimization problem (described in (4.7)) in discrete time using a nonlinear programming solver in the optimization toolbox. For real-time implementation the sequential quadratic programming (SQP) algorithm is used inside the solver, which is standard and widely used algorithm for nonlinear optimization. In this method, the function solves a quadratic programming (QP) sub-problem at each iteration. The computation time of the algorithm is in 100-200 millisecond range, which is within the expected range for real-time implementation.

The parameters of the host vehicle are chosen as $M_h = 1000$ kg, $C_D = 0.32$, $\rho_a = 1.184$ kg/m^3, $A_h = 2.5$ m^2, $g = 9.8$ m/s^2, and $\mu = 0.015$. The safe time headway t_{hd}^* and the minimum spacing s_0 parameters are set as 1.5 s and 7 m, respectively. The desired velocity v_d of the MPC is set as 22.23 m/s (80 km/h), and the velocity and acceleration constraints are set as $v_h \in [0, 26]$ m/s and $u_h \in [-5, 2]$ m/s^2, respectively. A suitable prediction horizon $T = 10$ s with 20 steps and the step size of $dt = 0.5$ s is chosen. The initial position x_h and velocity v_h of the host vehicle are set at $x_h(0) = 0$ m and $v_h(0) = 22.23$ m/s (80 km/h). The parameters of the IDM are set as $v_d = 80$ km/h, $s_0 = 2$ m, and $t_{hd}^* = 1.5$ s with maximum acceleration and comfortable deceleration of 1.5 m/s^2 and -2.5 m/s^2, respectively.

We evaluate the performance of the EDS using microscopic traffic simulations and conduct all simulations in four parts as follows

- At first, we run the simulation on a typical artificial road section of about 1.5 km with different altitude and shape of slopes to tune the fuzzy weights. The purpose is to obtain the optimum weight w_1 of the first term (velocity related) of the objective function (4.7), which gives the

minimum fuel consumption and CO_2 emission for the same travel time. From the simulation, the optimum w_1 of the MPC is obtained as 0.15. The fuzzy weights are inferred based on the road slope angle and the current speed at any location of the host vehicle on the slope. The optimum fuzzy weights are obtained as 0.060, 0.120, 0.172, and 0.105, respectively, through tuning.

- Secondly, we evaluate the effectiveness of the proposed EDS on typical common road scenarios, such as up-down and down-up slopes.
- Then, we validate the EDS for the host vehicle on a real road section (with complex up-down slopes of various degrees) located in Fukuoka City, Japan, using the GPS data and road slope information obtained from the digital road map.
- Finally, we evaluate the effectiveness of the proposed EDS to improve the overall driving performance for a group of following traditional vehicles considering the presence of the preceding vehicle.

For comparison purposes, three types of driving control systems are simulated, i.e., the IDM, which is considered as a fixed speed drive (FSD), the EDS using conventional (fixed-weight) MPC and the proposed fuzzy-tuned MPC EDS. The FSD system maintains constant velocity of vehicles by accurately generating the appropriate control action on road slopes. For an unbiased comparison among the methods, we maintain the average velocity of vehicles to be almost equal, in order to demonstrate the improvement in fuel consumption and CO_2 emission of the proposed EDS without compromising the travel time. To investigate vehicle fuel consumption and CO_2 emission rates, the VT-Micro model is used (Rakha et al., 2004). This model is well accepted for calculating fuel consumption and emissions of vehicles.

4.5.1 Performance Evaluation on Representative Hilly Road

Figure 25 shows the simulation results of driving on typical hilly road sections with an up-down slope (left) and a down-up slope (right). The first two

graphs from the top show the road altitude and percentage of road slop, the next two graphs illustrate comparative velocity trajectories and equivalent acceleration (“equiv accel” for short) profiles. The last three graphs show instantaneous fuel consumption, CO_2 emission, and total fuel consumption for traveling a distance from 200 m to 800 m (because the peak of up-down and down-up slopes are located at 500 m). The Fuzzy-MPC EDS vehicle increases its velocity in advance before entering the up-slope to avoid high acceleration when going up.

On the other hand, at the down-slope, the EDS vehicle utilizes the advantage of gravitational force to increase the velocity to be increased to some extent, so that it can travel further without accelerating and also avoid unnecessary braking. It can also be seen that the EDS vehicle smoothly varies its velocity on the slope. The performance of FSD, conventional MPC, and Fuzzy-MPC EDS is illustrated in Table 2, where it is found that for an up-down slope and a down-up slope, the proposed Fuzzy-MPC EDS outperforms the traditional human driving by 7.8% and 13.2% respectively in fuel economy, and 6.4% and 10.8% respectively in CO_2 emission reduction.

4.5.2 Performance Evaluation on Real Hilly Road

Next, the strength of our proposed fuzzy-MPC EDS is further demonstrated and validated using data of a real road called Yuniba Dori and its extended part located in Fukuoka City, Japan, as shown in Figure 26. The length of the route is approximately 2.5 km. The route altitude information is acquired from Fukuoka City’s digital road maps at every 5 m interval and the slope angle is calculated using (4.5). The altitude of the route is 6 m at the north end and 25 m at the south end. The route is situated in a hilly area and there are varying shapes of up and down slopes in the route. Figure 27 shows the road elevation of the route, where is complicated with multiple up and down slopes of varying shapes.

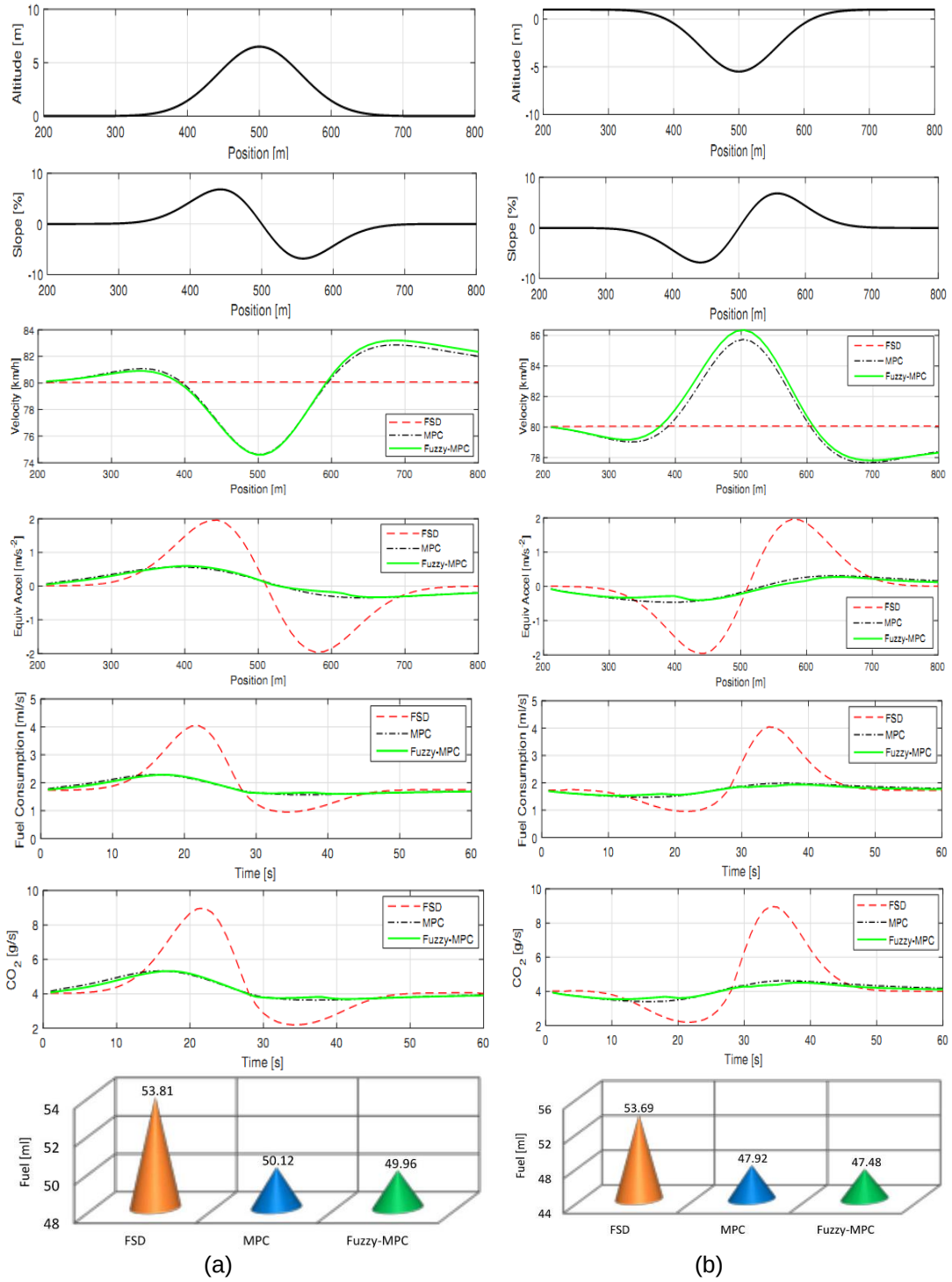

Figure 25: Drive along the hilly road sections (a) an up-down slope and (b) a down-up slope.

Table 2: Performance comparison between FSD and Fuzzy-MPC for driving along up-down and down-up slopes

	FSD	MPC	Fuzzy-MPC EDS
Up-down slope:			
Velocity [km/h]	80.07	80.08	80.10
Fuel economy [m/ml]	11.15	11.96	12.02
CO_2 emission [g/m]	0.2059	0.1937	0.1928
Down-up slope:			
Velocity [km/h]	80.07	80.20	80.23
Fuel economy [m/ml]	11.16	12.52	12.64
CO_2 emission [g/m]	0.2055	0.1853	0.1832

Figure 26: The experimental route in Fukuoka City, Japan, taken from Google maps.

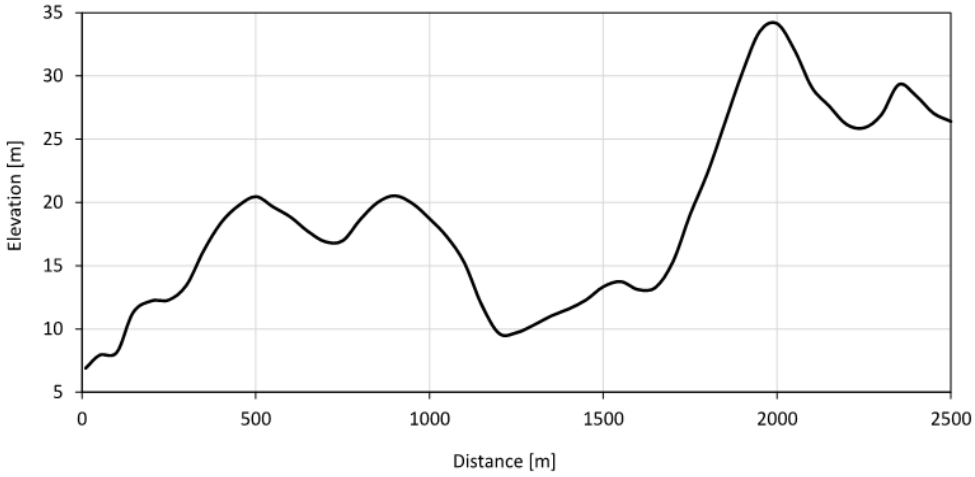

Figure 27: The road elevation of the experimental route obtained from digital road maps of Fukuoka City, Japan.

Figure 28 shows the simulation results of driving on the experimental route from the north end to the south end (N-S) and from the south end to the north end (S-N). The performance of FSD, conventional MPC, and Fuzzy-MPC EDS is given in Table 3. It is found that the proposed Fuzzy-MPC EDS saves more fuel than the traditional human driving by 8.4% (for N-S) and 11.2% (for S-N). The EDS also reduces CO_2 emission 6.8% and 9.4% compared to the traditional human driving for N-S and S-N, respectively. These results demonstrate the ability of the superiority of the proposed EDS over traditional human driving, in reducing fuel consumption and CO_2 emission.

Finally, we investigate impact of the Fuzzy-MPC EDS of the host vehicle on the driving performance for a number of following TDS vehicles running on a real hilly road. Specifically, a group of twelve vehicles is considered including the preceding vehicle, while they are traveling in synchronous flow traffic, i.e., the speed of traffic is lower than the free flow speed due to high traffic density. The initial velocity and the desired velocity of vehicles are set at 65 km/h. In this case we run two types of simulation, firstly we observe the traffic flow behaviour when all vehicles are traditional and human driven, and secondly, we consider the host vehicle as the EDS vehicle whereas the preceding and the following vehicles are the TDS vehicles.

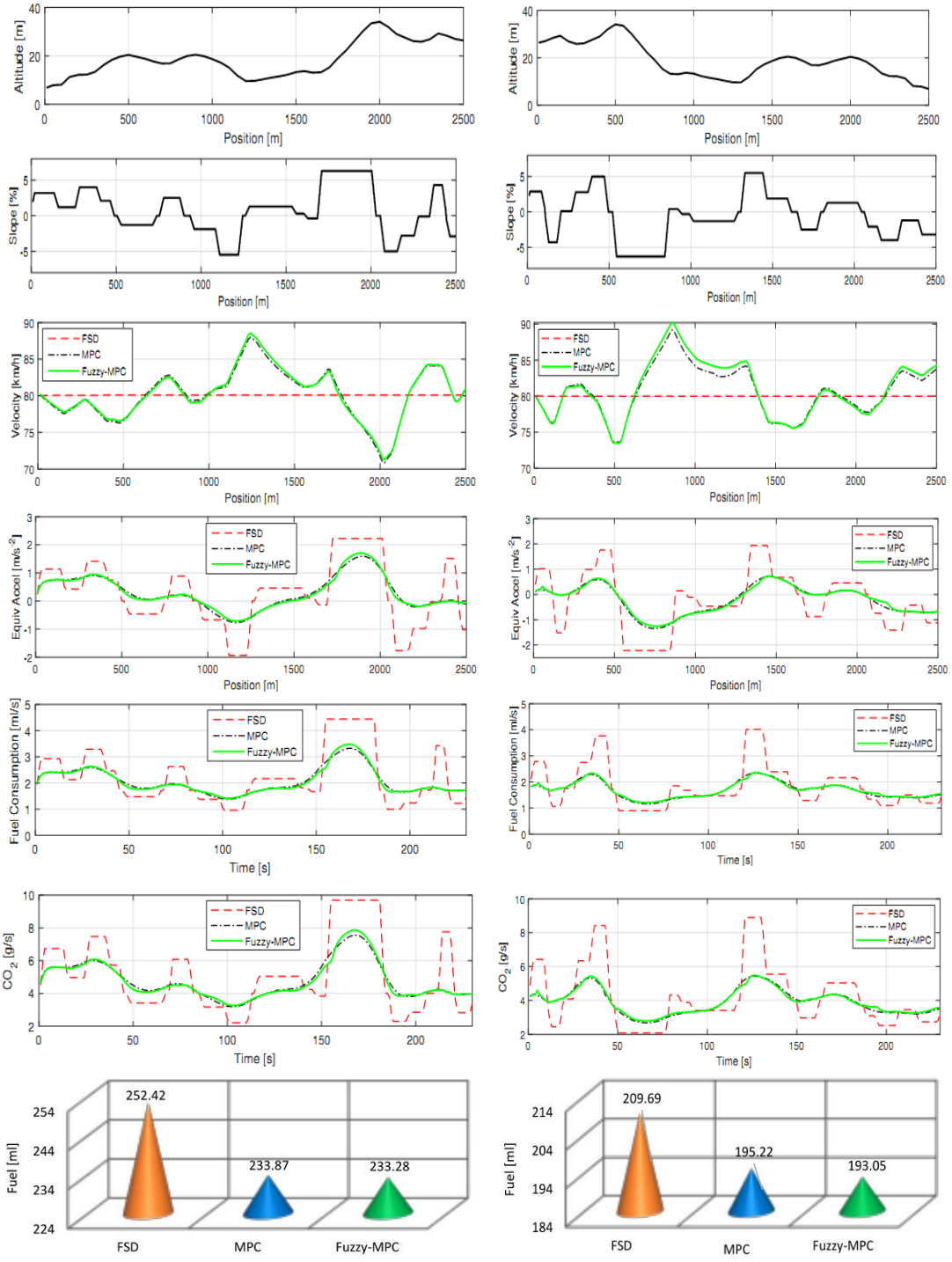

(a) (b)

Figure 28: Drive along the experimental route (a) from the north end to the south end and (b) from the south end to the north end.

Table 3: Performance comparison between FSD and Fuzzy-MPC for driving along the experimental route

	FSD	MPC	Fuzzy-MPC EDS
North to South:			
Velocity [km/h]	80.08	80.12	80.20
Fuel economy [m/ml]	9.90	10.68	10.76
CO_2 emission [g/m]	0.2302	0.2162	0.2145
South to North:			
Velocity [km/h]	80.08	80.26	80.32
Fuel economy [m/ml]	11.92	13.15	13.26
CO_2 emission [g/m]	0.1894	0.1751	0.1716

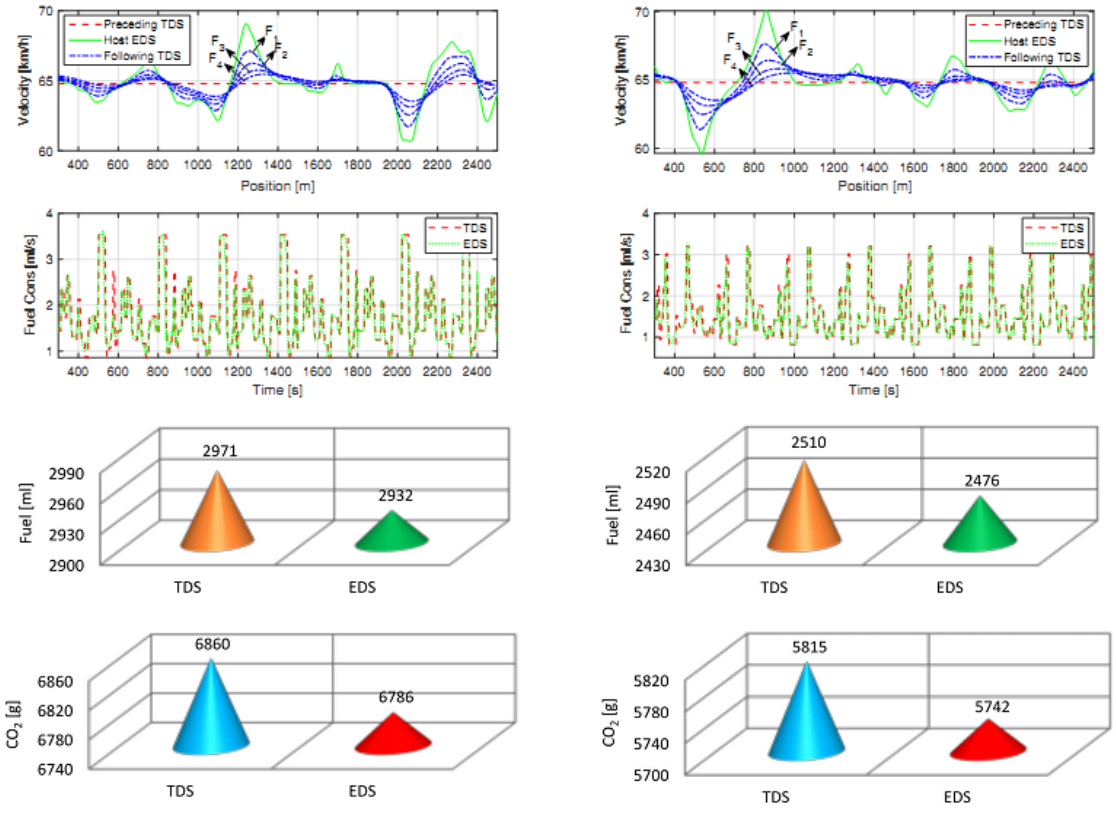

Figure 29: Evaluation of traffic flow performance when driving (a) from the north end to the south end and (b) from the south end to the north end.

Figure 29 illustrates the simulation results of traffic flow performance when the vehicles are traveling from the north end to the south end and from the south end to the north end, respectively. It is found that the traffic using the TDS consumes total 2,971 ml of fuel and emits 6,860 g of CO_2, while the traffic using the EDS consumes total 2,932 ml of fuel and emits 6,786 g of CO_2 when traveling from the north end to the south end. On the other hand, when the vehicles are traveling from the south end to the north end, the total fuel consumption of the TDS and the EDS are 2,510 ml and 2,476 ml, whereas the CO_2 emissions are 5,815 g and 5,742 g, respectively. Table 4 summarizes the comparison between the TDS and the EDS of the host vehicle H and the following vehicles F1 to F4 in synchronous driving mode for traveling from the north end to the south end and from the south end to the north end. The average fuel consumption of the TDS is obtained as 272.16 ml from the north end to the south end and 226.25 ml from the south end to the north end. Specifically, we observe that the proposed EDS has the highest impact on fuel consumption of the first following vehicle and gradually decreases until the fifth following vehicle. This improvement is achieved because the EDS vehicle forces the following vehicles to drive in the optimal ecological way.

Table 4: Traffic flow performance between the TDS and the EDS

	H	**F1**	**F2**	**F3**	**F4**
N-S	260.01	262.95	265.03	267.38	269.55
% Imp	4.6	3.8	2.6	1.8	1.1
S-N	216.07	219.10	221.10	223.57	225.44
% Imp	4.6	3.1	2.5	1.7	1.2

4.6 Summary

In this chapter, we have developed a novel dynamic ecological driving system (EDS) based on Fuzzy-MPC that reduces fuel consumption and CO_2 emission of a vehicle when moving on dense roads with uphill and downhill

sections. A nonlinear optimization problem is formulated considering longitudinal motion dynamics of the host vehicle, state of the preceding vehicle, and information of the road slope ahead, which is obtained from the digital road map. The objective function is minimized using MPC to generate the optimal velocity trajectory for ecological driving. To further improve the performance of the EDS, a weight of the objective function is dynamically varied using fuzzy inference techniques, based on the instantaneous velocity of the host vehicle and the road grade angle. The fuzzy weights are tuned based on a typical hilly road, whilst the proposed EDS is evaluated and validated on real hilly road scenarios. It is found that that fuzzy-MPC EDS has performed much better than the traditional human driving system. The proposed EDS fully utilizes gravitational potential energy by smoothly varying the velocity of a vehicle on the slope, which ensures the minimum energy waste due to braking. Thus, the EDS maintains the fuel consumption in the optimum level.

Based on different scenarios the fuel-saving potential of the proposed EDS ranges from 7.8 – 13.2%. Also, the proposed EDS reduces the CO_2 emission by 6.4 – 10.8%. Finally, we evaluate the potential of the proposed EDS to improve the overall traffic performance in a real hilly road scenario. It is found that the proposed EDS ensures the optimal driving strategy for a group of vehicles in synchronous driving mode.

For future research, we will consider the effect of curvature on hilly roads and investigate the traffic flow performance with different penetration rates of the EDS vehicles. Moreover, the proposed method will be extended for multi-lane traffic flow.

Chapter 5

5 Eco-driving Strategy for Horizontal Curved Roads

On horizontal curved roads, fuel consumption and emissions of a vehicle are also highly influenced by driving behaviour. In this chapter, we develop a novel dynamic eco-driving system (EDS) based on model predictive control (MPC) for a host vehicle traveling on horizontal curved roads. Previous works on vehicle control strategies for horizontal curves (Section 2.3) mainly developed different speed control algorithms for driving safety rather than eco-driving. Some existing eco-driving strategies on horizontal curves found that the fuel consumption should be minimum for a constant speed despite variations in road curvature, which is not feasible in real-world scenarios. Also, they did not consider the effect of various road-surface conditions. Our proposed method overcomes the limitations of those works by calculating the optimal speed based on both curvatures and road-surface conditions, while ensuring driving safety. Our proposed method does not require information of entire driving cycle before the trip compared with the previous DP-based approach. Thus, our method is suitable for real-time implementation.

In the proposed EDS, we formulate a nonlinear optimization problem considering a suitable prediction horizon and an objective function based on the factors affecting vehicle fuel consumption and safety. We derive a method to precisely calculate road-curvatures (with various radii) using high-accuracy digital road map data. The EDS dynamically computes the optimal velocity trajectory for the host vehicle considering its dynamical model, the state of the preceding vehicle, information of road-curvature, and road-surface conditions, such as dry, wet, snow, and ice. We evaluate the effectiveness of the EDS using microscopic traffic simulations on typical horizontal curved roads with different curvatures and road-surface conditions. It is found that the EDS

substantially reduces fuel consumption and CO_2 emission of the host vehicle compared to the traditional driving system (TDS), while ensuring safe driving.

The rest of this chapter is organized as follows. The fundamental concept of our proposed EDS is described in Section 5.1 and the model of vehicle motion dynamics on horizontal curved roads is discussed in Section 5.2. In Section 5.3, we derive a method to accurately calculate the road curvature and then in Section 5.4, we formulate the model predictive control algorithm. In Section 5.5, we present the simulation results and finally, Section 5.6 provides the summary of this chapter.

5.1 Fundamental Concept

It is well known that driving behaviour and road-geometry features have significant impact on fuel consumption and emissions of a vehicle. To drive a vehicle on horizontal curves in an optimal ecological and safe manner, it is important to anticipate future road traffic situations and driving states including information of road-curvatures and road-surface conditions. But, such anticipations are hardly possible for a human driver. Hence, an eco-driving system can be developed using advanced control algorithms to assist drivers for fuel-efficient and safe manoeuvring on curved roads.

The fundamental concept of our proposed MPC-based EDS on a horizontal curve is illustrated in Figure 30. We consider a single lane road for simplicity without lane changing and overtaking manoeuvres. The EDS uses the host vehicle's longitudinal motion dynamic model in the presence of a preceding vehicle, information of curvatures, and road-surface conditions (dry, wet, snow, and ice) to calculate the optimal velocity to minimize fuel consumption and CO_2 emission over the traveling interval. The vehicle's location is obtained from the global positioning system (GPS) and the road-surface condition is known from the vehicle mounted sensors. The coordinates of the whole trajectory is obtained from the digital road map, which is then used to calculate the curvature (radii) of the road with high accuracy. The preceding vehicle is

considered to be traditionally driven (human-driven) and called the TDS vehicle hereafter, whose dynamic behaviour is modelled according to a microscopic car-following model called the Intelligent Driver Model (IDM) (Treiber et al., 2000). The IDM captures the effect of road-curvatures in the input acceleration of a vehicle. To evaluate the effectiveness of the EDS, a suitable objective function is formulated and optimized in a receding horizon control approach. The following sections describe vehicle dynamical model, road-curvature calculation method, the performance index, and the control method in detail.

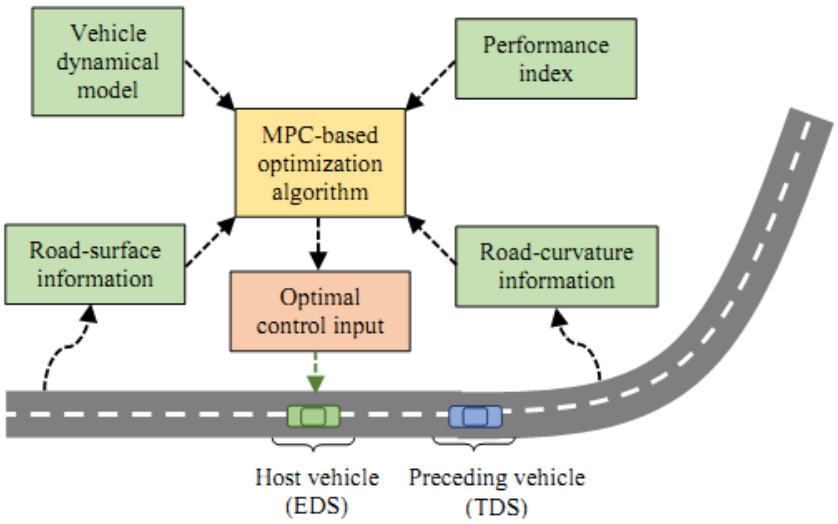

Figure 30: Fundamental concept of the proposed EDS on a horizontal curved road using MPC.

5.2 Vehicle Dynamics on Curved Roads

In this section, we present the vehicle dynamics, its technological settings, and operational hypotheses to design an MPC controller and make the system realistic. Since fuel consumption and CO_2 emission are directly related to the longitudinal movement, we only consider the host vehicle's longitudinal motion control (integrating lateral dynamics) for eco-driving on the horizontal curved road. We made some assumptions before modeling as:

1. The front wheel angle is equal to the angle of the steering wheel

2. The attributes of the tire cornering properties are in a linear range due to small slip angle and small variation of the tire load.

The nonlinear state equation of the vehicle is given as

$$\dot{y}(t) = f(y(t), u_h(t), z(t)), \tag{5.1}$$

where $y(t) = \left[x_h(t), v_h(t), x_p(t), v_p(t)\right]^{\mathrm{T}} \in \mathbb{R}^4$ denotes the state vector representing position x_h and velocity v_h of the host vehicle, position x_p and velocity v_p of the preceding vehicle, respectively, u_h is the control input relating to the traction force, and $z(t)$ is a time varying external parameter representing acceleration u_p of the preceding vehicle, whose value can be approximated by the measured speeds.

In traction mode, the motion of the vehicle on a curved road can be given by

$$\begin{aligned} & M_h\left(\frac{dv_{hx}(t)}{dt} - v_{hy}(t)\dot{w}_z(t)\right) \\ & = F_T(t) - \frac{1}{2}C_D\rho_a A_v v_{hx}^2(t) - \mu M_h g\cos\theta - F_{yf}\sin\delta_f, \end{aligned} \tag{5.2}$$

where v_{hx}, v_{hy}, and $\dot{w}_z$ are the longitudinal velocity, the lateral velocity, and the yaw rate of the host vehicle, F_{yf} is the tire lateral force of the front wheel, and δ_f is the front wheel steering angle, which is used to control the vehicle lateral dynamics on the curve. The traction force is given by the product of the mass of the vehicle and the equivalent acceleration as $F_T(t) = M_h u_h(t)$. We assume that the road slope angle θ is very small and thus, $\cos\theta \approx 1$ is considered for computational simplicity. On horizontal curves, the relation between vehicles longitudinal velocity and lateral velocity can be expressed as $v_{hy} = \beta v_{hx}$ where β is the host vehicles sideslip angle.

Next, we analyse the tyre-slip stiffness characteristics on a curved road. The front tires slip angle α_f and the rear tires slip angle α_r are given as

$$\alpha_f = \delta_f - \varphi_{vf},$$

$$\alpha_r = -\varphi_{vr}, \tag{5.3}$$

where φ_{vf} and φ_{vr} are the front and rear tires velocity angle given as

$$\varphi_{vf} = \frac{v_{hy} + l_f \dot{w}_z}{v_{hx}},$$

$$\varphi_{vr} = \frac{v_{hy} - l_r \dot{w}_z}{v_{hx}}, \tag{5.4}$$

where l_f and l_r respectively are the front tyre and the rear tyre distances from the centre of gravity of the host vehicle. Then, the lateral tyre forces for the front wheels and the rear wheels of the vehicle can be expressed as

$$F_{yf} = 2C_{\alpha f}\left(\delta_f - \varphi_{vf}\right),$$

$$F_{yr} = 2C_{\alpha r}(-\varphi_{vr}), \tag{5.5}$$

where $C_{\alpha f}$ and $C_{\alpha r}$ are cornering stiffness of the front tyre and the rear tyre, respectively. Thus, (5.4) becomes

$$F_{yf} = 2C_{\alpha f}\left(\delta_f - \beta - \frac{l_f \dot{w}_z}{v_{hx}}\right),$$

$$F_{yr} = 2C_{\alpha r}\left(-\beta + \frac{l_r \dot{w}_z}{v_{hx}}\right), \tag{5.6}$$

Finally, the nonlinear state equation of the host vehicle on a curved road can be written as

$f\left(y, u_h(t), z(t)\right) =$

$$\begin{bmatrix} v_h \\ -\frac{1}{2M_h} C_D \rho_a A_v v_{hx}^2 - \mu g - \frac{1}{M_h} F_{yf} \sin\delta_f + u_h(t) \\ v_p \\ u_p(t) \end{bmatrix}, \tag{5.7}$$

Where the term $-\frac{1}{2M_h}C_D\rho_a A_v v_{hx}^2 - \mu g - \frac{1}{M_h}F_{yf}\sin\delta_f + u_h(t)$ is the apparent acceleration. The control input u_h of the host vehicle is applied through its throttle or brake. The curved road coordinate information is available from the digital road map, which is used to calculate the curvature described in the next section.

5.3 Curvature Calculation Method

Horizontal curves provide transitions between two tangent lengths of a roadway, which are required in order to progressively change direction where a direct point of intersection is not feasible, e.g., highways, high speed routes with a steady stream of traffic etc. The radius of horizontal curves can be categorized as small, medium, and large radius curves. The small radius curves with a radius of less than 150 m are characteristic of low-speed roadways, usually below 70 km/h. On high-speed rural roads, such small curves are uncommon and require guideline speed limits, warning signs, or other driver alerts. The medium radius curves with a radius between 150 and 850 m refer to typical curve radii present on rural highways. The design speeds in the medium radius curves ranges between 70 and 120 km/h, which is the normal speed range for high-speed highways. The large radius curves correspond to radii greater than 850 m and the speed is usually above 120 km/h.

There are several methods to accurately calculate the curvature/radius of horizontal curves (Carlson, 2005; Cvitanić & Maljković; 2019). For the following purposes, it is important to calculate the radius of a curved road.

- Set advisory speeds for curve
- Predict operating speeds of vehicles
- Delimit curve spacing measures, such as markers created for retroreflective paving and chevrons
- Carry out traffic safety assessments

- Evaluate road accidents

The most probable way to measure the radius of a curve is usually to look at a sequence of plan sheets stored in the local transport department. Although this is definitely a viable approach for evaluating curve radii, it can also be time-consuming. Also, accessibility to such data is often quite challenging for researchers. Therefore, many scholars, crash investigators, and transport field crew department use a range of radius-estimating techniques, such as field survey, chord length, lateral acceleration, ball bank indicator (BBI), plan sheet, GPS, operating speed, and vehicle yaw rate. In functional terms, the plan sheet method and the GPS approach have the lowest mean relative errors to estimate radii as -0.9% and 1.2%, respectively.

Here we develop a method to calculate varying curvature/radius of a road using (X,Y) coordinate data obtained from the high accuracy digital road map. In particular, we fit circular curves considering three consecutive coordinate points to calculate road curvature. We presume that the curvature is uniform between these points; this assumption is not restrictive if the measurement interval is small (which is easy to achieve). Suppose (X_1, Y_1), (X_2, Y_2), and (X_3, Y_3) be the coordinates of a road and using these coordinates, a circular curve of radius R_c can be formed. The general equation of a circle can be expressed as

$$\mathcal{A}X^2 + \mathcal{A}Y^2 + \mathcal{B}X + \mathcal{P}Y + \mathcal{Q} = 0 \tag{5.8}$$

After substituting the points in (5.8), the set of equations of the circular curve can be represented by the determinant as

$$\begin{vmatrix} X^2+Y^2 & X & Y & 1 \\ X_1^2+Y_1^2 & X_1 & Y_1 & 1 \\ X_2^2+Y_2^2 & X_2 & Y_2 & 1 \\ X_3^2+Y_3^2 & X_3 & Y_3 & 1 \end{vmatrix} = 0 \tag{5.9}$$

The coefficients $\mathcal{A}$, $\mathcal{B}$, $\mathcal{P}$, and $\mathcal{Q}$ are obtained by solving the following determinants

$$\mathcal{A} = \begin{vmatrix} X_1 & Y_1 & 1 \\ X_2 & Y_2 & 1 \\ X_3 & Y_3 & 1 \end{vmatrix}, \qquad \mathcal{B} = -\begin{vmatrix} X_1^2 + Y_1^2 & Y_1 & 1 \\ X_2^2 + Y_2^2 & Y_2 & 1 \\ X_3^2 + Y_3^2 & Y_3 & 1 \end{vmatrix}, \qquad \mathcal{P} = \begin{vmatrix} X_1^2 + Y_1^2 & X_1 & 1 \\ X_2^2 + Y_2^2 & X_2 & 1 \\ X_3^2 + Y_3^2 & X_3 & 1 \end{vmatrix},$$

$$\mathcal{Q} = -\begin{vmatrix} X_1^2 + Y_1^2 & X_1 & Y_1 \\ X_2^2 + Y_2^2 & X_2 & Y_2 \\ X_3^2 + Y_3^2 & X_3 & Y_3 \end{vmatrix}$$

Then, the radius R_c and the curvature $\mathcal{C}$ of the circular curve can be calculated as

$$R_c = \sqrt{\frac{\mathcal{B}^2 + \mathcal{P}^2 - 4\mathcal{A}\mathcal{Q}}{4\mathcal{A}^2}} \tag{5.10}$$

$$\mathcal{K} = \frac{1}{R_c} \tag{5.11}$$

A large value of $\mathcal{C}$ indicates sharp turning and vice-versa. Then the critical velocity $v_{c,\kappa}$ as a function of the radius can be given as

$$v_{c,\kappa} = f\big(R_c(x_h)\big) \approx \zeta f(x_h) \tag{5.12}$$

where $\zeta < 1$ is a positive threshold. For different road-surface conditions (dry, wet, snow, and ice) $v_{c,\kappa}$ is calculates as

$$v_{c,\kappa}(x_h) = \sqrt{\mu_s g R_c} \tag{5.13}$$

where μ_s is the road-surface friction coefficient (lateral friction coefficient with which a vehicle skids on a road) and g is the gravitational acceleration. Note that, $v_{c,\kappa}$ significantly varies with the variation of R_c along the curve. Furthermore, $v_{c,\kappa}$ is highly influenced by μ_s due to considerable change in friction supply to tires. Table 5 shows the friction coefficient μ_s for different road-surface conditions (Zhao et al., 2017). The computational cost of our curvature estimation method above is almost negligible and hence, not difficult to implement.

Table 5: Friction coefficient for various road-surface conditions

Road-surface conditions	**Friction coefficient μ_s**
Dry	1.20
Wet	0.60
Snow	0.20
Ice	0.05

5.4 Model Predictive Control

We recall that the acceleration and braking rates of a vehicle are directly associated with the input force and variation of engine torque. A high level of acceleration or braking is not beneficial for fuel efficiency as well as driving comfort. The proposed MPC-based EDS measures the states of the host vehicle at any time t and derives the optimal velocity trajectory required for an efficient and safe travel in the prediction horizon. Specifically, we formulate an optimization algorithm to calculate the optimal velocity where the constraints of the optimization problem include the constraints for velocity, acceleration, and safe headway. A suitable value of the prediction horizon (analogous with anticipation of human driver) is considered. Since traffic flow experiences significant variation, a long horizon would not be beneficial. The safe headway (distance) s_d of the host vehicle from the preceding vehicle is given as

$$s_d(t) = s_0 + t_{hd}^* v_{hx}(t), \tag{4.6}$$

where s_0 is the minimum spacing between vehicles and t_{hd}^* is the safe (reference) headway time while following the preceding vehicle.

To implement the MPC with state dynamics (5.1) and (5.7), an optimal control problem is solved, where an objective function is minimized at each time t and expressed as

$$J\big(y(t),u_h(t)\big)=\int_{t}^{t+T}[w_1(v_{hx}(t)-v_d)^2+w_2u_h^2(t)+$$

$$+w_3(1+e^{-\sigma(t_{\mathrm{hd}}^{*}-t_{\mathrm{hd}}(t))})^{-1}]\,dt, \qquad (5.13)$$

Subject to

$$v_{\min}\le v_{hx}(t)\le v_{\max},$$
$$\mathrm{u}_{\min}\le u_h(t)\le u_{\max},$$
$$v_{hx}(t)-v_{\max,\mathrm{r}}(x_h)<0,$$
$$x_p(t)-x_h(t)\ge S_d(t),$$

where T is the prediction horizon from current time t, v_d is the constant desired velocity, σ is a positive constant, and w_1, w_2, and w_3 are the weighting factors related to the velocity, acceleration, and safe distance terms, respectively. The first term of the objective function implies a penalty when the host vehicle's current speed deviates from v_d. The second term reflects the cost of the vehicle's acceleration force on the horizontal curve. The third term represents a penalty because of the deviation from the reference headway, which gives a high value if the host vehicle is near the preceding vehicle and a negligible value when the preceding vehicle is far. The maximum velocity at various locations of the horizontal curve is calculated as $v_{\max,\mathrm{r}}(x_h)=\min(v_{\mathrm{c},\kappa},v_{\max,\iota})$, where $v_{\max,\iota}$ is the speed limit of the road. Thus, the optimization considers both R_c and μ_s to control the trajectory of the host vehicle dynamically. The smooth variations of speed with respect to the curvature and road-surface can significantly improve fuel economy and CO_2 emission of the host vehicle.

5.5 Simulation Results and Discussion

To implement the proposed EDS for horizontal curved roads we developed a simulation framework in MATLAB and solved a nonlinear constrained optimization problem (described in (5.12)) in discrete time using a

nonlinear programming solver in the optimization toolbox. For real-time implementation the sequential quadratic programming (SQP) algorithm is used inside the solver, which is standard and widely used algorithm for nonlinear optimization. In this method, the function solves a quadratic programming (QP) sub-problem at each iteration. The computation time of the algorithm is in 100-200 millisecond range, which is within the expected range for real-time implementation.

The parameters of the host vehicle are chosen as $M_h = 1000$ kg, $C_D = 0.32$, $\rho_a = 1.184$ kg/m^3, $A_h = 2.5$ m^2, $g = 9.8$ m/s^2, $\mu = 0.015$, $l_f = 1.4$ m, $l_r = 1.4$ m, $C_{\alpha f} = 59000$ N/rad, and $C_{\alpha r} = 59000$ N/rad. The safe time headway t_{hd}^* and the minimum spacing s_0 parameters are set as 1.5 s and 7 m, respectively. The desired velocity v_d of the MPC is set as 22.23 m/s (80 km/h), and the velocity and acceleration constraints are set as $v_h \in [0, 26]$ m/s and $u_h \in [-5, 2]$ m/s^2, respectively. The speed limit $v_{\mathrm{max,r}}$ of the road is set as 25 m/s (90 km/h). The simulation step is set at $dt = 0.5$ and the prediction horizon is chosen as $T = 10$ s, which is divided into 20 steps. The initial position x_h and velocity v_{hx} of the host vehicle are set at $x_h(0) = 0$ m and $v_{hx}(0) = 22.23$ m/s (80 km/h). The parameters of the IDM are set as $v_d = 80$ km/h, $s_0 = 2$ m, and $t_{\mathrm{hd}}^* = 1.5$ s with maximum acceleration and comfortable deceleration of 1.5 m/s^2 and -2.5 m/s^2, respectively.

We evaluate the effectiveness of the proposed EDS using microscopic traffic simulations for different curvatures and road-surface conditions, and benchmarked with the TDS. To investigate vehicle fuel consumption and CO_2 emission rates, a well-known fuel consumption and emissions model called the VT-Micro model is used (Rakha et al., 2004). A single lane representative horizontal curved road with various curvatures (radii) is considered for the simulation. The curved road profile (in the XY coordinate) and the curve angle are shown in Figure 31(a) and (b), respectively. The sequencing of curves is set according to the design guidelines for the Asian highway network, where the greater radius curve is followed by the smaller radius horizontal curve at a

ratio of not more than 1.5 and consecutive curves is separated by a straight section in addition to transition curves. The centre of the curves are located at 550 m, 980 m, and 1540 m along the route with the maximum radius of 175 m, 215 m, and 250 m, respectively. Figure 32 and 33 show the simulation results of speed trajectories, acceleration profiles, instantaneous fuel consumption, and CO_2 emission and for dry and wet (rainy) road-surface conditions, respectively.

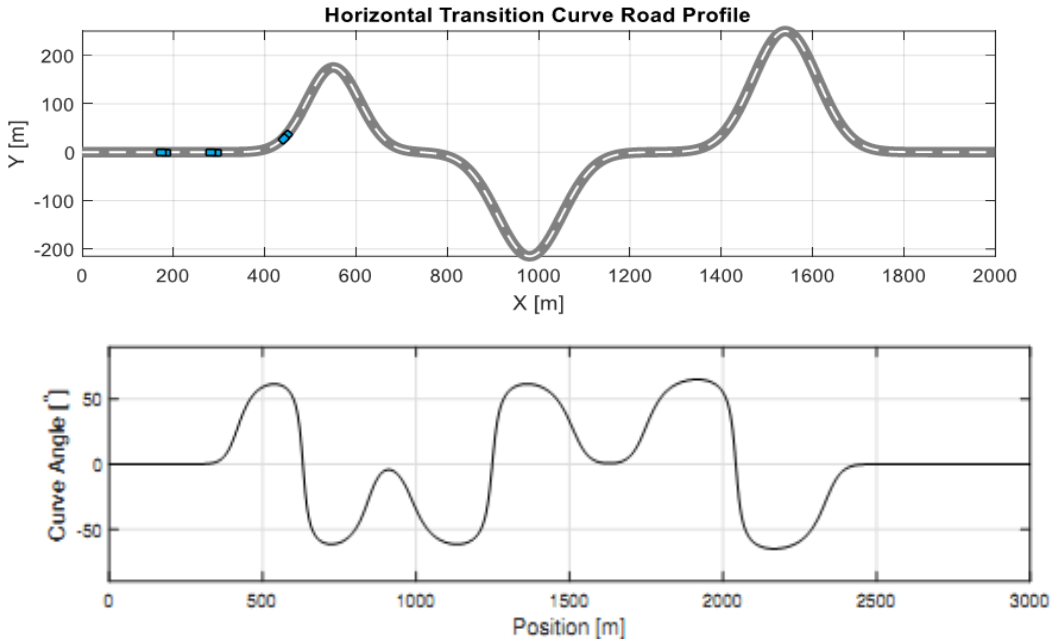

Figure 31: (a) The horizontal curved road profile in the XY coordinate system and (b) the curve angle.

When approaching the curve, the TDS rapidly slows down by generating appropriate control actions, travels up to the middle of the curve, and then quickly accelerates back to the initial velocity. Such rapid variations in motion, deceleration, and acceleration affect fuel consumption and CO_2 emission of vehicles on a curved road. In addition to the curvature effect, road-surface conditions affect human driving behaviour and drivers tend to perform unnecessary acceleration and braking, while delivering extra effort to control the vehicle when the road-surface condition is wet. These actions cause additional fuel consumption and CO_2 emission.

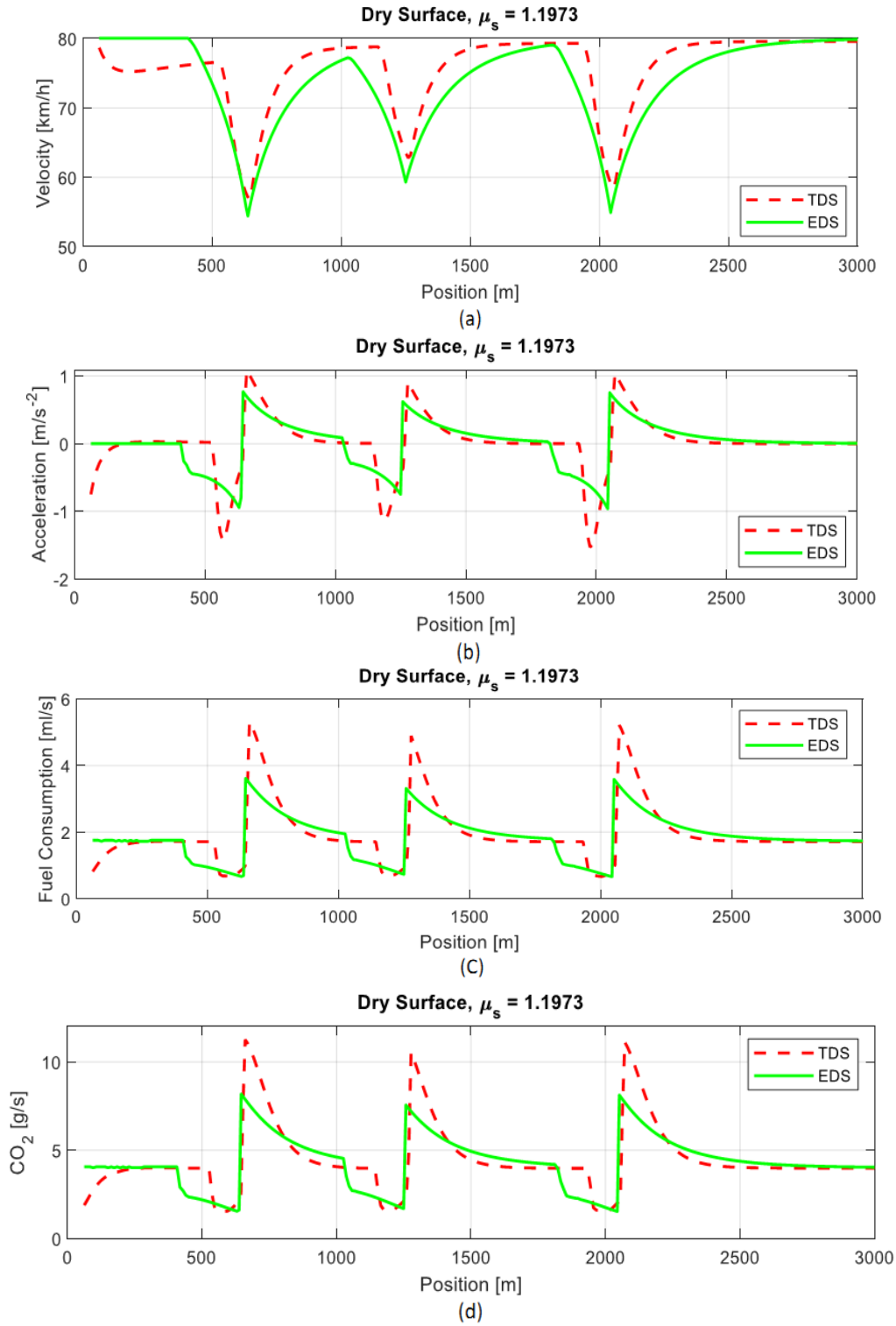

Figure 32: Drive under dry surface condition. (a) Speed trajectories, (b) acceleration profiles, (c) instantaneous fuel consumption, and (d) instantaneous CO_2 emission for the EDS and the TDS.

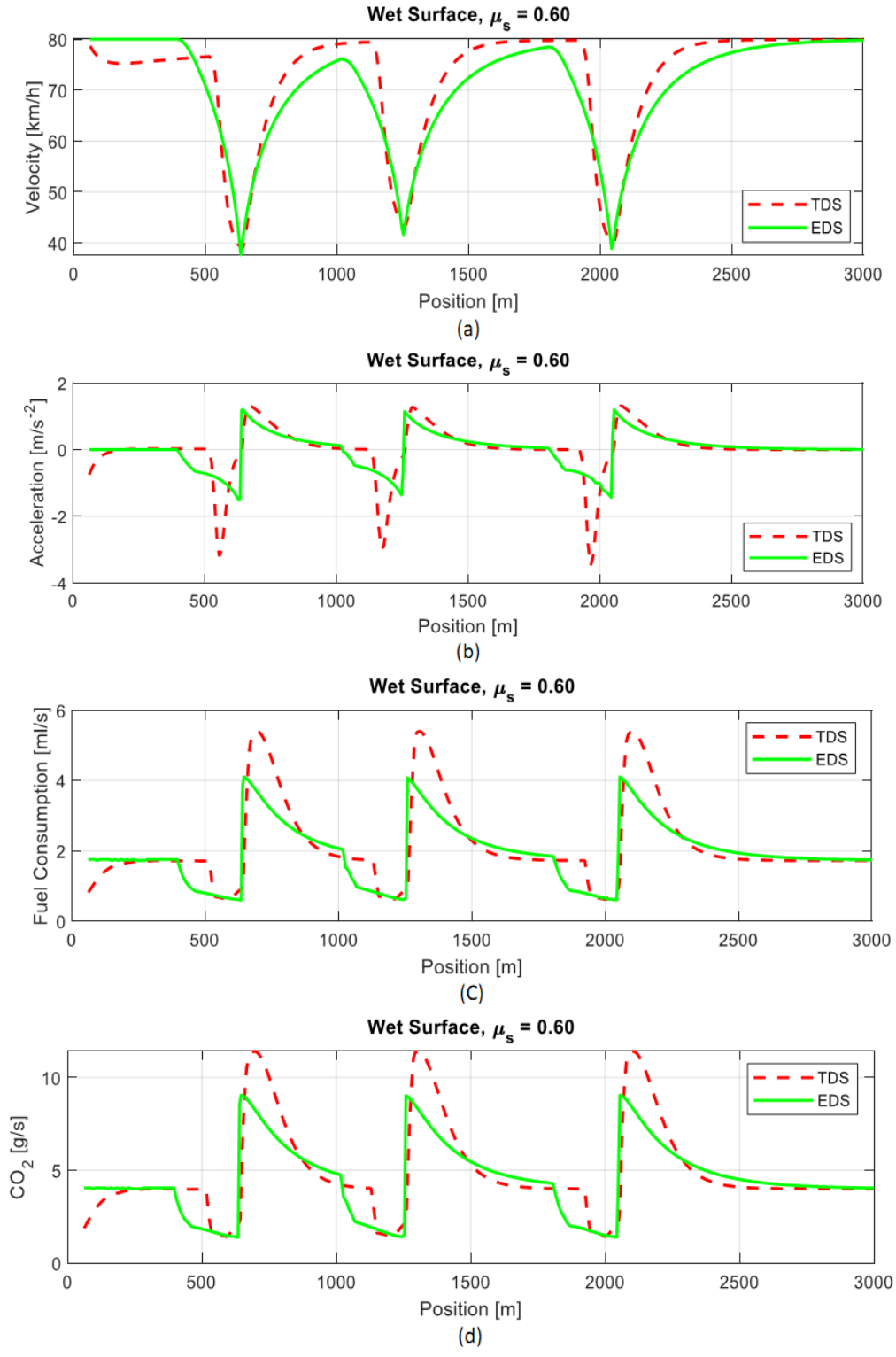

Figure 33: Drive under wet surface condition. (a) Speed trajectories, (b) acceleration profiles, (c) instantaneous fuel consumption, and (d) instantaneous CO_2 emission for the EDS and the TDS.

On the other hand, during winter season, the road-surface is usually covered with snow in many countries. Driving on snow surface becomes difficult as the road friction μ_s (to tires) decreases considerably and drivers cannot realize that fact to adjust their speed sufficiently. Sometimes, there is a thin coating of glaze ice (formed about the freezing point) on the road-surface, which is even more challenging because it is invisible and is called the *black ice*. Figure 34 and 35 show the simulation results for snow and ice road-surface conditions, respectively.

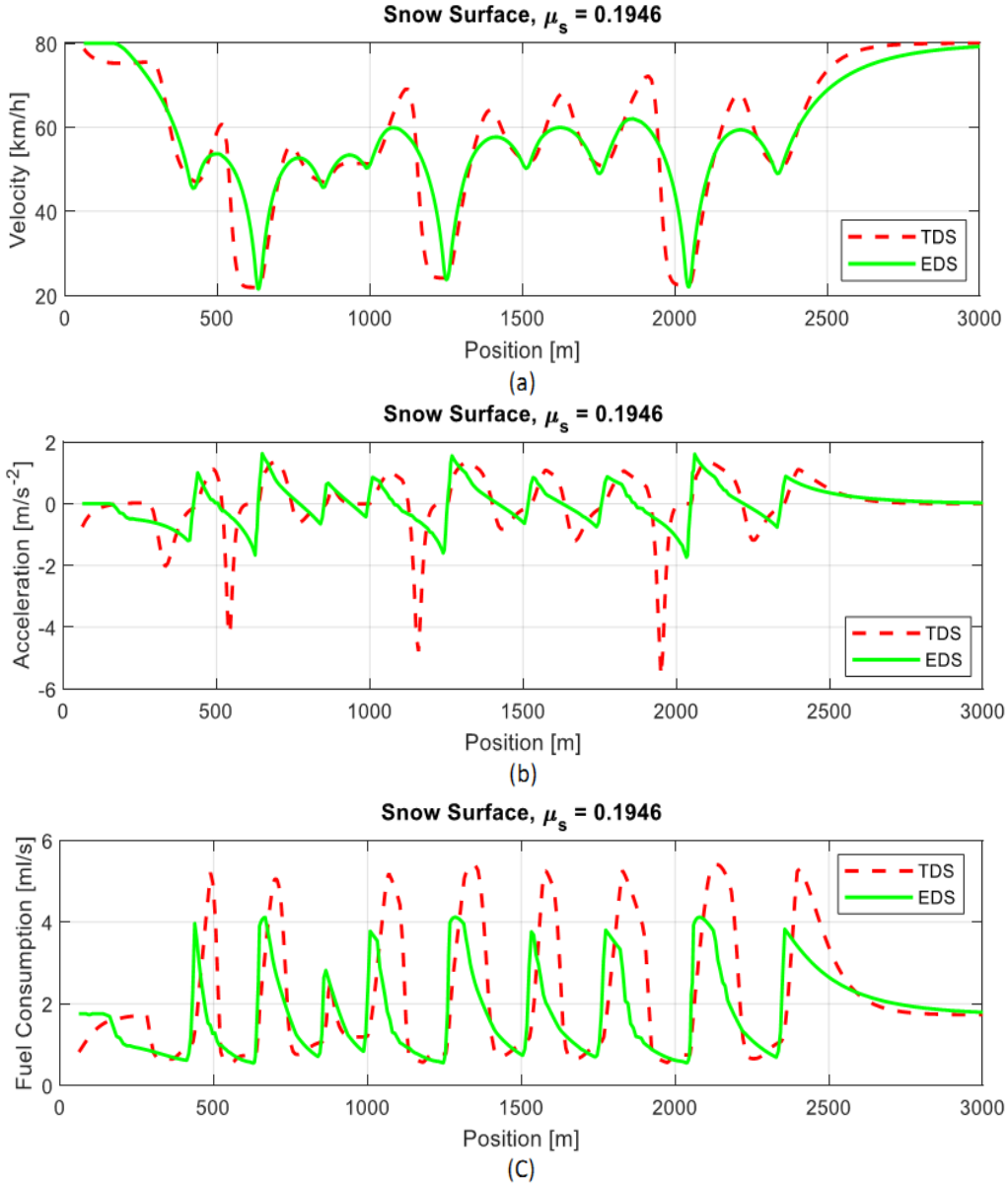

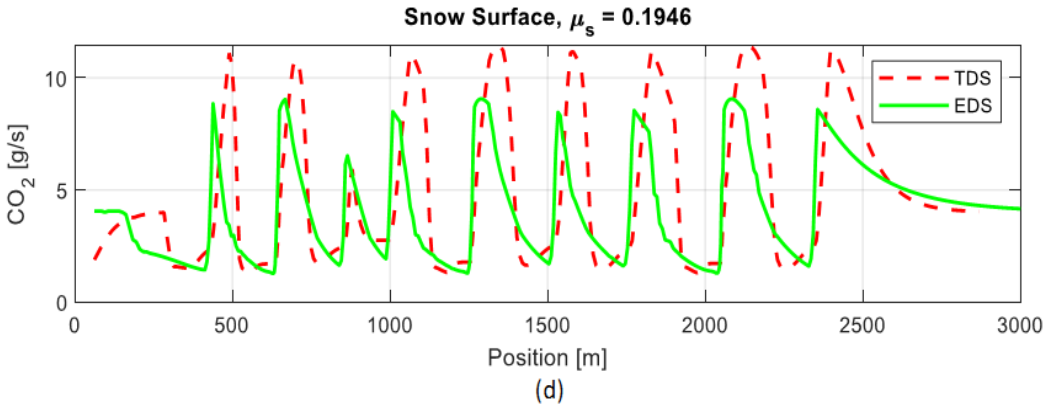

Figure 34: Drive under snow surface condition. (a) Speed trajectories, (b) acceleration profiles, (c) instantaneous fuel consumption and (d) instantaneous CO_2 emission for the EDS and the TDS.

It is found that for various road-surface conditions the EDS performs much better than the TDS. This is due to the fact that when traversing the horizontal curve the EDS vehicle smoothly varies its velocity and keeps the acceleration (control input) in the optimal level considering road-curvatures and road-surface conditions. Figure 36(a) and (b) show the simulation results of total fuel consumption and total CO_2 emission. Table 6 summarizes the comparison between the TDS and the EDS of the host vehicle for different road-surface conditions when driving along the horizontal curves. It is found that the proposed EDS saves fuel by 4.5–10.2% and reduces CO_2 emission by 3.4–8.2% compared to the traditional human driving. These findings illustrate the potential of the proposed EDS to be superior to conventional human driving in reducing fuel consumption and CO_2 emission.

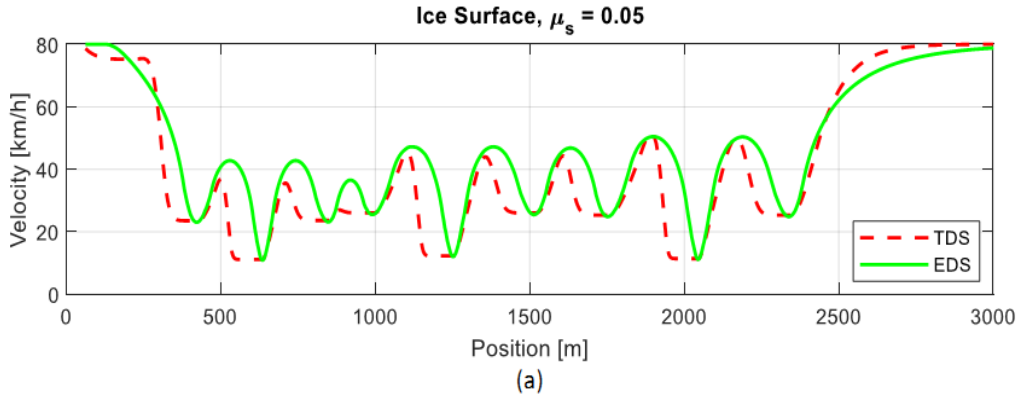

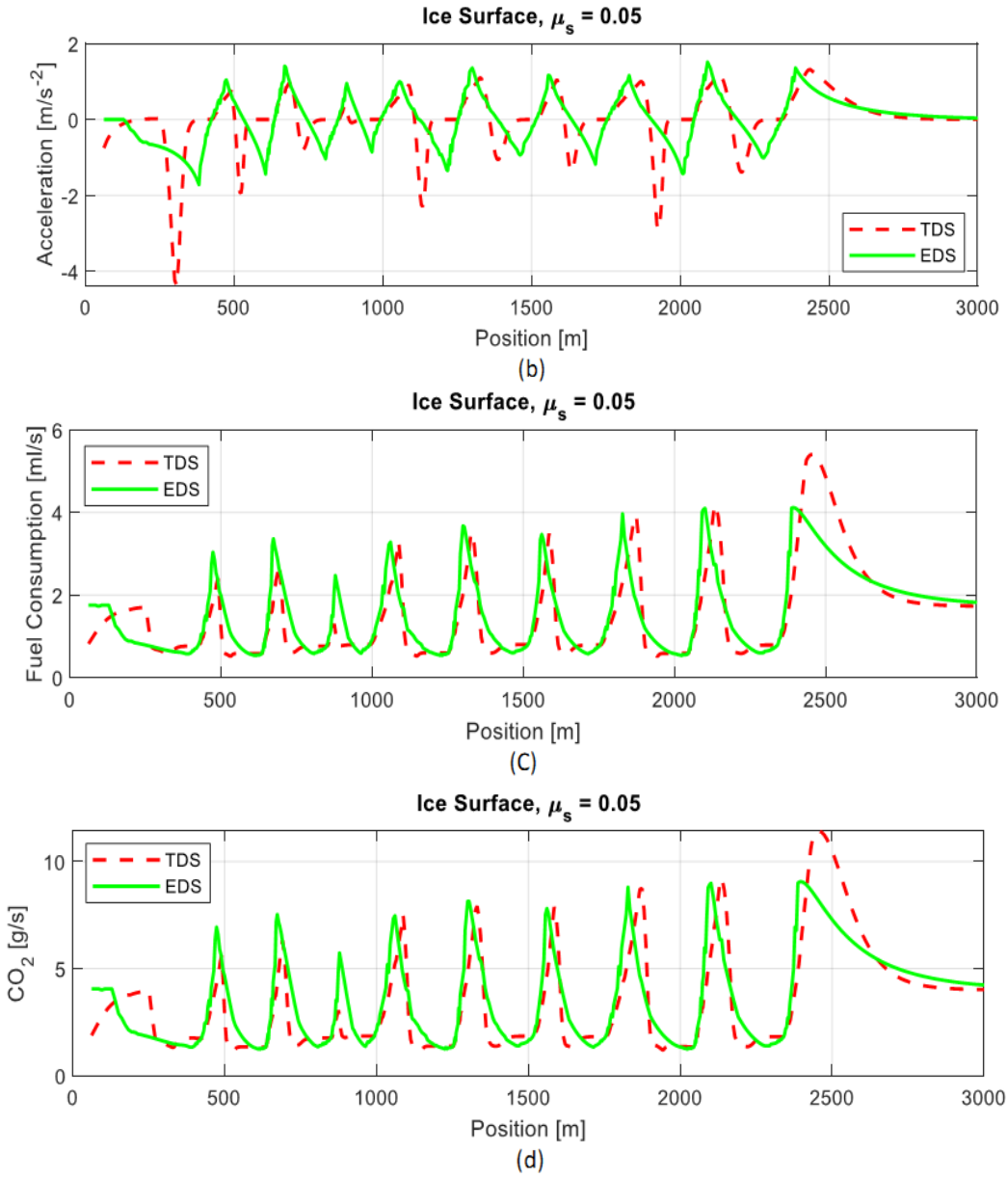

Figure 35: Drive under snow surface condition. (a) Speed trajectories, (b) acceleration profiles, (c) instantaneous fuel consumption, and (d) instantaneous CO_2 emission for the EDS and the TDS.

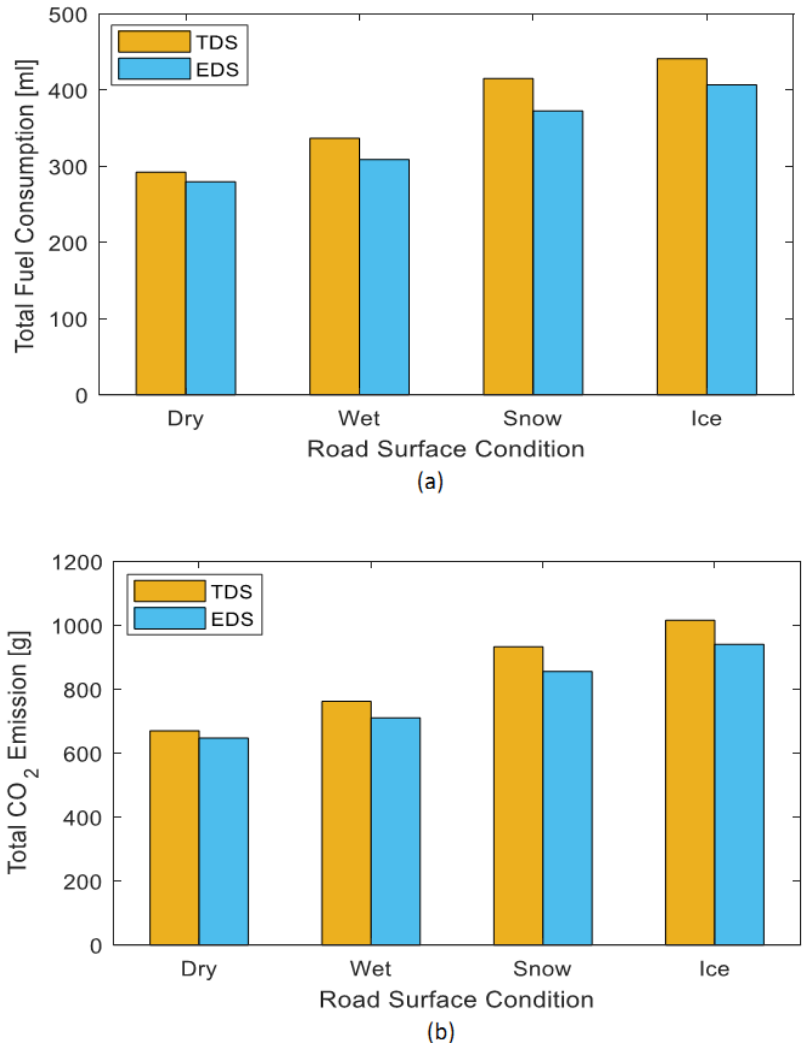

Figure 36: Comparison of (a) total fuel consumption and (b) total CO_2 emission between the EDS and the TDS.

Table 6: Performance comparison between the TDS and the EDS for various road-surface conditions

	Total Fuel Consumption [ml]		**Total CO_2 Emission [g]**		**% Fuel Savings**
	TDS	EDS	TDS	EDS	
Dry Surface	292.04	279.41	669.98	646.96	4.5
Wet Surface	336.69	308.65	761.87	710.22	8.4
Snow Surface	414.99	372.54	932.49	855.65	10.2
Ice Surface	441.14	406.84	1015.32	940.39	7.9

5.6 Summary

In this chapter, we have developed a novel dynamic EDS using MPC that reduces fuel consumption and CO_2 emission of a host vehicle on horizontal curves with various curvatures and road-surface conditions. We derived a method to precisely calculate the curvature and formulate a nonlinear optimization problem considering the host vehicle's longitudinal motion dynamics, state of the preceding vehicle, information of curvature, and road-surface conditions. The proposed EDS maintains proper deceleration when approaching a tangent to curve and then accelerates with an appropriate acceleration level after passing the middle of the curve, which ensures the minimum energy waste due to acceleration/braking. Hence, the EDS keeps the fuel consumption in the optimum level and performs much better than the traditional human driving system. Based on the scenario and various road-surface conditions, the fuel-saving capability of the proposed EDS ranges from 4.5-10.2%, while ensuring driving safety.

In future research, we will investigate traffic flow performance for different penetration rates of the EDS vehicle under mixed-automated vehicle environment. Also, we will extend the model for multi-lane traffic flow.

Chapter 6

6 Eco-driving Strategy for Roundabouts

Uncoordinated merging of vehicles is one of the main causes of traffic congestion in roundabouts, which directly affects travel time, fuel consumption, and emissions of individual vehicles. Connected vehicle technologies along with the cooperative control of automated vehicles (AVs) can play an important role to improve traffic flow performance in a roundabout. Therefore, to improve driving scenarios in the existing roundabout environment, here we have developed a novel roundabout coordination system (RCS) for AVs to achieve eco-driving (fuel-efficient driving) as well as safe and smooth traffic flows under a connected vehicle environment. Previous research on vehicle control strategies for roundabouts (Section 2.4) mainly developed ramp metering signal control systems to improve mobility and safety during peak hours. But it is expensive to upgrade traffic signal infrastructures and also, modern roundabouts do not encourage the use of ramp metering because it has been proven that a roundabout is more efficient than a signalized intersection. Our proposed method does not require ramp metering to improve traffic performance at roundabouts. Existing roundabout coordination systems for CAVs did not investigate different traffic demands on the roundabout capacity. Our proposed method can deal with different traffic demands up to the capacity of the roundabout.

The coordination of vehicles is implemented in a bi-level framework using a roundabout coordination unit (RCU), where in the higher level, vehicles in the entry lane approaching the roundabout are coordinated to form clusters based on traffic flow volume, whereas in the lower level, the vehicles' optimal sequences and roundabout merging times are calculated by solving a combinatorial optimization problem using a receding horizon control (RHC) approach. The proposed RCS aims to minimize the total time taken for all

approaching vehicles to enter the roundabout, whilst minimally affecting movement of circulating vehicles. Using microscopic simulations, we demonstrate the effectiveness of the RCS, comparing against the current traditional roundabout system (TRS) for various traffic flow scenarios. The results show that the proposed RCS produces significant improvement in traffic flow performance, e.g., average velocity, average fuel consumption, and average travel time in the roundabout. The work in this chapter is being reviewed by the IEEE Transactions on Intelligent Transportation Systems.

The rest of this chapter is organized as follows. In Section 6.1, we describe the fundamental concept of the proposed roundabout coordination system (RCS). In Section 6.2, we develop traffic flow modeling in a four-leg roundabout. In Section 6.3, we formulate the optimization problem including higher level coordination and lower level coordination. We present simulation results in Section 6.4 and finally, Section 6.5 gives the summary of the chapter.

6.1 Fundamental Concept

The concept of the proposed bi-level roundabout coordination system in a connected vehicle environment is illustrated in Figure 37. We consider an unsignalized four-legged single-lane roundabout; the legs are equally spaced at 90˚, and each leg has an entry and an exit lane. We consider a roundabout coordination unit that can communicate in two-ways (I2V and V2I) with negligible delay to globally coordinate the vehicles. The full signal coverage range of the RCU is about 200 meters. The vehicles frequently transmit their information, such as the current position and velocity to the RCU within the coverage range. For simplicity, all vehicles are assumed to be automated; such an assumption is reasonable, as traditional connected vehicles can be considered to comply with speed advice generated by the RCU.

Specifically, we define two zones for the implementation of the bi-level coordination, namely the *clustering zone* and the *merging-execution zone*. As shown in Figure 37, we define the clustering zone as the road segment

between 60 m to 200 m from the roundabout merging point, and the merging execution zone is from the merging point to 60 m away (between the merging point and the clustering zone). The RCU then determines if it is necessary to form a cluster; if necessary, then vehicles in the clustering zone will be directed to form clusters. In the merging-execution zone, the RCU computes the optimal sequence of merging and merging time at each of the four merging points simultaneously. Based on that information, the vehicles locally decide their required acceleration for smooth and safe merging at the roundabout.

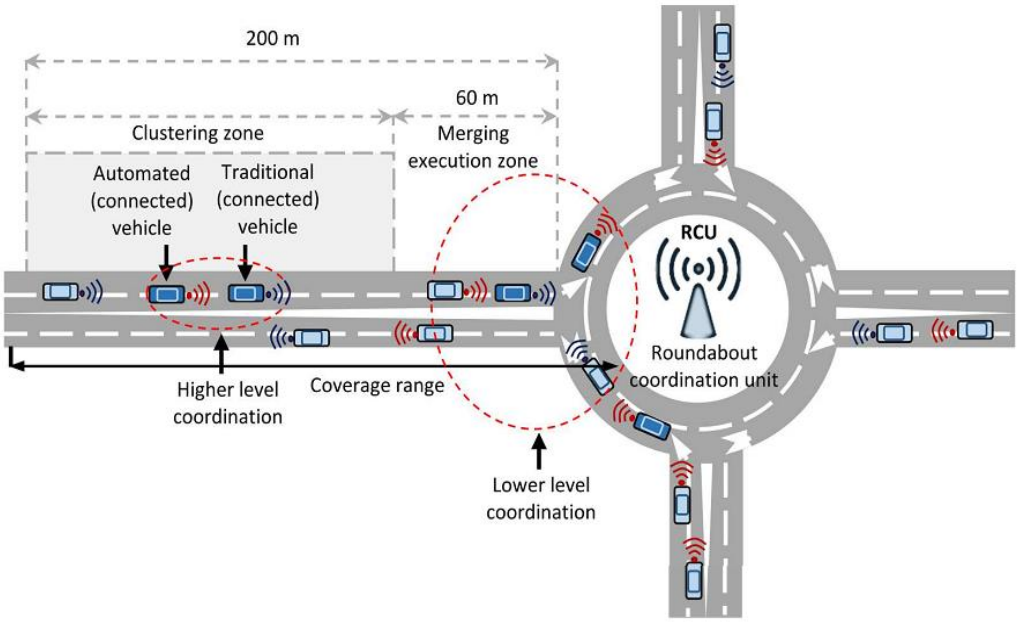

Figure 37: Fundamental concept of the proposed roundabout coordination system (RCS).

6.2 Traffic Flow Modeling

The position and velocity of vehicle i at time t are calculated using the kinematic equation given by

$$x_i(t+1) = x_i(t) + v_i(t)\Delta t + 0.5u_i(t)\Delta t^2,$$
$$v_i(t+1) = v_i(t) + u_i(t)\Delta t, \tag{6.1}$$

where x_i, v_i, and u_i are the position, velocity, and input acceleration of vehicle i, respectively, and Δt is the step size. The controller of vehicle i uses the

information of its preceding vehicle i-1 to decide a safe control acceleration u_i as

$$u_i(t) = f(x_i(t), v_i(t), x_{i-1}(t), v_{i-1}(t), v_i(t)\ ), \tag{6.2}$$

where $f(\cdot)$ is the driving decision function (which could possibly be an adaptive cruise control (ACC) or a car-following model), and v_i is the target speed, which is generated by the automated vehicle according to the instruction given by the RCU.

The traffic flow volumes in veh/min of the four-legged roundabout can be given by the entry flows q_κ, circulating flows ρ_κ, merged flows σ_κ, and exit flows p_κ with respect to each merging junction $\mathrm{J}_{\kappa\in\{1,2,3,4\}}$ as shown graphically using a single-line flow diagram (SLFD) in Figure 38. A guidance on permissible entry flow and circulating flow rates with respect to the number of lanes within a roundabout can be found in (Rodegerdts, 2010) and is shown in Figure 39. Traffic flow at each junction J_κ can be given by the following relationship

$$\mathrm{J}_\kappa : \begin{bmatrix} \sigma_\kappa = q_\kappa + \rho_\kappa, \\ \rho_\kappa = \sigma_{\kappa-1} - p_\kappa, \end{bmatrix} \quad \kappa \in \{1,2,3,4\}, \tag{6.3}$$

where σ_0 is understood as σ_4. Using (6.3) the flows ρ_κ of traffic in the roundabout can be obtained using the measured entry flows q_κ and exit flows p_κ. As all vehicles are connected, these flows over a certain time interval, e.g., 1 min, can be directly obtained. Such information of the entry flows and circulating flows is required to determine the necessity of vehicle clustering before entering the merging zone. Vehicle clustering is important because it requires a minimum time to merge in the roundabout than individual vehicles. As there is limited space within the roundabout, the coordination which can be achieved is also limited. A coordination performed before the vehicles are approaching the roundabout merging point will also help more efficient coordination.

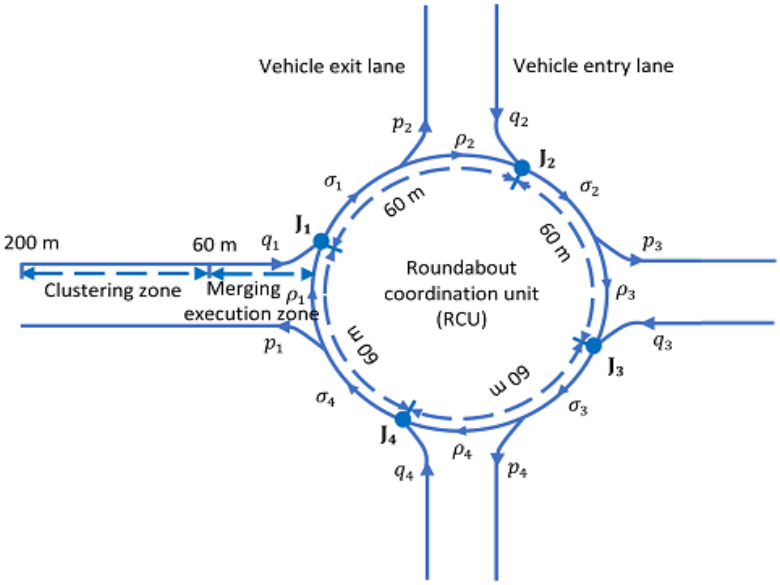

Figure 38: Single-line flow diagram (SLFD) of a single lane four-legged roundabout with four merging junctions.

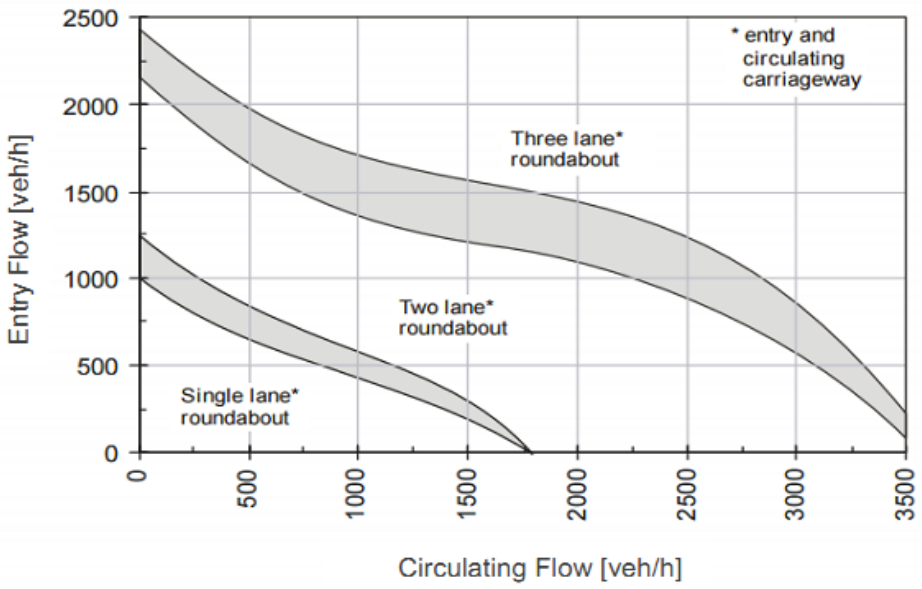

Figure 39: Roundabout entry flow and circulating flow rates with respect to the number of lanes.

6.3 Formulation of Optimization Problem

In this section we formulate the optimization problem including higher level coordination and lower level coordination.

6.3.1 Higher Level Coordination

A vehicle can simply follow another vehicle on the same lane with a minimum following gap of f_g sec, and both vehicles can pass over the merging point if there is no vehicle approaching from the other (circulating) lane. However, when a vehicle passes the merging point after or before a vehicle from the other lane, it requires additional safety merging gap m_g sec, i.e., two vehicles from different lanes at the merging point requires at least a time gap of m_g sec. Therefore, a pattern involving only a single vehicle merging between two circulating vehicles may slow down the overall traffic flows and reduce the capacity of the roundabout. Considering that fact, a *higher level coordination* is incorporated into the RCS to direct adjacent vehicles in the clustering zone to form clusters (or platoons) for smooth merging prior to entering the merging-execution zone. The function of the higher level coordination is described in this sub-section.

Initially, the necessity of forming clusters is determined using the information of traffic flow rates. At any junction, J_κ, using the entry flow rate q_κ (veh/min) and the circulating flow rate ρ_κ (veh/min), the number of vehicles (per minute) that leads a cluster, which corresponds to the required number of clusters (per minute) is determined by

$$n_\kappa = \frac{60 - f_g(q_\kappa + \rho_\kappa)}{m_g}. \tag{6.4}$$

When the total traffic flow $(q_\kappa + \rho_\kappa)$ at merging point J_κ exceeds its capacity, the number of clusters becomes $n_\kappa < 1.0$, means all vehicle should form a single cluster. Such an over-saturated traffic condition may create evolving queues and congestion at the roundabout. From the number of clusters n_κ, the recommended cluster size (the average number of vehicles in the cluster) s_κ in the entry flow is calculated as

$$s_\kappa = \frac{q_\kappa}{\max(1, n_\kappa)}. \tag{6.5}$$

When $s_\kappa > 1$, some vehicles will need to form clusters, so that the lower level coordination can facilitate smooth merging and avoid a long queue.

Specifically, as illustrated in Figure 40, the RCU coordinates the clustering by calculating recommended speeds for the vehicles in the entry lane. When vehicle i enters the clustering zone, the required possible set of speed of vehicle i to reach the end of the clustering zone (at a distance d_i) are obtained, based on the recommended arrival time of (preceding) vehicle $i-1$. Then, the RCU calculates the required speed v_{jci} for vehicle i to join a cluster (jc) with vehicle $i-1$, whilst maintaining a projected time gap f_g as

$$v_{jci} = \frac{d_i}{\tau_{i-1} + f_g}, \tag{6.6}$$

where $\tau_{i-1} = d_{i-1}/v_{i-1}$ is the estimated arrival time of the preceding vehicle at the end of clustering zone. If it is not possible to form a cluster with the preceding vehicle, then vehicle i will start a (new) cluster (sc) with its following vehicle (if any), by maintaining a gap $c_g = f_g + m_g$ with vehicle $i-1$ (such that a circulating vehicle can pass through), then the corresponding required speed v_{sci} is calculated as

$$v_{sci} = \frac{d_i}{\tau_{i-1} + c_g}. \tag{6.7}$$

If there is no following vehicle, then vehicle i will drive at its desired speed v_d. Using the actual speeds v_{jci} and v_{sci}, as well as the desired speed v_d, we can calculate v_{reci}, which is the recommended speed for the automated vehicle as

$$v_{reci} = \begin{cases} v_{jci}, & if\ v_{sci} \le v_{jci} \le v_{max}, \\ v_{sci}, & if\ v_{jci} \ge v_{max}, v_{sci} \le v_{max}, \\ v_d, & otherwise, \end{cases} \tag{6.8}$$

where v_{max} is the maximum allowable cluster speed that can be adjusted according to the desired cluster size s_κ. The local controller of each automated vehicle utilizes this $v_i = v_{reci}$ to compute the acceleration using

(6.2) and safely drive. In this way, the difficulty in merging is reduced, by flexibly coordinating the arrival patterns of automated vehicles.

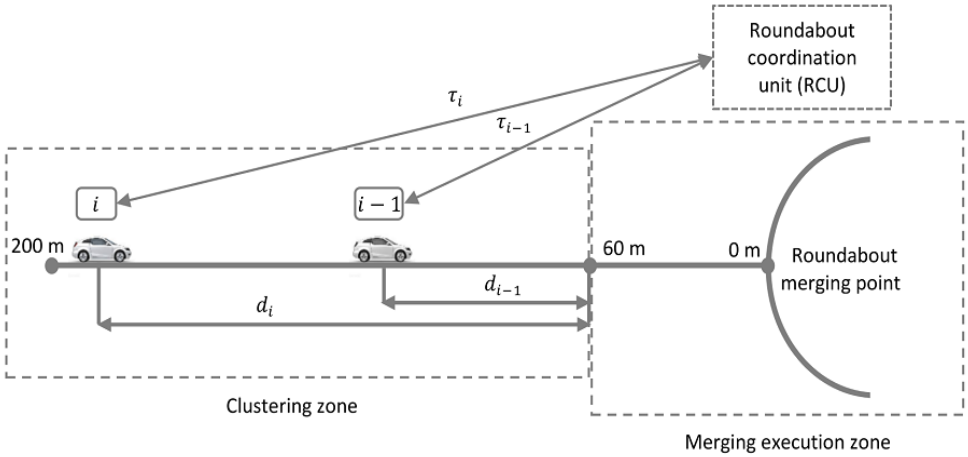

Figure 40: Clustering principle in the higher level coordination.

6.3.2 Lower Level Coordination

The main problem that causes vehicles to stop prior to entering a roundabout is that they arrive at the merging point almost at the same time of a circulating vehicle. When this happens, the entering vehicles decelerate or stop, increasing fuel consumption and travel time, whilst decreasing average velocity and overall roundabout capacity. Hence, to prevent collision or aggressive braking and minimize idling time, the lower level coordination calculates the optimal time for each vehicle to arrive at the merging point. To mitigate for any abrupt and unforeseen changes in traffic flow, the optimal merging algorithm is implemented successively using a receding horizon control approach. Note that if a group of vehicles comes as a cluster (from the clustering zone), then very likely the merging algorithm will allow them to merge as a cluster, which will minimize the waiting time at the merging point.

A lower level controller for each junction J_κ is used to obtain the optimal merging sequence and timings for the vehicles in both the entry and circulating lanes approaching the merging point. The controller considers the vehicles in both the roundabout circulating lane segment (r) and entry lane (e) of the merging-execution zone as shown in Figure 41. Let $\mathcal{E}$ and $\mathcal{R}$ be the tuples of

vehicles in a sequence on the entry lane (n vehicles) and circulating lane (m vehicles), respectively, given by

$$\mathcal{E} = \{e_1, e_2, \dots\dots, e_n\}, \qquad \mathcal{R} = \{r_1, r_2, \dots\dots, r_m\},$$

where e_1 and r_1 are the vehicles closest to the merging point on the respective lanes. For simplicity, junction index κ is omitted in this description.

Let v_α be the speed and d_α the distance to the immediate merging point of vehicle $\alpha \in \mathcal{E} \cup \mathcal{R}$. We assume that vehicle α decreases its speed linearly to merge in the roundabout. Thus, the unrestrained time a vehicle takes to arrive at the merging point is given by

$$\tau_\alpha = f_{merge}(v_\alpha, d_\alpha, \psi_\alpha) = \frac{d_\alpha}{\frac{1}{2}(v_\alpha + \psi_\alpha)}, \tag{6.9}$$

where ψ_α is the recommended merging-speed. The optimal merging sequence of the set of vehicles $\mathcal{E} \cup \mathcal{R}$ is obtained considering the constraint that a vehicle is not allowed to overtake on the same lane. Therefore, the search space or the feasible solutions$\Omega$of the merging sequences can be given by a tuple as

$$\Omega = \begin{cases} W = (w_1, w_2, \dots\dots, w_{n+m}) | \forall w_i \in \mathcal{E} \cup \mathcal{R} \\ s.t. \begin{bmatrix} w_i \neq w_j, \ \ for\ \forall i \neq j, \\ \tau_{wi} < \tau_{wi+1}, \ \ for\ w_i, w_{i+1} \in \mathcal{E} \\ \tau_{wi} < \tau_{wi+1}, \ \ for\ w_i, w_{i+1} \in \mathcal{R} \end{bmatrix} \end{cases} \tag{6.10}$$

where, for brevity, the first vehicle in W (i.e., w_1) passes the merging point first, and the rest follows sequentially. According to (6.10), a vehicle can only be picked one time in W from $\mathcal{E} \cup \mathcal{R}$ and a following vehicle on the same lane cannot appear before its preceding vehicle.

The objective of the lower level coordination is to obtain the optimal sequence W^* of merging by solving

$$\min_{W \in \Omega} J(W) = \sum_{i=1}^{n+m} \beta_{wi}\, \tau^*_{wi}, \tag{6.11}$$

where $\boldsymbol{\beta_{wi}}$ denotes the weight of individual vehicle and $\boldsymbol{\tau^*_{wi}}$ is the optimal passing time of a vehicle $\boldsymbol{w_i}$ for a given feasible sequence $\boldsymbol{W}$, which is obtained successively for $i = 1,2, \dots \dots, n+m$, as

$$\tau^*_{wi} = \max\left(\tau_{wi}, \tau^*_{wi} + \gamma(\, w_{i-1},\, w_i)\right), \tag{6.12}$$

where τ_{wi} is the unrestrained arrival time obtained from (6.9), and $\gamma(\, w_{i-1},\, w_i)$ denotes the minimum time gap between two vehicles at the merging point given by

$$\gamma(\, w_{i-1},\, w_i) = \begin{cases} \delta_e, & if\ \ w_{i-1},\, w_i \in \mathcal{E}, \\ \delta_r, & if\ \ w_{i-1},\, w_i \in \mathcal{R}, \\ \delta_m, & otherwise, \end{cases} \tag{6.13}$$

$\delta_e, \delta_r,$ and δ_m denote the minimum time gaps between two successive vehicles at the merging point according to their originating lanes.

The above problem falls into the class of combinatorial optimization, and computation time rises drastically with the number of instants or vehicles. Therefore, we optimize only four vehicles at a time, i.e., two from each lane ($n = 2, m = 2$) in a successive optimization technique as shown in Figure 41. Such an approach is reasonable, because in a short distance between two merging points, there will usually be no more than two vehicles in a steady flow condition. Even when three or more vehicles are present in a lane, the motion of the 3rd vehicle onwards are optimized successively after the leading vehicle has merged, i.e., multiple optimization problems are solved successively.

As there are four elements (vehicles) in $\mathcal{E} \cup \mathcal{R}$, there are 6 feasible combinations of vehicle sequences considering the vehicle order constraints in the same lane as (6.10). Hence, the optimization (6.10) is simplified as to pick one of the six possible combinations given in Ω using a brute-force algorithm that systematically computes all possible candidates for the solution. Even if multiple optimization problems need to be resolved successively, the total computation time will remain relatively short.

Once the optimal sequence W^* of vehicles is determined, each vehicle receives the corresponding recommended merging time τ_{wi}^*, and determines the desired speed by considering the distance to the merging point. However, the final merging into the roundabout s only executed if there is sufficient safety gap, according to the lane change model called minimizing overall braking induced by lane change (MOBIL) (Kesting et al., 2007). Specifically, according to MOBIL, a merging manoeuvre is only executed if estimated acceleration of the merging entering vehicle on the roundabout is higher than -4.0 m/s^2. When a vehicle or a cluster of vehicles enters the roundabout, the controller will optimize movements of the next set of vehicles, by repeating the movements of remaining vehicles optimized previously. Thus, the controller successively uses the receding horizon approach to mitigate for inaccurate estimation and prediction, or any changes in vehicle states.

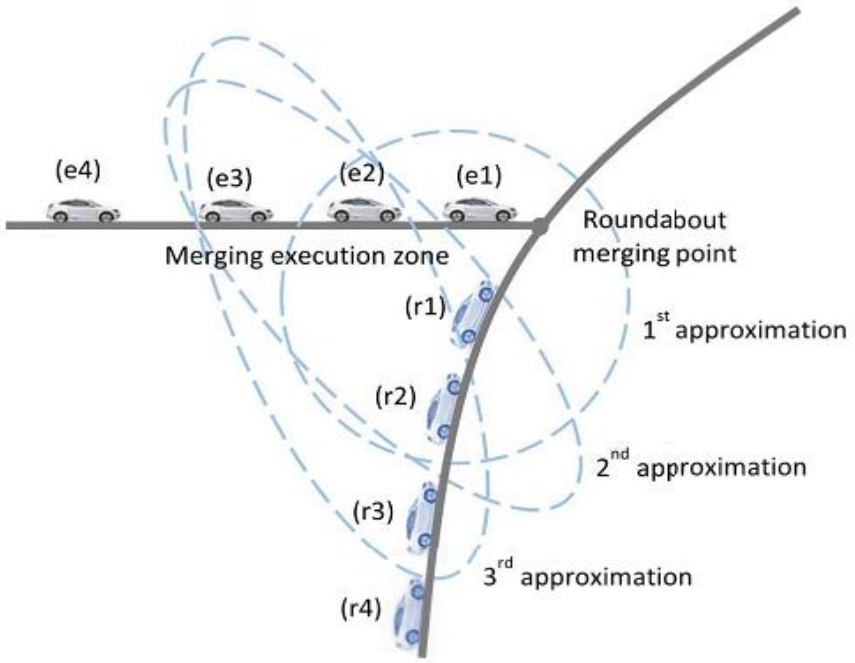

Figure 41: Successive optimization of vehicles in a receding horizon approach in the lower level coordination.

6.4 Simulation Results and Discussion

To demonstrate the effectiveness of the proposed RCS, we have developed a simulation environment in MATLAB. The roundabout has 4 legs, each with an entry and exit lane, and equally spaced at the roundabout and named North, South, East, and West lanes. Referring to Figure 27, the circumference of the roundabout is set at 240 m long, while the distance between two merging points is 60 m. Each entry (approaching) lane is considered 300 m long. The control zones, i.e., the clustering zone and the merging execution zone are 140 m and 60 m, respectively. The RCU coverage radius is considered as 250 m (according to IEEE 802.11p). The arrival of vehicles in the entry lanes is given randomly in the simulation using Poisson distribution for different traffic flow rates. The intelligent driver model is used as the vehicle controlled function (6.2), with different values of parameters for human driven vehicles and automated (or ACC) vehicles (Kesting et al., 2008). Each vehicle is 5 m long, with a flow gap of $f_g = 1$ sec and a merge gap of $m_g = 2.5$ sec for AVs. These time gaps are set for the traditional roundabout system (TRS) as $f_g = 2$ sec and $m_g = 4$ sec. The vehicles approach the roundabout, circulate in it, and exit independently, and are coordinated only when entering the clustering zone and the merging execution zone. All simulations are run in discrete-time with step size of $\Delta t = 0.5$ sec.

We set the arrival (free-flow) velocity when exiting the clustering zone to be no more than 13.89 m/s (50 km/h) and no less than 10 m/s (36 km/h) in order not to affect the flow of following traffic. It should be noted that though the desired velocity is high, the vehicle may move much slower (as the local controller may determine), depending on the preceding vehicle. The maximum allowable merging velocity of vehicles is set at $\psi_\alpha = 30$ km/h. To achieve the maximum traffic flow, the circulating vehicles are assigned with higher priority than entry lane vehicles because delaying the circulating flow will equally affect all lanes, and cause traffic congestion. We set the maximum and minimum

velocities of circulating vehicles to be 9.72 m/s (35 km/h) and 5.56 m/s (20 km/h), respectively.

We simulate two traffic flow cases to demonstrate the effectiveness of the proposed RCS for various traffic flow rates (free flow to congested flow near the capacity). In Case 1, all entry lanes have the same traffic flow rates (balanced flow) beginning with 200 veh/h and increased in intervals of 200 veh/h to 1000 veh/h (which is close to the capacity of a single lane roundabout). The flow rates circulating in the roundabout are assumed to be the same as the entry lane flow rates, i.e., vehicles exit from the roundabout with equal probability. In Case 2, the traffic flow rates in the perpendicular lanes are twice the flow rates of the other two lanes. The purpose is to create traffic congestion in specific areas, which is a common phenomenon during peak hours. To this end, the traffic flow rate at East and West lanes are initially set at 200 veh/h and the flow rate at North and South lanes are 400 veh/h. Then East and West lane flow rates are increased to 600 veh/h in increments of 100 veh/h, while the North and South lane flow rates are increased by double. Firstly the simulations are run to observe the performance of TRS, where all vehicles are driven by humans, with dynamics represented by the intelligent driver model representing function (6.2) to decide acceleration, and the lane change model MOBIL is used to execute safe merging. Then, simulations are conducted using the RCS proposed in work.

The comparison of simulation results between RCS and TRS are assessed via five performance matrices of traffic flow, namely (i) average traveling time, (ii) average idling time, (iii) average velocity, (iv) minimum average velocity, and (v) average fuel consumption. The traveling time is the total time taken by vehicles to traverse the roundabout and the idling time is the total time spent by vehicles to stop and wait at the roundabout junctions. The average velocity is the sum of velocities of all vehicles divided by the number of vehicles throughout the simulation and the minimum average velocity is the lowest average velocity of vehicles. The average fuel

consumption is the total fuel consumption divided by the number of vehicles in the network. The fuel consumption of each vehicle is estimated by the method proposed in (Kamal et al., 2011).

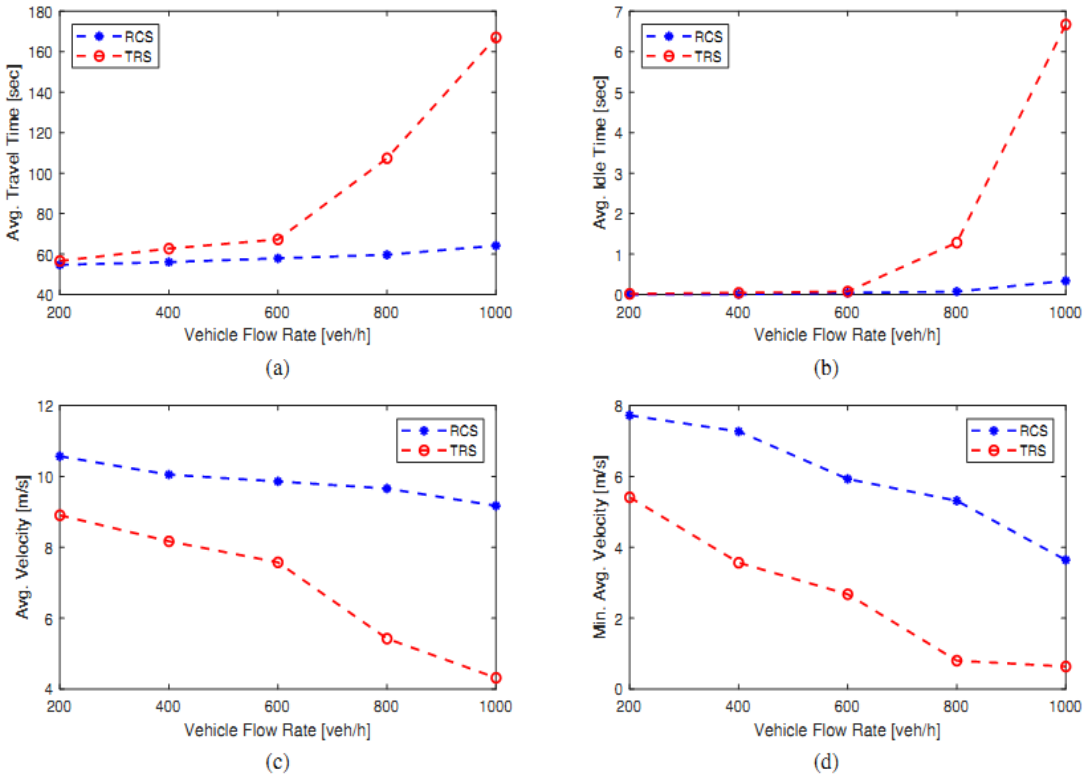

Figure 42: Case 1 performance comparison of roundabout control system (RCS) and traditional roundabout system (TRS).

Figures 42 and 43 show the simulation results for Cases 1 and 2, respectively, which demonstrate that the proposed RCS causes average traveling and idling times to be significantly lower, compared to the TRS. This is because coordinated vehicles require minimum waiting time before entering the roundabout. However, there may be trivial increase of traveling time and idling time, where the coordination of vehicles is not possible due to high density of circulating flow. Moreover, the proposed RCS significantly improves average velocity and minimum average velocity because coordinated vehicles do not need to slow down or stop in most of the cases before entering the roundabout, which ensures smooth flow. Figure 44 shows the average fuel consumption of both cases and it is clear that the proposed RCS outperforms the TRS for different traffic demands particularly, when traffic flow is near capacity. The

percentage improvement in average travel time, average velocity, and average fuel consumption for Cases 1 and 2 are summarized in Table 7.

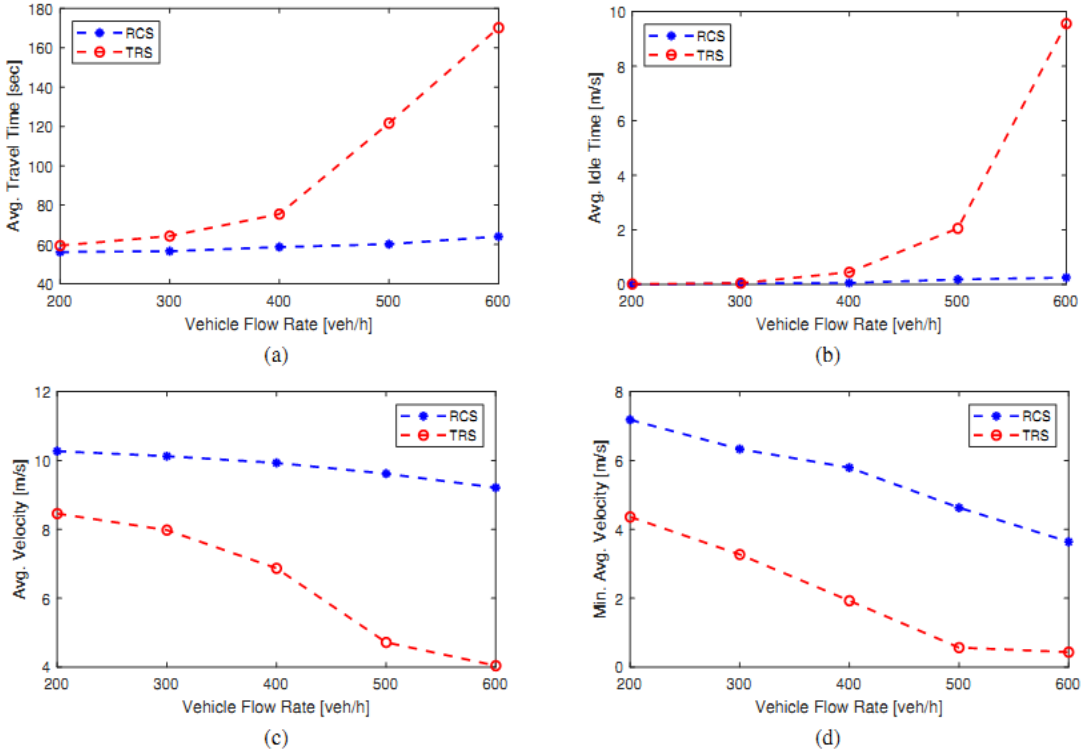

Figure 43: Case 2 performance comparison of roundabout control system (RCS) and traditional roundabout system (TRS).

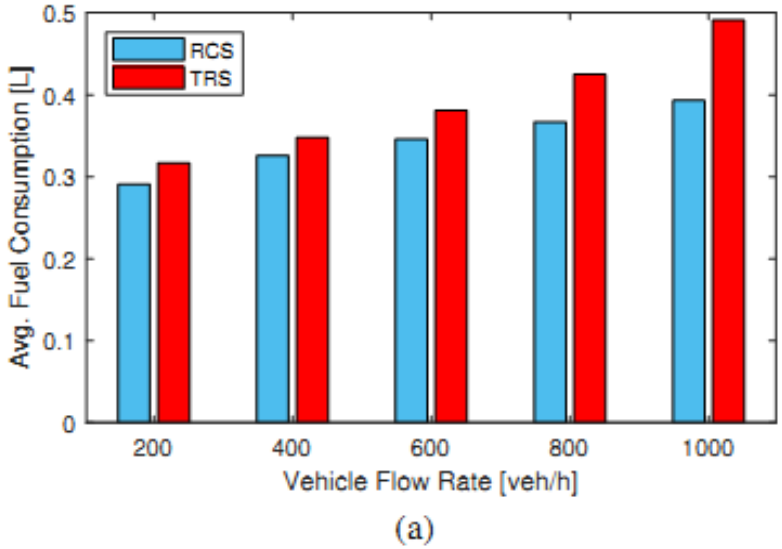

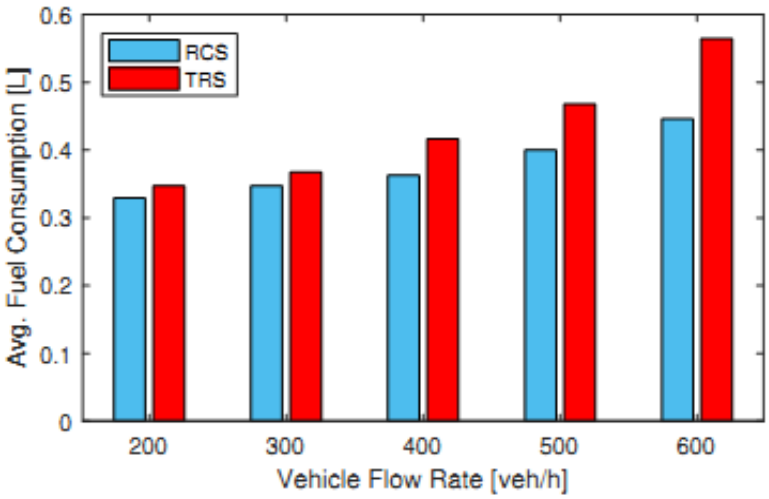

Figure 44: Average fuel consumption of vehicles, (a) Case 1 with balanced traffic flow, and (b) Case 2 with unbalanced traffic flow.

Table 7: Performance comparison between RCS and TRS

	TRS	RCS	Improvement
Case 1:			
Avg. Velocity [km/h]	24.76	35.45	42.73%
Avg. Travel Time [sec]	92.20	58.52	36.52%
Avg. Fuel Cons [ml]	392	344	12.24%
Case 2:			
Avg. Velocity [km/h]	23.08	35.36	53.20%
Avg. Travel Time [sec]	98.20	59.13	39.78%
Avg. Fuel Cons [ml]	432	376	12.96%

6.5 Summary

In this chapter, we have developed a novel roundabout control system (RCS) for AVs at a four-leg roundabout. The vehicles are coordinated in a bi-level framework using a roundabout coordination unit (RCU). The higher level coordination forms clusters of vehicles based on traffic flow information before preparing for merging. In the lower level coordination, a combinatorial

optimization problem is solved to calculate the target times for individual vehicles to enter the roundabout. Following that, local controller determines the acceleration of automated vehicles for smooth merging and avoiding collision with circulating vehicles. The roundabout coordination is not affected if any vehicle fails to follow the sequence. The proposed RCS is evaluated using a four-leg roundabout considering various traffic demands, i.e., both balanced and unbalanced traffic flow rates and the performance is compared to the traditional roundabout system (TRS). From the results, it is evident that the proposed RCS yields significant improvement in fuel consumption, travel time, and average velocity of vehicles for different traffic scenarios. The proposed system can be implemented online as the computational burden is negligible.

The current simulation is considered for a single lane roundabout that can be extended for multi-lane roundabouts in the future. The proposed scheme can be used to cluster and optimize more vehicles for coordination with additional computational cost. Moreover, the scheme can be extended further using distributed model predictive control (MPC) for individual vehicles.

7 Conclusion and Future Works

In this thesis, we have developed intelligent vehicle control strategies for eco-driving at signalized intersections, hilly roads, horizontal curved roads, and four-legged roundabouts. The eco-driving strategy at the intersection is based on naturalistic learning from driving data and traffic signal conditions, the strategy on hilly roads and curved roads are based on fuzzy-tuned MPC and MPC, respectively, and the strategy at the roundabout is based on intelligent coordination of CAVs using successive receding horizon control approach.

The proposed EDS for signalized intersections takes into account the presence of disturbances and preceding vehicles, and the speed advisory system recommends the optimal velocity to the vehicle. The vehicle either retains a steady cruising speed or performs an appropriate level of acceleration to avoid red signal when it observes a switch to the green signal. When there is a shift to the red signal, the vehicle slows down to its minimum velocity and slowly approaches the intersection to minimize idling time. The EDS for hilly roads generates the optimal velocity for the host vehicle based on the fuzzy-tuned MPC that helps efficiently utilize the gravitational potential energy and avoids braking (which wastes energy) at down-slopes. The proposed EDS also ensures the optimal driving strategy for a group of TDS vehicles in synchronous driving mode. The EDS for curved roads computes the optimal velocity trajectory for the host vehicle using MPC considering its dynamical model, the state of the preceding vehicle, information of road-curvatures, and various road-surface conditions. On the other hand, the proposed eco-driving strategy for roundabouts coordinates vehicles centrally in a bi-level framework using a roundabout coordination unit.

To evaluate the performance of the proposed scheme, microscopic traffic simulations are conducted and compared with the traditional driving systems. It is found that for various scenarios the proposed eco-driving strategies outperform the traditional human driving system in fuel economy,

CO_2 emission, and travel time, while ensuring driving safety. The proposed EDS maintains fuel consumption in the optimum level. In particular, the eco-driving strategies have improved fuel consumption for an isolated signalized intersection by 3.9%, for hilly roads (with various up and down slopes) by 7.8-13.2%, for a horizontal curved road (with different road-surface conditions) by 4.5-10.2%, and for a four-legged roundabout by about 13%. The proposed eco-driving strategies are fast enough to be implemented in real-time.

The eco-driving strategies developed in this study apply to different road-traffic scenarios with single lane. In the future, multi-lane traffic flow will be considered including lane change model. Also, the traffic flow performance will be investigated for different market penetration rates of the EDS vehicle.

8 References

[1] Schrank, D., Eisele, B., Lomax, T., & Bak, J. (2015). 2015 urban mobility scorecard.

[2] European Comission. Directorate-General for Mobility and Transport. (2011). *White Paper on Transport: Roadmap to a Single European Transport Area: Towards a Competitive and Resource-Efficient Transport System*. Publications Office of the European Union.

[3] EIA, U. S. (2019). *Annual energy outlook 2015: with projections to 2050*. US Department of Energy, DOE/EIA, Washington, DC, 20585.

[4] Desai, M., & Harvey, R. P. (2017). Inventory of US greenhouse gas emissions and sinks: 1990-2015. *Federal Register*, *82*(30), 10767.

[5] Guerreiro, C. B., Foltescu, V., & De Leeuw, F. (2014). Air quality status and trends in Europe. *Atmospheric environment*, *98*, 376-384.

[6] Zhang, K., & Frey, H. C. (2006). Road grade estimation for on-road vehicle emissions modeling using light detection and ranging data. *Journal of the Air & Waste Management Association*, *56*(6), 777-788.

[7] Barth, M., Collins, J., Scora, G., Davis, N., & Norbeck, J. (2006). Measuring and modeling emissions from extremely low-emitting vehicles. *Transportation Research Record*, *1987*(1), 21-31.

[8] Bishop, J., Nedungadi, A., Ostrowski, G., Surampudi, B., Armiroli, P., & Taspinar, E. (2007). *An engine start/stop system for improved fuel economy* (No. 2007-01-1777). SAE technical paper.

[9] Mendez, S., & Thirouard, B. (2009). Using multiple injection strategies in diesel combustion: potential to improve emissions, noise and fuel economy trade-off in low CR engines. *SAE International Journal of Fuels and Lubricants*, *1*(1), 662-674.

[10] Berry, I. M. (2010). *The effects of driving style and vehicle performance on the real-world fuel consumption of US light-duty vehicles* (Doctoral dissertation, Massachusetts Institute of Technology).

[11] Knowles, M., Scott, H., & Baglee, D. (2012). The effect of driving style on electric vehicle performance, economy and perception. *International Journal of Electric and Hybrid Vehicles*, *4*(3), 228-247.

[12] Saboohi, Y., & Farzaneh, H. (2009). Model for developing an eco-driving strategy of a passenger vehicle based on the least fuel consumption. *Applied Energy*, *86*(10), 1925-1932.

[13] Margiotta, R. A., & Snyder, D. (2011). *An agency guide on how to establish localized congestion mitigation programs* (No. FHWA-HOP-11-009). United States. Federal Highway Administration. Office of Operations.

[14] Tang, T. Q., Yi, Z. Y., & Lin, Q. F. (2017). Effects of signal light on the fuel consumption and emissions under car-following model. *Physica A: Statistical Mechanics and its Applications*, *469*, 200-205.

[15] Xia, H., Boriboonsomsin, K., Schweizer, F., Winckler, A., Zhou, K., Zhang, W. B., & Barth, M. (2012, September). Field operational testing of eco-approach technology at a fixed-time signalized intersection. In *2012 15th International IEEE Conference on Intelligent Transportation Systems* (pp. 188-193). IEEE.

[16] Toyota. (2006). Toyota Australia Eco-Driving Guide. Energy Conservation Centre,Japan, https://www.toyota.com.au/static/pdfs/ecodriving/ecodriving-guide.pdf

[17] Boriboonsomsin, K., & Barth, M. (2009). Impacts of road grade on fuel consumption and carbon dioxide emissions evidenced by use of advanced navigation systems. *Transportation Research Record*, *2139*(1), 21-30.

[18] Carrese, S., Gemma, A., & La Spada, S. (2013). Impacts of driving behaviours, slope and vehicle load factor on bus fuel consumption and emissions: a real case study in the city of Rome. *Procedia-Social and Behavioral Sciences*, *87*, 211-221.

[19] Silva, C. M., Farias, T. L., Frey, H. C., & Rouphail, N. M. (2006). Evaluation of numerical models for simulation of real-world hot-stabilized fuel consumption and emissions of gasoline light-duty vehicles. *Transportation Research Part D: Transport and Environment*, *11*(5), 377-385.

[20] Ko, M. (2015). Incorporating Vehicle Emissions Models into the Geometric Highway Design Process: Application on Horizontal Curves. *Transportation Research Record*, *2503*(1), 1-9.

[21] Van Mierlo, J., Maggetto, G., Van de Burgwal, E., & Gense, R. (2004). Driving style and traffic measures-influence on vehicle emissions and fuel

consumption. *Proceedings of the Institution of Mechanical Engineers, Part D: Journal of Automobile Engineering*, *218*(1), 43-50.

[22] Cheng, Q., Nouveliere, L., & Orfila, O. (2013, June). A new eco-driving assistance system for a light vehicle: Energy management and speed optimization. In *2013 IEEE Intelligent Vehicles Symposium (IV)* (pp. 1434-1439). IEEE.

[23] Barth, M., Mandava, S., Boriboonsomsin, K., & Xia, H. (2011, June). Dynamic ECO-driving for arterial corridors. In *2011 IEEE Forum on Integrated and Sustainable Transportation Systems* (pp. 182-188). IEEE.

[24] Hu, J., Shao, Y., Sun, Z., Wang, M., Bared, J., & Huang, P. (2016). Integrated optimal eco-driving on rolling terrain for hybrid electric vehicle with vehicle-infrastructure communication. *Transportation Research Part C: Emerging Technologies*, *68*, 228-244.

[25] Kamal, M. A. S., Mukai, M., Murata, J., & Kawabe, T. (2011). Ecological vehicle control on roads with up-down slopes. *IEEE Transactions on Intelligent Transportation Systems*, *12*(3), 783-794.

[26] Wang, M., Daamen, W., Hoogendoorn, S. P., & van Arem, B. (2014). Rolling horizon control framework for driver assistance systems. Part I: Mathematical formulation and non-cooperative systems. *Transportation research part C: emerging technologies*, *40*, 271-289.

[27] Xia, H., Wu, G., Boriboonsomsin, K., & Barth, M. J. (2013, October). Development and evaluation of an enhanced eco-approach traffic signal application for connected vehicles. In *16th International IEEE Conference on Intelligent Transportation Systems (ITSC 2013)* (pp. 296-301). IEEE.

[28] Rakha, H., & Kamalanathsharma, R. K. (2011, October). Eco-driving at signalized intersections using V2I communication. In *2011 14th international IEEE conference on intelligent transportation systems (ITSC)* (pp. 341-346). IEEE.

[29] Beusen, B., Broekx, S., Denys, T., Beckx, C., Degraeuwe, B., Gijsbers, M., ... & Panis, L. I. (2009). Using on-board logging devices to study the longer-term impact of an eco-driving course. *Transportation research part D: transport and environment*, *14*(7), 514-520.

[30] Barth, M., & Boriboonsomsin, K. (2009). Energy and emissions impacts of a freeway-based dynamic eco-driving system. *Transportation Research Part D: Transport and Environment*, *14*(6), 400-410.

[31] Mensing, F., Bideaux, E., Trigui, R., & Jeanneret, B. (2013). Trajectory 107 rocedia 107 ion for eco-driving–an experimentally verified 107 rocedia 107 ion method. *International Journal of Vehicle Systems Modelling and Testing*, *8*(4), 295-315.

[32] Post, K., Kent, J. H., Tomlin, J., & Carruthers, N. (1985). Vehicle characterization and fuel consumption prediction using maps and power demand models. *International Journal of Vehicle Design*, *6*(1), 72-92.

[33] Akcelik, R. (1989). Efficiency and drag in the power-based model of fuel consumption. *Transportation Research Part B: Methodological*, *23*(5), 376-385.

[34] Barth, M., An, F., Younglove, T., Scora, G., Levine, C., Ross, M., & Wenzel, T. (2000). Comprehensive Modal Emission Model (CMEM), version 2.0 user's guide. *University of California, Riverside*, *4*.

[35] Hellinga, B., Khan, M. A., & Fu, L. Analytical Emission Models for Signalized Arterials in The Canadian Society of Civil Engineers 3rd Transportation Specialty Conference. 2000. *London, Ontario, CA*.

[36] Fröberg, A., Hellström, E., & Nielsen, L. (2006). *Explicit fuel optimal speed profiles for heavy trucks on a set of topographic road profiles* (No. 2006-01-1071). SAE Technical Paper.

[37] Simpson, A. G. (2005). Parametric modelling of energy consumption in road vehicles.

[38] Rakha, H., Ahn, K., & Trani, A. (2004). Development of VT-Micro model for estimating hot stabilized light duty vehicle and truck emissions. *Transportation Research Part D: Transport and Environment*, *9*(1), 49-74.

[39] Kamal, M. A. S., Mukai, M., Murata, J., & Kawabe, T. (2012). Model predictive control of vehicles on urban roads for improved fuel economy. *IEEE Transactions on control systems technology*, *21*(3), 831-841.

[40] Li, L., Wen, D., & Yao, D. (2013). A survey of traffic control with vehicular communications. *IEEE Transactions on Intelligent Transportation Systems*, *15*(1), 425-432.

[41] Gáspár, P., & Németh, B. (2014). Design of adaptive cruise control for road vehicles using topographic and traffic information. *IFAC Proceedings Volumes*, *47*(3), 4184-4189.

[42] Azizi, M. (2015). Incorporating Connected Vehicles into the Transportation Planning Process. AMPO Annual Meeting, U.S. Department of Transportation.

[43] Hamida, E. B., Noura, H., & Znaidi, W. (2015). Security of cooperative intelligent transport systems: Standards, threats analysis and cryptographic countermeasures. *Electronics*, *4*(3), 380-423.

[44] Yang, K., Guler, S. I., & Menendez, M. (2016). Isolated intersection control for various levels of vehicle technology: Conventional, connected, and automated vehicles. *Transportation Research Part C: Emerging Technologies*, *72*, 109-129.

[45] Rios-Torres, J., & Malikopoulos, A. A. (2016). Automated and cooperative vehicle merging at highway on-ramps. *IEEE Transactions on Intelligent Transportation Systems*, *18*(4), 780-789.

[46] SAE On-Road Automated Vehicle Standards Committee. (2014). Taxonomy and definitions for terms related to on-road motor vehicle automated driving systems. *SAE Standard J*, *3016*, 1-16.

[47] Fenton, R. E. (1970). Automatic vehicle guidance and control—A state of the art survey. *IEEE Transactions on Vehicular Technology*, *19*(1), 153-161.

[48] Pue, A. J. (1979). Implementation trade-offs for a short-headway vehicle-follower automated transit system. *IEEE Transactions on Vehicular Technology*, *28*(1), 46-55.

[49] Caudill, R. J., Kornhauser, A. L., & Wroble, J. R. (1979). Hierarchical vehicle management concept for automated guideway transportation systems. *IEEE Transactions on Vehicular Technology*, *28*(1), 11-21.

[50] Shladover, S. E., Desoer, C. A., Hedrick, J. K., Tomizuka, M., Walrand, J., Zhang, W. B., ... & McKeown, N. (1991). Automated vehicle control

developments in the PATH program. *IEEE Transactions on vehicular technology*, *40*(1), 114-130.

[51] Sheikholeslam, S., & Desoer, C. A. (1993). Longitudinal control of a platoon of vehicles with no communication of lead vehicle information: A system level study. *IEEE Transactions on vehicular technology*, *42*(4), 546-554.

[52] Varaiya, P. (1993). Smart cars on smart roads: problems of control. *IEEE Transactions on automatic control*, *38*(2), 195-207.

[53] Rajamani, R., Tan, H. S., Law, B. K., & Zhang, W. B. (2000). Demonstration of integrated longitudinal and lateral control for the operation of automated vehicles in platoons. *IEEE Transactions on Control Systems Technology*, *8*(4), 695-708.

[54] Li, M., Boriboonsomsin, K., Wu, G., Zhang, W. B., & Barth, M. (2009). Traffic energy and emission reductions at signalized intersections: a study of the benefits of advanced driver information. *International Journal of Intelligent Transportation Systems Research*, *7*(1), 49-58.

[55] Nishuichi, H., & Yoshii, T. (2005, November). A study of the signal control for the minimization of CO2 emission. In *Proceedings of the 12th World Congress on Intelligent Transport Systems, San Francisco, CA*.

[56] Cools, S. B., Gershenson, C., & D'Hooghe, B. (2013). Self-organizing traffic lights: A realistic simulation. In *Advances in applied self-organizing systems* (pp. 45-55). Springer, London.

[57] Priemer, C., & Friedrich, B. (2009, October). A decentralized adaptive traffic signal control using V2I communication data. In *2009 12th International IEEE Conference on Intelligent Transportation Systems* (pp. 1-6). IEEE.

[58] Maccubbin, R. P., Staples, B. L., Kabir, F., Lowrance, C. F., Mercer, M. R., Philips, B. H., & Gordon, S. R. (2008). *Intelligent transportation systems benefits, costs, deployment, and lessons learned: 2008 update* (No. FHWA-JPO-08-032).

[59] Vander Werf, J., Shladover, S. E., Miller, M. A., & Kourjanskaia, N. (2002). Effects of adaptive cruise control systems on highway traffic flow capacity. *Transportation Research Record*, *1800*(1), 78-84.

[60] Ioannou, P. A., & Stefanovic, M. (2005). Evaluation of ACC vehicles in mixed traffic: Lane change effects and sensitivity analysis. *IEEE Transactions on Intelligent Transportation Systems*, *6*(1), 79-89.

[61] Kesting, A., Treiber, M., Schönhof, M., & Helbing, D. (2008). Adaptive cruise control design for active congestion avoidance. *Transportation Research Part C: Emerging Technologies*, *16*(6), 668-683.

[62] Pananurak, W., Thanok, S., & Parnichkun, M. (2009, February). Adaptive cruise control for an intelligent vehicle. In *2008 IEEE International Conference on Robotics and Biomimetics* (pp. 1794-1799). IEEE.

[63] Van Arem, B., Van Driel, C. J., & Visser, R. (2006). The impact of cooperative adaptive cruise control on traffic-flow characteristics. *IEEE Transactions on intelligent transportation systems*, *7*(4), 429-436.

[64] Shladover, S., Nowakowski, C. V., Cody, D., Bu, F., O'Connell, J., Spring, J., … & Nelson, D. (2009). *Effects of cooperative adaptive cruise control on traffic flow: testing drivers' choices of following distances*. California PATH Program, Institute of Transportation Studies, University of California at Berkeley.

[65] Naus, G., Vugts, R., Ploeg, J., van de Molengraft, R., & Steinbuch, M. (2010, June). Cooperative adaptive cruise control, design and experiments. In *Proceedings of the 2010 American control conference* (pp. 6145-6150). IEEE.

[66] Öncü, S., Ploeg, J., Van de Wouw, N., & Nijmeijer, H. (2014). Cooperative adaptive cruise control: Network-aware analysis of string stability. *IEEE Transactions on Intelligent Transportation Systems*, *15*(4), 1527-1537.

[67] Mandava, S., Boriboonsomsin, K., & Barth, M. (2009, October). Arterial velocity planning based on traffic signal information under light traffic conditions. In *2009 12th International IEEE Conference on Intelligent Transportation Systems* (pp. 1-6). IEEE.

[68] Asadi, B., & Vahidi, A. (2010). Predictive cruise control: Utilizing upcoming traffic signal information for improving fuel economy and reducing trip time. *IEEE transactions on control systems technology*, *19*(3), 707-714.

[69] Kamal, M. A. S., Taguchi, S., & Yoshimura, T. (2015, September). Intersection vehicle cooperative eco-driving in the context of partially

connected vehicle environment. In *2015 IEEE 18th International Conference on Intelligent Transportation Systems* (pp. 1261-1266). IEEE.

[70] Jiang, H., Hu, J., An, S., Wang, M., & Park, B. B. (2017). Eco approaching at an isolated signalized intersection under partially connected and automated vehicles environment. *Transportation Research Part C: Emerging Technologies*, *79*, 290-307.

[71] Mahler, G., & Vahidi, A. (2014). An optimal velocity-planning scheme for vehicle energy efficiency through probabilistic prediction of traffic-signal timing. *IEEE Transactions on Intelligent Transportation Systems*, *15*(6), 2516-2523.

[72] Morsink, P. L., van Nes, N., Walta, L., & Marchau, V. (2008). In-car speed assistance to improve speed management. In *15th World Congress on Intelligent Transport Systems and ITS America's 2008 Annual MeetingITS AmericaERTICOITS JapanTransCore*.

[73] Spyropoulou, I., & Karlaftis, M. G. (2008, April). Parameters related to modelling intelligent speed adaptation systems with the employment of a microscopic traffic model. In *Proceedings of European Conference on Human Centred Design for Intelligent Transport Systems* (p. 163).

[74] Lee, J., & Park, B. (2012). Development and evaluation of a cooperative vehicle intersection control algorithm under the connected vehicles environment. *IEEE Transactions on Intelligent Transportation Systems*, *13*(1), 81-90.

[75] Kamal, M. A. S., Imura, J. I., Hayakawa, T., Ohata, A., & Aihara, K. (2014). A vehicle-intersection coordination scheme for smooth flows of traffic without using traffic lights. *IEEE Transactions on Intelligent Transportation Systems*, *16*(3), 1136-1147.

[76] Dresner, K., & Stone, P. (2008). A multiagent approach to autonomous intersection management. *Journal of artificial intelligence research*, *31*, 591-656.

[77] de La Fortelle, A. (2010, September). Analysis of reservation algorithms for cooperative planning at intersections. In *13th International IEEE conference on intelligent transportation systems* (pp. 445-449). IEEE.

[78] Huang, S., Sadek, A. W., & Zhao, Y. (2012). Assessing the mobility and environmental benefits of reservation-based intelligent intersections using an integrated simulator. *IEEE Transactions on Intelligent Transportation Systems*, *13*(3), 1201-1214.

[79] Li, L., & Wang, F. Y. (2006). Cooperative driving at blind crossings using intervehicle communication. *IEEE Transactions on Vehicular technology*, *55*(6), 1712-1724.

[80] Yan, F., Dridi, M., & El Moudni, A. (2009, October). Autonomous vehicle sequencing algorithm at isolated intersections. In *2009 12th International IEEE conference on intelligent transportation systems* (pp. 1-6). IEEE.

[81] Jin, Q., Wu, G., Boriboonsomsin, K., & Barth, M. (2012, December). Multi-agent intersection management for connected vehicles using an optimal scheduling approach. In *2012 International Conference on Connected Vehicles and Expo (ICCVE)* (pp. 185-190). IEEE.

[82] Makarem, L., & Gillet, D. (2013, October). Model predictive coordination of autonomous vehicles crossing intersections. In *16th International IEEE Conference on Intelligent Transportation Systems (ITSC 2013)* (pp. 1799-1804). IEEE.

[83] Cao, W., Mukai, M., Kawabe, T., Nishira, H., & Fujiki, N. (2015). Cooperative vehicle path generation during merging using model predictive control with real-time optimization. *Control Engineering Practice*, *34*, 98-105.

[84] Yu, K., Yang, J., & Yamaguchi, D. (2015). Model predictive control for hybrid vehicle ecological driving using traffic signal and road slope information. *Control theory and technology*, *13*(1), 17-28.

[85] De Nunzio, G., De Wit, C. C., Moulin, P., & Di Domenico, D. (2016). Eco-driving in urban traffic networks using traffic signals information. *International Journal of Robust and Nonlinear Control*, *26*(6), 1307-1324.

[86] Park, S., & Rakha, H. (2006). Energy and environmental impacts of roadway grades. *Transportation research record*, *1987*(1), 148-160.

[87] Schwarzkopf, A. B., & Leipnik, R. B. (1977). Control of highway vehicles for minimum fuel consumption over varying terrain. *Transportation Research*, *11*(4), 279-286.

[88] Chang, D. J., & Morlok, E. K. (2005). Vehicle speed profiles to minimize work and fuel consumption. *Journal of transportation engineering*, *131*(3), 173-182.

[89] Saerens, B., & Van den Bulck, E. (2013). Calculation of the minimum-fuel driving control based on Pontryagin's maximum principle. *Transportation Research Part D: Transport and Environment*, *24*, 89-97.

[90] Hellström, E., Ivarsson, M., Åslund, J., & Nielsen, L. (2009). Look-ahead control for heavy trucks to minimize trip time and fuel consumption. *Control Engineering Practice*, *17*(2), 245-254.

[91] Kirschbaum, F., Back, M., & Hart, M. (2002). Determination of the fuel-optimal trajectory for a vehicle along a known route. *IFAC Proceedings Volumes*, *35*(1), 235-239.

[92] Luu, H. T., Nouveliere, L., & Mammar, S. (2010). Dynamic programming for fuel consumption optimization on light vehicle. *IFAC Proceedings Volumes*, *43*(7), 372-377.

[93] Wang, J., Yu, Q., Li, S., Duan, N., & Li, K. (2014). Eco speed optimization based on real-time information of road gradient. *J Automotive Safety and Energy*, *5*, 257-262.

[94] Hu, J., Shao, Y., Sun, Z., Wang, M., Bared, J., & Huang, P. (2016). Integrated optimal eco-driving on rolling terrain for hybrid electric vehicle with vehicle-infrastructure communication. *Transportation Research Part C: Emerging Technologies*, *68*, 228-244.

[95] Li, L., Li, X., Wang, X., Song, J., He, K., & Li, C. (2016). Analysis of downshift's improvement to energy efficiency of an electric vehicle during regenerative braking. *Applied Energy*, *176*, 125-137.

[96] Kaku, A., Kamal, M. A. S., Mukai, M., & Kawabe, T. (2013). Model predictive control for ecological vehicle synchronized driving considering varying aerodynamic drag and road shape information. *SICE Journal of Control, Measurement, and System Integration*, *6*(5), 299-308.

[97] Polus, A., Fitzpatrick, K., & Fambro, D. B. (2000). Predicting operating speeds on tangent sections of two-lane rural highways. *Transportation Research Record*, *1737*(1), 50-57.

[98] Schurr, K. S., McCoy, P. T., Pesti, G., & Huff, R. (2002). Relationship of design, operating, and posted speeds on horizontal curves of rural two-lane highways in Nebraska. *Transportation Research Record*, *1796*(1), 60-71.

[99] Chen, X. L., Lu, M., Zhang, D. Z., Chi, R., & Wang, J. (2010, June). Integrated safety speed model for curved roads. In *Proceedings of the 2010 World Automotive Congress. London: FISITA* (pp. 1-7).

[100] Khan, G., Bill, A. R., Chitturi, M. V., & Noyce, D. A. (2013). Safety evaluation of horizontal curves on rural undivided roads. *Transportation research record*, *2386*(1), 147-157.

[101] Zhang, D., Xiao, Q., Wang, J., & Li, K. (2013). Driver curve speed model and its application to ACC speed control in curved roads. *International journal of automotive technology*, *14*(2), 241-247.

[102] Matsumoto, S., Tange, S., Suzuki, T., & Yoshizawa, H. (2008). *U.S. Patent No. 7,337,055*. Washington, DC: U.S. Patent and Trademark Office.

[103] Ding, F., & Jin, H. (2018). On the optimal speed profile for eco-driving on curved roads. *IEEE Transactions on Intelligent Transportation Systems*, *19*(12), 4000-4010.

[104] Yang, X., Li, X., & Xue, K. (2004). A new traffic-signal control for modern roundabouts: method and application. *IEEE Transactions on Intelligent Transportation Systems*, *5*(4), 282-287.

[105] Zohdy, I. H., & Rakha, H. A. (2013). Enhancing roundabout operations via vehicle connectivity. *Transportation research record*, *2381*(1), 91-100.

[106] Hummer, J. E., Milazzo, J. S., Schroeder, B., & Salamati, K. (2014). Potential for metering to help roundabouts manage peak period demands in the United States. *Transportation research record*, *2402*(1), 56-66.

[107] Martin-Gasulla, M., García, A., & Moreno, A. T. (2016). Benefits of metering signals at roundabouts with unbalanced flow: Patterns in spain. *Transportation Research Record*, *2585*(1), 20-28.

[108] Xu, H., Zhang, K., & Zhang, D. (2016). Multi-level traffic control at large four-leg roundabouts. *Journal of Advanced Transportation*, *50*(6), 988-1007.

[109] Ahn, K., Kronprasert, N., & Rakha, H. (2009). Energy and environmental assessment of high-speed roundabouts. *Transportation Research Record*, *2123*(1), 54-65.

[110] Gastaldi, M., Meneguzzer, C., Rossi, R., Della Lucia, L., & Gecchele, G. (2014). Evaluation of air pollution impacts of a signal control to roundabout conversion using microsimulation. *Transportation research 115rocedia*, *3*, 1031-1040.

[111] Zhao, L., Malikopoulos, A., & Rios-Torres, J. (2018). Optimal control of connected and automated vehicles at roundabouts: An investigation in a mixed-traffic environment. *IFAC-PapersOnLine*, *51*(9), 73-78.

[112] Alessandrini, A., Campagna, A., Delle Site, P., Filippi, F., & Persia, L. (2015). Automated vehicles and the rethinking of mobility and cities. *Transportation Research Procedia*, *5*(2015), 145-160.

[113] Bakibillah, A. S. M., Kamal, M. A. S., Tan, C. P., Hayakawa, T., & Imura, J. I. (2019). Event-driven stochastic eco-driving strategy at signalized intersections from self-driving data. *IEEE Transactions on Vehicular Technology*, *68*(9), 8557-8569.

[114] Treiber, M., Hennecke, A., & Helbing, D. (2000). Congested traffic states in empirical observations and microscopic simulations. *Physical review E*, *62*(2), 1805.

[115] Nagel, K., Wagner, P., & Woesler, R. (2003). Still flowing: old and new approaches for traffic flow modeling Operations. *Research*, *51*, 681-710.

[116] Liebner, M., Baumann, M., Klanner, F., & Stiller, C. (2012, June). Driver intent inference at urban intersections using the intelligent driver model. In *2012 IEEE Intelligent Vehicles Symposium* (pp. 1162-1167). IEEE.

[117] Sivak, M. (2013). *Effects of vehicle fuel economy, distance travelled, and vehicle load on the amount of fuel used for personal transportation: 1970-2010*. University of Michigan, Ann Arbor, Transportation Research Institute.

[118] Koller, D., & Friedman, N. (2009). *Probabilistic graphical models: principles and techniques*. MIT press.

[119] Mihaly, A., & Gáspár, P. (2013, November). Look-ahead cruise control considering road geometry and traffc flow. In *2013 IEEE 14th International Symposium on Computational Intelligence and Informatics (CINTI)* (pp. 189-194). IEEE.

[120] Zadeh, L. A. (1965). Information and control. *Fuzzy sets*, *8*(3), 338-353.

[121] Mamdani, E. H., & Assilian, S. (1975). An experiment in linguistic synthesis with a fuzzy logic controller. *International journal of man-machine studies*, *7*(1), 1-13.

[122] Er, M. J., & Sun, Y. L. (2001). Hybrid fuzzy proportional-integral plus conventional derivative control of linear and nonlinear systems. *IEEE Transactions on Industrial Electronics*, *48*(6), 1109-1117.

[123] Li, H. X., & Gatland, H. B. (1995). A new methodology for designing a fuzzy logic controller. *IEEE transactions on systems, man, and cybernetics*, *25*(3), 505-512.

[124] Hsu, F. Y., & Fu, L. C. (2000). Intelligent robot deburring using adaptive fuzzy hybrid position/force control. *IEEE Transactions on Robotics and Automation*, *16*(4), 325-335.

[125] Jang, J. S., & Sun, C. T. (1995). Neuro-fuzzy modeling and control. *Proceedings of the IEEE*, *83*(3), 378-406.

[126] Iancu, I. (2012). A Mamdani type fuzzy logic controller. *Fuzzy Logic: Controls, Concepts, Theories and Applications*, 325-350.

[127] Robinson, B. W., Rodegerdts, L., Scarborough, W., Kittelson, W., Troutbeck, R., Brilon, W., … & Mason, J. (2000). *Roundabouts: An informational guide* (No. FHWA-RD-00-067; Project 2425). United States. Federal Highway Administration.

[128] Kesting, A., Treiber, M., & Helbing, D. (2007). General lane-changing model MOBIL for car-following models. *Transportation Research Record*, *1999*(1), 86-94.

[129] Liu, B., Ai, X., Liu, P., Zhang, C., Hu, X., & Dong, T. (2015). Fuel economy improvement of a heavy-duty powertrain by using hardware-in-loop simulation and calibration. *Energies*, *8*(9), 9878-9891.

[130] Nair, B. M., & Cai, J. (2007, June). A fuzzy logic controller for isolated signalized intersection with traffic abnormality considered. In *2007 IEEE intelligent vehicles symposium* (pp. 1229-1233). IEEE.

[131] Shen, G., Ma, T., & Sun, Y. (2002, June). Application of fuzzy control theory in multi-phase traffic control of single intersection. In *Proceedings of the 4th World Congress on Intelligent Control and Automation (Cat. No. 02EX527)* (Vol. 2, pp. 1017-1022). IEEE.

[132] Murat, Y. S., & Gedizlioglu, E. (2005). A fuzzy logic multi-phased signal control model for isolated junctions. *Transportation Research Part C: Emerging Technologies*, *13*(1), 19-36.

[133] Li, Z., Chitturi, M. V., Zheng, D., Bill, A. R., & Noyce, D. A. (2013). Modeling reservation-based autonomous intersection control in VISSIM. *Transportation research record*, *2381*(1), 81-90.

[134] Mirheli, A., Hajibabai, L., & Hajbabaie, A. (2018). Development of a signal-head-free intersection control logic in a fully connected and autonomous vehicle environment. *Transportation Research Part C: Emerging Technologies*, *92*, 412-425.

[135] Zohdy, I. H., & Rakha, H. A. (2016). Intersection management via vehicle connectivity: The intersection cooperative adaptive cruise control system concept. *Journal of Intelligent Transportation Systems*, *20*(1), 17-32.

[136] Dong, H., Zhuang, W., Yin, G., Chen, H., & Wang, Y. (2020, July). Energy-Optimal Velocity Planning for Connected Electric Vehicles at Signalized Intersection with Queue Prediction. In *2020 IEEE/ASME International Conference on Advanced Intelligent Mechatronics (AIM)* (pp. 238-243). IEEE.

[137] Cicero-Fernández, P., Long, J. R., & Winer, A. M. (1997). Effects of grades and other loads on on-road emissions of hydrocarbons and carbon monoxide. *Journal of the Air & Waste Management Association*, *47*(8), 898-904.

[138] Fitzpatrick, K., Elefteriadou, L., Harwood, D. W., Collins, J. M., McFadden, J., Anderson, I. B., … & Passetti, K. (2000). *Speed prediction for two-lane rural highways* (No. FHWA-RD-99-171). United States. Federal Highway Administration.

[139] Misaghi, P., & Hassan, Y. (2005). Modeling operating speed and speed differential on two-lane rural roads. *Journal of Transportation Engineering*, *131*(6), 408-418.

[140] Gong, H., & Stamatiadis, N. (2008). Operating speed prediction models for horizontal curves on rural four-lane highways. *Transportation Research Record*, *2075*(1), 1-7.

[141] Shallama, R. D. K., & Ahmed, A. M. (2016). Operating Speed Models on Horizontal Curves for Two-lane Highways. *Transportation Research Procedia*, *17*, 445-451.

[142] Wang, B., Hallmark, S., Savolainen, P., & Dong, J. (2018). Examining vehicle operating speeds on rural two-lane curves using naturalistic driving data. Accident Analysis & Prevention, 118, 236-243.

[143] Cvitanić, D., & Maljković, B. (2019). Determination of Applicable Adjacent Horizontal Curve Radii Using Operating Speed. Promet-Traffic&Transportation, 31(4), 443-452.

[144] Schneider, W. H., Savolainen, P. T., & Zimmerman, K. (2009). Driver injury severity resulting from single-vehicle crashes along horizontal curves on rural two-lane highways. Transportation Research Record, 2102(1), 85-92.

[145] Hamzeie, R. (2016). The interrelationships between speed limits, geometry, and driver behavior: a proof-of-concept study utilizing naturalistic driving data.

[146] Machiani, S. G., Medina, A., Gibbons, R., & Williams, B. (2016). Driver behavior modeling on horizontal curves for two-lane rural roads using naturalistic driving data (No. 16-4829).

[147] Dhahir, B., & Hassan, Y. (2018). Studying driving behavior on horizontal curves using naturalistic driving study data. *Transportation research record*, *2672*(17), 83-95.

[148] Kang, M. W., Shariat, S., & Jha, M. K. (2013). New highway geometric design methods for minimizing vehicular fuel consumption and improving safety. Transportation research part C: emerging technologies, 31, 99-111.

[149] You, B. (2017). The environmental impact of horizontal curves on two-lane rural highways (Doctoral dissertation, Texas Southern University).

[150] Llopis-Castelló, D., Pérez-Zuriaga, A. M., Camacho-Torregrosa, F. J., & García, A. (2018). Impact of horizontal geometric design of two-lane rural roads on vehicle CO2 emissions. *Transportation Research Part D: Transport and Environment*, *59*, 46-57.

[151] Gruppelaar, V., van Paassen, R., Mulder, M., & Abbink, D. (2018, October). A perceptually inspired Driver Model for Speed Control in curves. In *2018*

IEEE International Conference on Systems, Man, and Cybernetics (SMC) (pp. 1257-1262). IEEE.

[152] Shi, K., Wang, J., Zhong, S., Tang, Y., & Cheng, J. (2020). Non-fragile memory filtering of TS fuzzy delayed neural networks based on switched fuzzy sampled-data control. *Fuzzy Sets and Systems*, *394*, 40-64.

[153] Carlson, P. J., Burris, M., Black, K., & Rose, E. R. (2005). Comparison of radius-estimating techniques for horizontal curves. *Transportation research record*, *1918*(1), 76-83.

[154] Cvitanić, D., & Maljković, B. (2019). Determination of Applicable Adjacent Horizontal Curve Radii Using Operating Speed. *Promet-Traffic&Transportation*, *31*(4), 443-452.

[155] Zhao, Y. Q., Li, H. Q., Lin, F., Wang, J., & Ji, X. W. (2017). Estimation of road friction coefficient in different road conditions based on vehicle braking dynamics. *Chinese Journal of Mechanical Engineering*, *30*(4), 982-990.